



**POLITECNICO  
DI TORINO**  
Dipartimento  
di Ingegneria Meccanica  
e Aerospaziale

**UB**  
**University at Buffalo**

**CRA3ILAB**  
*CRashworthiness for Aerospace Structures and Hybrids Lab*

POLITECNICO DI TORINO

SCHOOL OF ENGINEERING

Master's Degree course in Aerospace Engineering

Master's Degree Thesis

# Venus Sample Return Mission

Conceptual Solar System Exploration Mission

**Supervisor**

Prof. Manuela Battipede

**Candidate**

Pietro Aiazzone

**Internship Tutor at  
New York State University at Buffalo (NY)**

Dr. Javid Bayandor

July 2020

This work is subject to the Creative Commons Licence



## **Abstract**

Despite several previous missions and decades of researches, the Earth's planetary neighbour, Venus, remains a mysterious reality with many fundamental questions about the evolution of its atmosphere and climate, the composition of its surface and the materials beneath it, the interactions between this two systems, the atmosphere and the surface, and the presence of any forms of life. A new mission concept that employs an atmospheric entry lander and a back-to-Earth vehicle to return both atmospheric and surface samples can answer many of these questions.

Therefore, the main purpose of this thesis is to present a new concept of a Venus Sample Return Mission, developed with the collaboration of the CRASH Lab of the State University of New York at Buffalo, that fully satisfies a list of requirements given by NASA-JPL, describing step by step both the mathematical calculations and the model concepts that have been derived and created to design the main systems and subsystems of the landing vehicle.

# Summary

The purpose of this thesis is to present in details the challenges and the importance related to any Venus Sample Return space missions and describe step by step both the mathematical calculations and the model concepts that have been derived and created to design the main systems and subsystems of a new conceptual solar system exploration mission that is capable to collect and return to Earth some samples from the Venusian soil and atmosphere. In particular, the present Master's thesis is composed of four chapters each of them dealing with different aspect of the conceptual design of a new Venus Sample Return Mission.

The first chapter gives a detailed overview of the environment where the mission occurs (which is the Venus environment), providing details both of the background scientific knowledge, gained thanks to decades of researches and space missions, and of the challenges involved in such a space mission. The aim of this chapter is to describe the Venusian system, listing the crucial open questions related to this Earth's neighbour planet and underlining the importance that a deeper knowledge about it would have not only in terms of space exploration, but also in terms of better understanding of terrestrial phenomena and constraints for the presence of life.

The second chapter focuses on the definition of a Venus Sample Return Mission in general, underlining why this type of space mission is so crucial in the understanding of the Venusian environment and which are the scientific goals and the objectives such a space mission has to (and would be able to) fulfill. Moreover, the list of requirements (given by NASA-JPL) this new conceptual Venus Sample Return Mission has to satisfy is listed and described in details.

The purpose of the third chapter is, then, to describe the main phases of the proposed conceptual mission, providing both an overview of the entire procedure, and mathematical and conceptual details of every designed operation involved. The description follows the order these phases are designed to occur, starting from the launch on Earth and ending with the return of the spacecraft from the Venusian planet.

The fourth chapter provides the detailed description of the designed systems and subsystems the landing vehicle consists of. The mathematical calculations, the CAD models and all the results obtained using engineering tools are described in details underlying both the strengths and the criticalities of the conducted design processes.

Lastly, conclusions and final considerations about the conducted research are shared in order to sum up the strengths and limitations of the entire research and provide inspiration or suggestions for future related works.

# Acknowledgements

Beyond the equations, the graphs and the tables present in the pages of this Master's Thesis there has been a long, challenging and extremely exciting adventure composed of months of research and calculations, sessions of brainstorming and discussions conducted in collaboration with the CRASH Lab of the State University of New York at Buffalo. This experience allowed me not only to increase my knowledge in the aerospace field, which I feel more and more interested in every day, but also to grow from an ethical and professional point of view. That is why I would like to dedicate this entire page to all the people who made this thesis project possible.

First of all, I would like to thank Professor Manuela Battipede, my advisor at Politecnico di Torino, for having increased my interest in orbital mechanics and interplanetary space missions with the course *Space Flight Mechanics*, for having been always available when I needed help or advice and, above all, for suggesting that I apply for this project at the State University of New York at Buffalo.

Special thanks go to my advisor at the State University of New York at Buffalo, Javid Bayandor: not only did he welcome me to the CRASH Lab (of which he is founder and director) as if I was part of a family, but also he encouraged and helped me with the research and the studies during the entire duration of the project (especially during the difficult months of spreading of COVID-19); without his contribution this thesis would not have been possible.

I would like to thank all the CRASH Lab members I had the opportunity to work with: Alex, Cameron, Clayton, Nicholas, Pradeep, Samuel and Suraj. All the discussions and the brainstorming conducted with each of them always resulted in great advice and suggestions for my research. It was a pleasure to work and spend time with all of them, I wish them the best of luck for their (undoubtedly brilliant) careers.

I would like to thank all those special people I met in Buffalo: life is not just about work and they really helped me to enjoy the experience and have a wonderful time during the past months. Thank you Andrew, Adrian (the American and Lucy), Adrian (the German), Hasan, Tony, Iris, Sreeya, Chitvan and the Sunday soccer group directed by Tom. I will never forget you.

# Contents

<b>Abstract</b>	I
<b>Summary</b>	II
<b>List of Tables</b>	VI
<b>List of Figures</b>	VIII
<b>1 Introduction and Scientific Background</b>	<b>1</b>
1.1 Introduction . . . . .	1
1.2 Venus Science Background . . . . .	2
1.2.1 Venus Geography . . . . .	3
1.2.2 Surface Geology . . . . .	4
1.2.3 Internal Structure . . . . .	5
1.2.4 Atmosphere and Climate . . . . .	6
1.2.5 Magnetic Field and Core . . . . .	9
1.3 Open Questions . . . . .	9
<b>2 Venus Sample Return Mission</b>	<b>11</b>
2.1 Advantages of Sample Return . . . . .	11
2.2 Proposed Mission Executive Summary . . . . .	12
2.3 Scientific Goals and Objectives . . . . .	13
2.3.1 Goal 1: Understand Venus’s early evolution and possible habitability to constrain the evolution of Venus-sized (exo)planets . . . . .	14
2.3.2 Goal 2: Understand composition and dynamics of Venus’s atmosphere	16
2.3.3 Goal 3: Understand the geologic history preserved on the Venusian surface and the present-day interactions between the surface and the atmosphere . . . . .	16
2.4 Mission Requirements . . . . .	17
<b>3 Mission Main Phases</b>	<b>19</b>
3.1 Launch . . . . .	19
3.2 Interplanetary Travel . . . . .	20
3.2.1 Interplanetary Hohmann Transfer . . . . .	21
3.2.2 Timing . . . . .	23
3.2.3 Launch Windows . . . . .	26

3.2.4	Planetary Departure . . . . .	28
3.2.5	Arrival at Venus . . . . .	30
3.2.6	Implementation on STK . . . . .	31
3.3	Descent and Landing . . . . .	31
3.3.1	Landing Site Selection . . . . .	32
3.3.2	Atmospheric Entry . . . . .	34
3.3.3	Landing Phase . . . . .	39
3.4	Surface Operations . . . . .	40
3.5	Ascent, Rendezvous with the Orbiter and Return to Earth . . . . .	41
<b>4</b>	<b>Systems and Subsystems</b> . . . . .	<b>43</b>
4.1	Venus Entry Aeroshell . . . . .	43
4.1.1	Heat Shield . . . . .	44
4.1.2	Backshell . . . . .	45
4.1.3	Parachute . . . . .	46
4.1.4	Aerodynamic Grid Fins . . . . .	48
4.2	Venus Lander . . . . .	50
4.2.1	Platform . . . . .	51
4.2.2	Helium Tanks . . . . .	52
4.2.3	Landing Ring . . . . .	57
4.2.4	Scientific Payload . . . . .	58
4.2.5	Thermal Protection System . . . . .	64
4.2.6	Mechanisms . . . . .	69
4.2.7	Communication System . . . . .	75
4.2.8	Power System . . . . .	76
4.3	Venus Ascent Vehicle . . . . .	79
4.3.1	Venus Ascent Balloon . . . . .	80
4.3.2	Venus Ascent Rocket . . . . .	92
4.4	Lander Overview . . . . .	112
	<b>Conclusions</b> . . . . .	<b>117</b>
	<b>Bibliography</b> . . . . .	<b>119</b>

# List of Tables

2.1	VEXAG Goals and Objectives of Venus's future exploration . . . . .	15
3.1	Launch Vehicles List . . . . .	20
3.2	Dimensions of the <i>SOI</i> of the planets in our Solar System . . . . .	21
3.3	Eccentricity and Inclination to the ecliptic plane . . . . .	21
3.4	Calculation of the interplanetary Hohmann transfer's characteristics . . . . .	23
3.5	Data used for Hohmann calculations . . . . .	24
3.6	Calculation of the $\Delta V$ using elliptical departure and target orbit . . . . .	24
3.7	Hohmann round trip timing . . . . .	26
3.8	Synodic period and Angular velocity difference . . . . .	27
3.9	Mean longitude at J2000 . . . . .	27
3.10	Launch windows . . . . .	28
3.11	Hyperbola calculations - Earth . . . . .	30
3.12	Hyperbola calculations - Venus . . . . .	31
3.13	Interplanetary transfer results obtained using STK . . . . .	32
3.14	Atmospheric Entry Input Parameters . . . . .	36
3.15	Heat Shield Main Properties - From Ref. [45] [46] . . . . .	37
3.16	Lander Main Properties . . . . .	38
4.1	Heat Shield Properties . . . . .	44
4.2	Backshell Properties . . . . .	46
4.3	Annular Parachute Properties . . . . .	47
4.4	Parachute Film Materials . . . . .	47
4.5	Parachute Fiber Materials . . . . .	48
4.6	Tensile Strength Analysis of Kapton and PBO . . . . .	48
4.7	Final Parachute Materials and Masses . . . . .	48
4.8	Waspaloy Main Properties . . . . .	49
4.9	Grid Fins Total Mass . . . . .	50
4.10	Titanium Alloy Grade 5 (Ti-6Al-4V) Main Properties . . . . .	51
4.11	Helium Cylindric Tanks Geometry and Mass Combinations . . . . .	53
4.12	Dimensions of the Helium Tanks . . . . .	53
4.13	Helium Cylindric Tanks Materials, Thickness and Mass Combinations . . . . .	56
4.14	Material, Dimensions and Masses of the designed Helium Tanks . . . . .	56
4.15	Landing Ring and Legs Masses . . . . .	58
4.16	Scientific Payload Properties . . . . .	62
4.17	Scientific Payload Containers Dimensions . . . . .	64
4.18	Scientific Payload Containers Masses . . . . .	64

4.19	AZ-93 Paint Main Properties [55]	65
4.20	Aerogel Main Properties [56]	65
4.21	Teflon (PTFE) Main Properties	66
4.22	Insulating Layers Thicknesses	67
4.23	Insulating Layers Thicknesses	69
4.24	Ammonia and Helium Cooling System Tanks	70
4.25	Samples Drilling Performances	71
4.26	Mechanical Arm Estimated Mass	72
4.27	Soil Samples Capsules Properties	74
4.28	Atmospheric Samples Capsules Properties	76
4.29	HiTall Batteries Target Performances - Ref. [60]	77
4.30	Drills Power Budget	77
4.31	Scientific Payload (Container 1) Power Budget	78
4.32	Scientific Payload (Container 2) Power Budget	78
4.33	Communication System Power Budget	79
4.34	Ascent Vehicle Power Budget	79
4.35	Batteries Mass Budget	79
4.36	Potential Balloon Film Materials - Ref. [62], [61]	82
4.37	Potential Corrosive Protection Materials	83
4.38	Balloon Potential Target Altitudes	87
4.39	Balloon Potential Target Altitudes	88
4.40	Balloon Ascent Characteristics	91
4.41	Final Balloon Specifications	92
4.42	Venus Ascent Rocket Target Orbit	94
4.43	Ascent Rocket Trajectory Parameters	100
4.44	Ascent Rocket Propellant Properties - Ref. [69]	102
4.45	Ascent Rocket Motor Properties	104
4.46	Possible Motor Case Materials	104
4.47	Motor Case Thickness and Mass	105
4.48	Motor Case Design	106
4.49	Properties of laminates made using six alternate layers of CCF and KP based EPDM prepregs - Ref. [72]	107
4.50	Motor Case Insulating Layer Thickness and Mass	107
4.51	Venus Ascent Rocket Nozzles Properties	109
4.52	Nozzles Design	110
4.53	Stages Baseline Mass	111
4.54	Nose Cone Potential Materials	112
4.55	Nose Cone Design	112
4.56	Preliminary Lander Mass Estimation	114

# List of Figures

1.1	Venus and Earth, companions in the cosmos that have much to tell us through an examination of their common processes and divergent natures (adapted from [1]) . . . . .	2
1.2	Southern hemisphere of Venus as seen in a time-averaged composite of Mariner 10 ultraviolet images (adapted from [3]), and Pioneer Venus OCPP data (adapted from [4]) . . . . .	3
1.3	Surface of Venus as captured in altimeter topography data from the Magellan spacecraft [7] . . . . .	4
1.4	The main tectonic and volcanic units that make up the surface of Venus [8]	4
1.5	Sapas Mons Volcano, 400 km across, 1.5 km high - The simulated hues are based on color images recorded by the Soviet Venera 13 and 14 spacecraft - Image Credit: NASA/JPL . . . . .	5
1.6	Cutaway view of possible internal structure of Venus - Courtesy of Calvin J. Hamilton . . . . .	6
1.7	Globally Averaged Venus Atmosphere Conditions [27] . . . . .	7
1.8	Venus's average pressure vs Altitude - Adapted from [31] . . . . .	8
1.9	Venus's average Temperature vs Altitude - Adapted from [31] . . . . .	9
1.10	Artist's impression showing how the solar wind shapes the magnetospheres of Venus - Adapted from [34] . . . . .	10
2.1	Venus in visible and ultraviolet light as seen from the Mariner 10 flyby in 1974 (Courtesy NASA) . . . . .	13
2.2	The basaltic plain of the Venera 14 landing site. . . . .	14
3.1	SpaceX Falcon fairing - Adopted from Ref. [39] . . . . .	20
3.2	Hohmann Transfer ellipse - Adopted from Figure 8.2 in Ref. [40] . . . . .	22
3.3	Geometry sketch . . . . .	25
3.4	Planets in circular orbit around the Sun - Fig. 8.3 in Ref. [40] . . . . .	26
3.5	Geometry of a hyperbolic orbit sketch . . . . .	29
3.6	Arrival at Venus Sketch - Adopted from Figure 8.14 in Ref. [40] . . . . .	31
3.7	Interplanetary Trajectory Transfer to Venus Sketch . . . . .	32
3.8	Geological Map of Venus - Unsafe units shown in black - Adopted from [34]	33
3.9	Geological Map of Venus - Lower scientific priorities units shown in gray - Adopted from [34] . . . . .	34
3.10	Zonal and Meridional winds - Adopted from Ref. [41] . . . . .	34
3.11	CAD Model of the spacecraft encapsulated inside the aeroshell . . . . .	35
3.12	Descent Phase Summary . . . . .	38

3.13	Landing Probe Descent - Altitude vs Time . . . . .	39
3.14	Landing Probe Descent - Altitude vs Velocity . . . . .	39
3.15	Ascent Phase Summary . . . . .	42
4.1	Heat Shield for Extreme Entry Environment Technology layers - Adopted from Ref. [49] . . . . .	44
4.2	Heat Shield for Extreme Entry Environment Technology configuration - Adopted from Ref. [49] . . . . .	45
4.3	Heat Shield for Extreme Entry Environment Technology model - Adopted from Ref. [49] . . . . .	45
4.4	Backshell CAD Model . . . . .	46
4.5	Annular Parachute Final Dimensions . . . . .	49
4.6	Single Grid Fin CAD Model . . . . .	50
4.7	Lander CAD Model . . . . .	51
4.8	Platform CAD Model . . . . .	52
4.9	Available Space for the Helium Tanks on the Platform . . . . .	54
4.10	Membrane Stresses in Vessels - Adopted from Ref. [51], page 21 . . . . .	54
4.11	Helium Tanks Location - CAD Model . . . . .	57
4.12	Plascore CrushLite Configurations - From Ref. [54] . . . . .	59
4.13	Landing Ring and Legs CAD Model . . . . .	59
4.14	Neutral Mass Spectrometer - Courtesy NASA . . . . .	60
4.15	Payload Containers CAD Model . . . . .	63
4.16	Insulating Layers Sketch . . . . .	66
4.17	Thermal Resistance Diagram of Lander Pressure Vessels . . . . .	66
4.18	Thermal Management System Concept - Ref. [57] . . . . .	68
4.19	Cooling System Cycles - Ref. [57] . . . . .	69
4.20	Honeybee HT actuator with remote (i.e., room temperature) interface electronics - Ref. [58] . . . . .	70
4.21	Sketches of the Pneumatic Transfer System Concept - Ref. [59] . . . . .	71
4.22	Detail of the Mechanical Arm Rods . . . . .	72
4.23	Sketch of the Collected Soil Samples Locations . . . . .	72
4.24	Telescopic Drill Compressed (left) and Extended (right) . . . . .	73
4.25	Sketches of the Atmospheric Collecting System Concept . . . . .	74
4.26	Soil Samples Handling System Concept . . . . .	75
4.27	Low-Gain Antennae (Left) and High-Gain Antennae (Right) Locations . . . . .	76
4.28	Venus's Atmosphere Overview . . . . .	80
4.29	PBO Chemical Structure . . . . .	82
4.30	Strength and Modulus versus Temperature - Ref. [63] . . . . .	83
4.31	Balloon Layers Specifications . . . . .	84
4.32	Natural Shape Balloon Evolution During the Ascent - Ref. [47] . . . . .	84
4.33	Balloon Characteristics vs Altitude . . . . .	85
4.34	Drag Losses and Atmospheric Density vs Altitude . . . . .	86
4.35	Average windspeed versus altitude within the Venus atmosphere - Ref. [65] . . . . .	86
4.36	Temperature and Pressure versus altitude within the Venus atmosphere . . . . .	87
4.37	Model of Venusian Atmosphere, 0 to 100 km - Ref. [66] . . . . .	88
4.38	Balloon Diameters with different Lifting Gases Comparison . . . . .	89
4.39	Balloon Shape at the target altitude of 51 km above the Venusian surface . . . . .	90

4.40	Balloon Profile During the Ascent . . . . .	90
4.41	Balloon Vertical Motion . . . . .	91
4.42	Definition of Burn Out Angle $\phi_{BO}$ . . . . .	94
4.43	Estimated First Stage Losses in terms of $\Delta V$ . . . . .	97
4.44	Venus Ascent Rocket GLOM vs Burnout Angle . . . . .	99
4.45	Venus Ascent Rocket GLOM vs Burnout Angle . . . . .	99
4.46	Venus Ascent Rocket Burn Times versus Burnout Angle . . . . .	100
4.47	Venus Ascent Rocket Flight Path . . . . .	101
4.48	Venus Ascent Rocket Flight Path . . . . .	102
4.49	Venus Ascent Rocket Propellant Configuration - Ref. [70] . . . . .	103
4.50	Motor Web Fraction vs L/D Ratio . . . . .	103
4.51	Conical Nozzle Geometry Sketch . . . . .	108
4.52	Nozzle Correction Factor and Nozzle Length to Exit Radius vs Nozzle Half Cone Angle - 1st Stage (left) and 2nd Stage (right) . . . . .	109
4.53	Venus Ascent Rocket CAD Model . . . . .	113
4.54	Falcon 9 Payload Fairing, Venus Lander and Orbiter . . . . .	113
4.55	Venus Lander Overview . . . . .	115

# Chapter 1

## Introduction and Scientific Background

### 1.1 Introduction

Born in the inner solar system and formed by the same cosmic material as Earth, Venus is considered the twin of Earth. Together with Mars and Mercury, these siblings are referred as terrestrial (or rocky) planets, they have nearly the same size, mass and density, both of them are characterized by solid surfaces with a comparable composition and they have an atmosphere and a weather system. However, there are many differences between the two planets too: Venus's atmosphere is 90 times more dense than that on Earth and it is made of  $\sim 97\%$  of  $CO_2$ , producing a huge greenhouse effect with a 90 atmospheres pressure and a  $470\text{ }^\circ\text{C}$  temperature on the surface; thick clouds made up of sulfuric acid shroud Venus's surface, which lacks water and presents faults and folds, and has been shaped mostly by volcanic activity; the upper clouds experience super-rotation, rotating at a rate 60 times faster than the surface, and are extremely reflective, making Venus the most reflective body in the Solar System (they reflect about 75% of the sunlight); moreover, an intrinsic magnetic field is apparently missing and that suggests the planet's interior might also be different from that of Earth.

All these differences indicate that Earth and Venus had distinct evolutionary paths. What is still unanswered is how their paths diverged, when it happened and why. Therefore, studying the evolution of Venus may help us not only to learn about the history of our Solar System and the formation of its planets, but also to better understand the possible future scenarios of our own planet's evolution. Additionally, solving these mysteries, we will be able to better define if conditions ever existed on Venus that could have hosted life, what processes determine the habitability of a planet and what paths lead to a habitable planet. The great progresses we achieved exploring Mars illustrate how in-depth explorations of nearby terrestrial planets can successfully help to investigate Earth processes: the exploration of Mars has revealed how physics and chemistry can shape another rocky world and, of course, the study of Venus could similarly improve our understanding of Earth processes and Earth-like worlds, offering radically different comparisons (Fig. 1.1). Moreover, as we learn how climate and geology work on a planet similar to our own, we

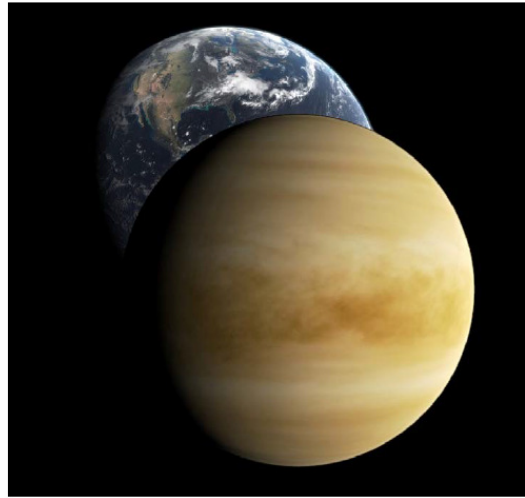


Figure 1.1: Venus and Earth, companions in the cosmos that have much to tell us through an examination of their common processes and divergent natures (adapted from [1])

gain a deeper understanding of the mechanisms currently at work in our own environment. With the threat of possible irreversible anthropogenic changes to the atmosphere, and the realization that we do not know well enough the Earth's climate system, comes a valid concern about the natural vulnerability of the planet where we were born. What is the limit of stability of the terrestrial global system under the influence of human activities and consumptions? Could the rapid emission of greenhouse gases cause irreversible and dangerous changes to our own environment? Has the Earth system already gone beyond a no return point? Thanks to the previous explorations of Venus, now we know that it may have had early oceans and that they probably boiled away because of a huge greenhouse effect. If this happened to Venus, could it happen to Earth as well?

Sometimes the understanding of natural phenomena can be difficult to discern on the Earth itself, but might be illuminated by deeper studies of Earth-like planets. In particular, Venus could provide a lot of climate feedbacks and advice that might be ultimately crucial for the physical safety and the economic security of our society.

## 1.2 Venus Science Background

Our knowledge of Venus's main characteristics (geography, surface geology, internal structure, atmosphere and climate, magnetic field and core) has come from the combination of advanced Earth-based observations and successful Russian, American, European and Japanese exploration missions launched toward our planetary neighbour since 1961.

Venus's present-day atmospheric environment is one of the most extreme in our inner solar system. The atmosphere, characterized by the predominance of  $CO_2$  and a small amount of  $N_2$ , exerts a pressure of  $\sim 90$  bar on the surface and is responsible of a  $\sim 470$  °C temperature due to the greenhouse effect, despite almost  $\sim 80\%$  of the incident solar energy is reflected back to space [2]. The planet is entirely shrouded by thick sulfuric acid haze and clouds. The atmosphere is also composed by  $H_2O$ ,  $CO$ ,  $SO_2$ , which all

are characterized by strong absorption bands in the Infra-Red spectral range and take part in trapping the thermal emissions from the surface and the deep atmosphere. The atmosphere is also known to experience superrotation with respect to the planet surface and to be characterized by two enormous vortices that rotate vertically over the poles of the planet and present very complex shapes and behaviours (Fig. 1.2). The surface is

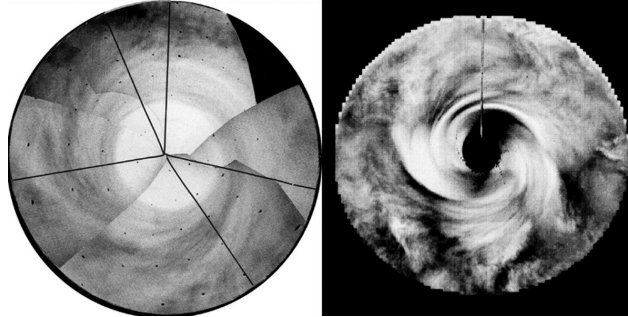


Figure 1.2: Southern hemisphere of Venus as seen in a time-averaged composite of Mariner 10 ultraviolet images (adapted from [3]), and Pioneer Venus OCPP data (adapted from [4])

characterized by a dry and rigid crust with no signs of plate tectonics, but with a great variety of volcanic structures, responsible for releasing heat from the interior of the planet (role played by plate tectonics on Earth). At present day there is no sign of water on the surface and the atmosphere has 100000 times less water than Earth, however, Venus could have harbored liquid water for as long as 2 billion years on the surface and could have been the first habitable planet of our solar system [5].

### 1.2.1 Venus Geography

The mapping process of Venus and its geological features involved surface radar images of the planet, creation of geological maps and identification of the stratigraphic history of the crust. The first global map of the surface of Venus was provided by the *Magellan* orbiter during 1990-1991 by exploiting the physical properties of wave reflection: long wavelength microwaves were used to penetrate the thick atmosphere and reach the surface and, depending on the different strength of the signals reflected by the surface, images useful to construct the map were produced [6]. After having collected the images of Venus's surface, scientists started to map and characterize different geologic materials and units according to distinct surface features.

As a result of the research we now know that Venus's surface is composed of a relatively small number of terrain units that can be divided into 3 categories: tectonized terrains ( $\sim 20\%$ ), volcanic terrains ( $\sim 80\%$ ) and impact-related materials ( $\sim 10\%$ ) [8]. Thus, volcanic and tectonized units represent the principal ones on the Venusian surface (Fig. 1.4).

The tectonized terrains are characterized by the presence of a great number of tectonic structures that strongly deform the original, likely volcanic, morphologic characteristics of the underlying materials of the precursor terrain.

The volcanic terrains are mostly characterized by a morphologically smooth surface with few local shield- and cone-like mounds which are interpreted as volcanic edifices.

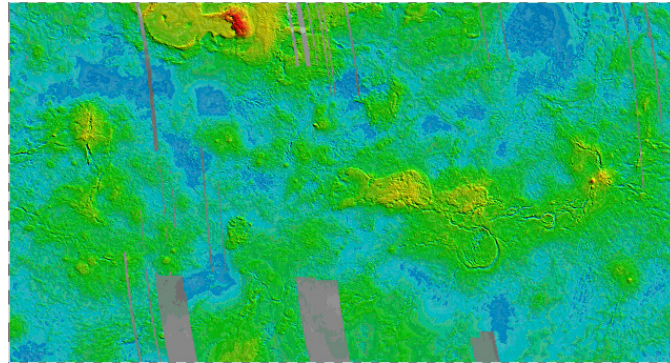


Figure 1.3: Surface of Venus as captured in altimeter topography data from the Magellan spacecraft [7]

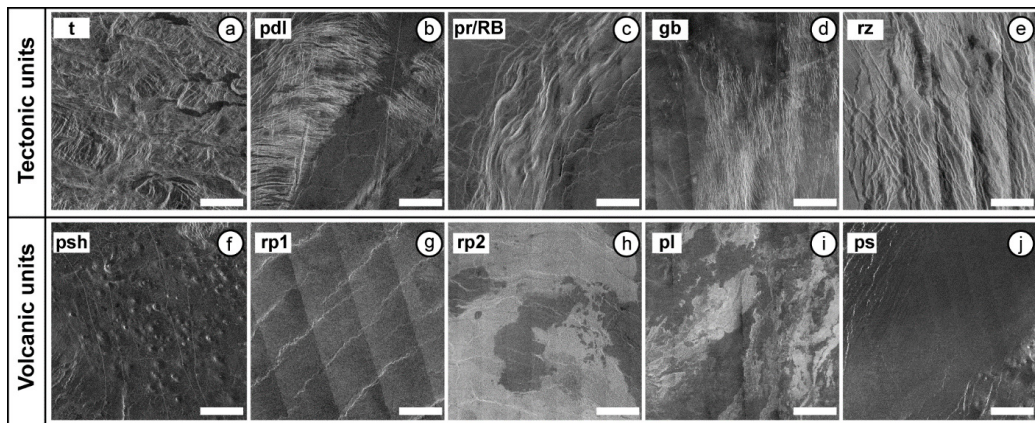


Figure 1.4: The main tectonic and volcanic units that make up the surface of Venus [8]

Lastly, the impact-related materials include the floor, walls and contiguous ejected objects of impact craters. Since there are less than 1000 craters on Venus, the surface must be estimated to be relatively young (between 300 and 700 million years) [9]). Venus's surface craters range from 3 to 280 km in diameter. There are no craters smaller than 3 km, due to the slowing action of the dense atmosphere on incoming objects: those objects that have less than a certain kinetic energy are slowed down so much by the thick and dense atmosphere that they do not generate an impact crater but they just fragment and burn up before reaching the ground [10].

### 1.2.2 Surface Geology

As we discussed in the previous section, most of Venus's surface appears to be shaped by volcanic activity. Our neighbour planet has several times as many volcanoes as Earth and it is characterized by more than 160 large volcanoes which are over 100 km across (Fig. 1.5). Only one volcanic complex of this size is present on Earth and it is the Big Island of Hawaii [11]. However, that does not mean Venus is more volcanically active than Earth, but depends on the fact that Venus's crust is older than Earth's one: in fact, the terrestrial

oceanic crust is constantly recycled by subduction at the interfaces of tectonic plates, and has an average age around 100 million years [12], while Venus’s surface is estimated to be between 300 and 700 million years.

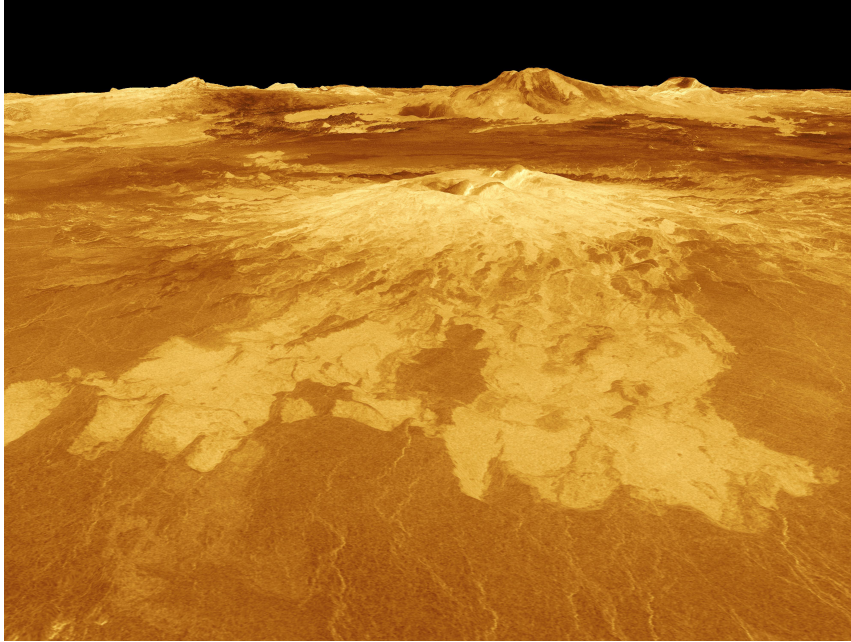


Figure 1.5: Sapas Mons Volcano, 400 km across, 1.5 km high - The simulated hues are based on color images recorded by the Soviet Venera 13 and 14 spacecraft - Image Credit: NASA/JPL

Several evidence that occurred during the years of research and missions toward Venus, suggest the presence of an ongoing volcanic activity on Venus. Spectroscopic evidence of lightning on Venus was obtained by Venera 9 orbiter [13] and the Venera 12 descent probe [14] and, later on, the ESA Venus Express spacecraft detected whistler waves confirming the occurrence of lightning on Venus [15]. An explanation is that ashes from a volcanic eruption were generating the lightning. Another piece of evidence came from measurements of the concentrations of sulfur dioxide in the atmosphere, which dropped between 1978 and 1986 by a factor of 10, jumped in 2006, and then dropped again [16]. Therefore, it may mean that levels had been boosted a lot of times by large volcanic eruptions. Lastly, in January 2020, scientists that had studied the behaviour of olivine, reported evidence that suggests that our neighbour planet is currently volcanically active [17].

### 1.2.3 Internal Structure

Without important seismic data, our knowledge on Venus’s interior is mostly theoretical and derived from Earth’s compositions: in the absence of data to characterize the density profile of Venus, the interior of the planet is commonly a rescaled model of Earth modified for Venus’s mass and radius (one-dimensional preliminary reference model (PREM) [18]). In fact, since they are similar in size and density, they could be similar in internal composition as well, presenting a core, a mantle and a crust (Fig. 1.6).

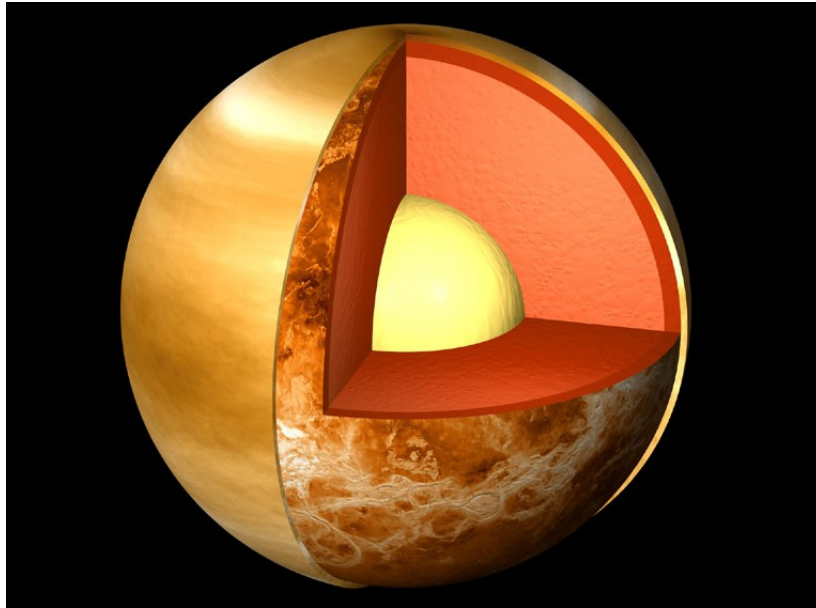


Figure 1.6: Cutaway view of possible internal structure of Venus - Courtesy of Calvin J. Hamilton

Similarly to the Earth's one, Venus's core is at least partially liquid because the two planets have been cooling at similar rate [19]. The thickness of the crust is still under debate, however, the latest theories concluded that the global crustal thickness is in the range of 12 to 65 km from a mean value of 25 km and that is consistent with the current known dynamic evolutive process of Venus [20]. A density range of  $2700\text{-}2900\text{ kg/m}^3$  (which corresponds to basaltic rocks) and the composition of the surface have been given by the various landers that reached the Venusian surface over the years [21].

Deep interior pressures of Venus are 24% lower than Earth's because of the slightly smaller size of the first one [22]. However, the principal difference between the two planets is represented by the lack of signs of plate tectonics on Venus, possibly due to the fact that its crust is too strong for subduction without water that makes it less viscous. Therefore, the planet is prevented from cooling because the heat losses are lower, and that may also be the reason why Venus lacks an internally generated magnetic field [23]. Instead, the internal heat of Venus may be lost through periodic major resurfacing events [24].

#### 1.2.4 Atmosphere and Climate

Compared to that of Earth's, the atmosphere of Venus is extremely dense: characterized by the 96.5% of carbon dioxide, the 3.5% of nitrogen and traces of other gases (including sulfur dioxide), Venus's atmosphere is 93 times heavier than the Earth's one; the pressure at its surface is equivalent to the pressure on Earth at a depth of nearly 1 km underwater; the density at the surface is  $65\text{ kg/m}^3$ , that is about 50 times the density of Earth's atmosphere at sea level. Due to the high presence of  $CO_2$ , Venus's atmosphere causes a huge greenhouse effect, which is responsible for the  $462\text{ }^\circ\text{C}$  temperature on the surface, which is, therefore, hotter than Mercury's one (maximum surface temperature of  $427\text{ }^\circ\text{C}$ ) [25] even

though the distance Sun-Mercury is half the distance Sun-Venus and thus it receives only 25% of Mercury’s solar radiation.

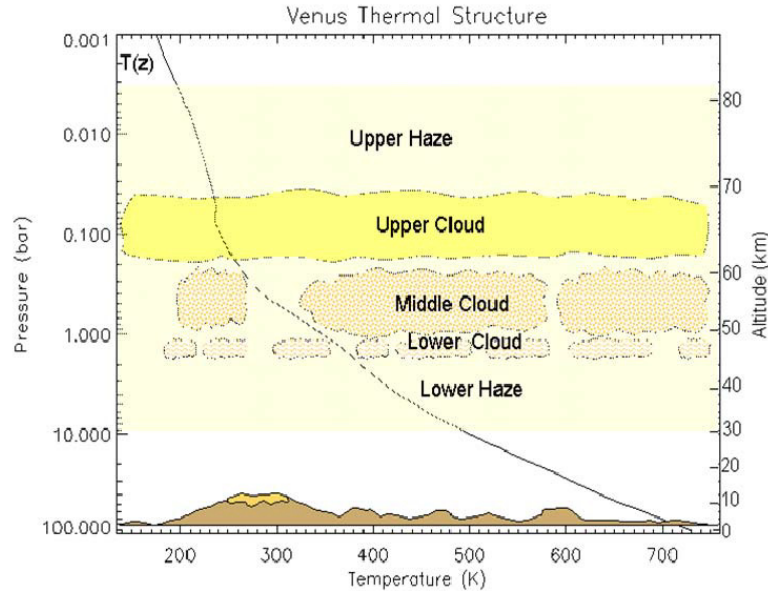


Figure 1.7: Globally Averaged Venus Atmosphere Conditions [27]

Researches about our neighbour planet have suggested that billion of years ago, its atmosphere could have been like the present-day terrestrial one and the planet could have hosted oceans of liquid water as well. However, after a period of about 600 million to few billion years, a runaway greenhouse effect was probably caused by the evaporation of that original water, which determined a critical level of greenhouse gases in its atmosphere [26] and started making the environment inhospitable. Moreover, The combination of thermal inertia and strong winds suggests that the temperature of Venus’s surface is not significantly different between the two hemispheres of the planet (those facing and not facing the Sun), even considering the slow rotation of Venus. But even if conditions on Venus’s surface are no longer hospitable for any Earth-like life, studies have suggested that in the upper cloud layers, at about 50 km of altitude, there may be the conditions for life, even if the environment is acidic, because temperature ranges between 30 °C and 80 °C.

The lower atmosphere of Venus has been poorly characterized, and represents one of the biggest mysteries about the Venusian system: since it is covered by thick and dense sulfuric clouds that make very difficult to collect detailed information, we know very little about its composition and dynamics. What is known is that altitude is one of the few factors that affect the temperature in within Venus’s lower atmosphere: the temperature transits quickly from values of 470 °C at the surface to values of 130 °C. In fact, the coolest point on Venus’s surface is also the highest one, that is Maxwell Montes, with a temperature around 380 °C. Even if it does not possess the superrotational winds of the upper clouds, the lower atmosphere is presumed to be windy and characterized by powerful convection currents caused by the great difference of temperatures at different altitudes.

The superrotational sulfuric acid clouds are part of the mid-atmosphere of Venus, which goes from 45 km to about 70 km. The sulfuric acid that makes up these clouds was probably spewed into the atmosphere from volcanic outgassing and upwelling convection currents that took place at the surface over time [28]. Additionally, ground-based observations using emission spectrum analysis of the Venusian atmosphere have shown that the clouds are absorbing a greater amount of UV radiation than sulfuric acid would theoretically do; therefore, another key chemical component may be present in the clouds and that may be  $FeCl_3$  or elemental sulfur [29]. Moreover, concentrations of water vapor have been found both in the lower and the mid atmosphere. As said before, the mid-atmosphere Venusian clouds experience superrotation: they orbit the planet in approximately 3 days at the mid-latitudes to the poles and 5 days at the equator [30]. Because of this almost constant rotational period of about 3 days in such a large continuous region, it has been suggested that near the poles the clouds may behave as a quasi-solid body with a much higher density than the lower latitudes clouds. Anyway, the average peak velocity is 80-110 m/s with oscillations due to the convective currents from the lower atmosphere [31]. These sulfuric acid clouds prevent visual observation of the Venusian surface and block and absorb most of the solar heat that reaches the planet so that the temperatures on the Venusian surface remain relatively constant. Even if Venus is nearer than Earth to the Sun, its surface receives less sunlight than our planet. The range of temperature of the mid-atmosphere of Venus goes from 110 °C in the lower part to -30 °C in the upper part.

Lastly, the upper atmosphere of Venus (which goes from about 65 km to 120 km) has relatively similar Earth-like conditions of temperatures, pressure and chemical composition, despite the harshness of the surface and the lower atmospheric layers. As the altitude increases, the atmosphere becomes thinner, with lower pressures and lower temperatures (see Fig. 1.8 and 1.9).

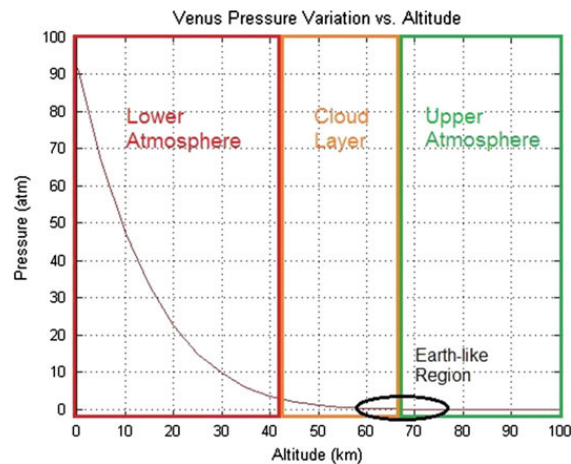


Figure 1.8: Venus's average pressure vs Altitude - Adapted from [31]

Similarly to the rest of the Venusian atmosphere, the upper layer is a  $CO_2$  based greenhouse with traces of N,  $O_2$  and CO, which are the most present components of Earth's atmosphere. However, though the conditions of this region seem to be benign for human and robotic use, strong winds are still present (80 to 100 m/s).

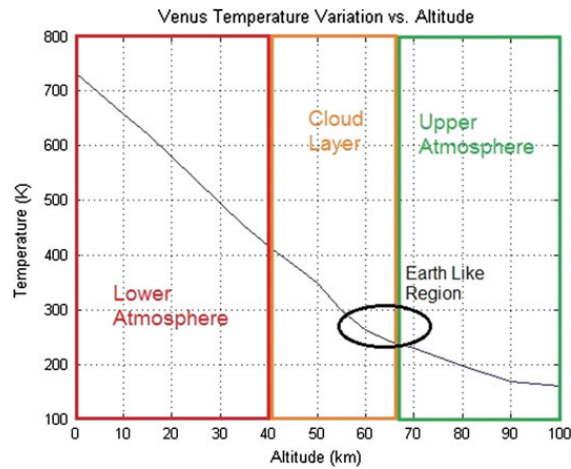


Figure 1.9: Venus’s average Temperature vs Altitude - Adapted from [31]

### 1.2.5 Magnetic Field and Core

Unlike Earth, Venus’s magnetic field is very weak. Induced by interactions between the ionosphere and the solar wind [32], it gives low protection to the atmosphere against cosmic radiations. Given the similar size to Earth, it was expected to contain a dynamo at its core, however, it was surprisingly found out the lack of an intrinsic magnetic field. In general, a dynamo requires the presence of a conducting liquid, rotation and convection, therefore, since Venus’s core is supposed to be electrically conductive and its rotation, though slow, seems to be enough to produce a dynamo, an intrinsic magnetic field is probably missing because of the lack of convection in Venus’s core [33].

Anyway, since the weak magnetosphere around Venus is caused by the interaction of the upper atmosphere with the solar wind, it is characterized by a cometary-type shape (Fig. 1.10). Here, the dissociation of neutral molecules from UV radiation creates ions of hydrogen and oxygen; then, the solar wind provides enough energy to escape Venus’s gravity to some of these ions. As a result, there is a steady loss of low-mass ions such as hydrogen, oxygen and helium ones and a retention of heavier molecules such as carbon dioxide. Therefore, this is the process that may had led the loss of most of Venus’s water over time [34].

## 1.3 Open Questions

As we have just seen from the previous sections, a reasonable knowledge about Venus and its characteristics has been created. However, a lot of key questions are still unanswered and further investigations are needed to address them and obtain more information, so we will be able to draw in detail the evolution, and maybe even the fate, of our neighbour planet.

Some of these questions include:

- What is the composition of Venus’s deep atmosphere?
- Why does the atmosphere rotate much faster than the surface of the planet?

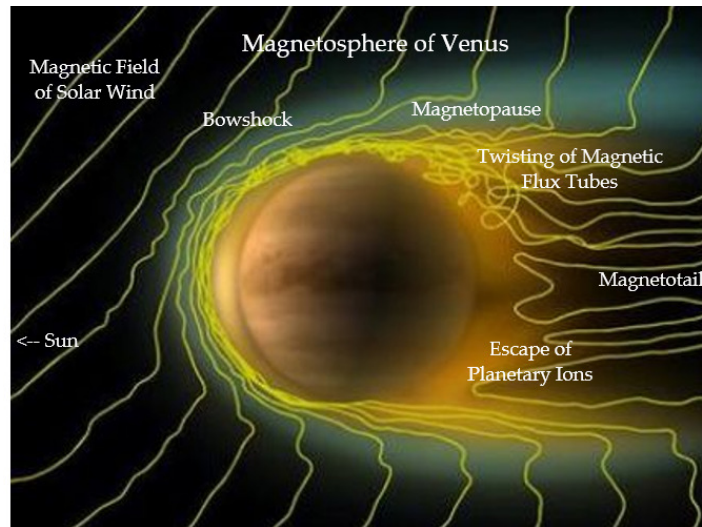


Figure 1.10: Artist's impression showing how the solar wind shapes the magnetospheres of Venus  
- Adapted from [34]

- What is the composition of the surface and the materials beneath it?
- What are the dynamics of the volcanism and the tectonism of the planet?
- What are the processes that shaped the surface of Venus?
- Is Venus really characterized by a Earth-like interior structure?
- What are the consequences of the hydrogen escape due to the interactions between ionosphere and solar wind?

## Chapter 2

# Venus Sample Return Mission

Venus is probably the most similar planet to Earth in our Solar System and represents a unique opportunity to better understand the evolutionary processes that our own planet will have to face with. However, the harsh conditions on its surface and its atmosphere make exploring Venus environment very difficult, leaving scientists with many open questions about both the past and the present of our neighbour planet. To answer these questions, further investigations and missions are needed, but manned mission to the planet have always been out of question so far, because of life-threatening reasons. Similarly, the unmanned probes that have been launched over time toward Venus, have highlighted the inadequacy of our present-day technology to face the challenges for a long life station on the Venusian soil. Moreover, even if they can operate for many years and collect a huge amount of data, orbiters around Venus are limited because of the lack of visibility through the planet's thick atmosphere. Therefore, in order to fully explore and collect more information about Venus, technological improvements must be made that allow probes to work properly in Venus's environment for more than the few hours they survived previously. That is why a Sample Return Mission can represent the best solution to obtain a much deeper understanding of Venus in the very next future: without the need to survive for long time on the hostile surface of our neighbour planet, samples of Venusian soil and atmosphere are collected and returned to Earth, where there are no limitations or challenges to face to and they can even be analyzed with high precisions instruments. And then, once we possess a deeper understanding of the Venusian phenomena and environment, we will be able to develop specific technologies that can be used for long-life *in situ* stations.

### 2.1 Advantages of Sample Return

Although we can obtain a huge amount of data about planetary objects through spectrometers, cameras and other instruments, and we can learn even more through *in situ* missions, a sample return mission provides unique opportunities not offered by either orbital or *in situ* missions in general. Returning material from the planetary body of interest, allows to study the samples in well equipped laboratories on Earth, without those constraints typical of a space mission: limited mass of the instruments, limited room inside the spacecraft,

harshness of the environment, limited time and so on. In particular, exploiting the instruments and the laboratories we have on Earth, we could determine the chemical, physical, mineralogical and structural properties of the returned material from the atomic scale up to the macroscopic level. And even if the laboratory instruments' technology readiness level was not high enough to perform specific measurements or to answer to certain questions, the samples can be preserved safely for decades and used by the future generations to solve not only those problems, but also to answer questions we have not even thought of. Moreover, the study of returned samples could verify and validate conclusions drawn by remote sensing (either Earth-based or by spacecraft) and *in situ* missions not only on the specific body of interest, but also of other different planetary objects.

However, sample return missions represent complex challenges that require very careful planning and execution. Not only they have to deal with the usual obstacles of both orbital and landing missions, but also they need to face and handle very unique hazards and to successfully perform all the operations in a limited time. A sample return mission, for example, requires the instruments to work outside pressure vessels, facing the harshness of the environment, in order to collect planetary material.

Therefore, even though a precise design of the systems, subsystems and the operations must be performed, making trade-offs between science goals and costs, between complexity of the mission and risks, the return of sample material from another planetary body can really provide valuable and unique information to increase the level of understanding of the world around us.

## 2.2 Proposed Mission Executive Summary

The sample return mission to Venus involves a complex set of equipment and maneuvers. A Falcon 9 lifter rocket is used to send the spacecraft out of the Earth's sphere of influence. A helium-pressurized bipropellant system that uses Hydrazine as the fuel and mixed oxides of nitrogen as the oxidant is used for Venus orbit insertion. It has a thrust of  $\sim 416$  N and a specific impulse of  $\sim 286$  s. Four pairs of 10 thrusters (4 primary, 4 redundant) provide trajectory and attitude control when needed. The rendezvous with Venus occurs 146 day after leaving Earth and the orbiter maneuvers into a circular Venus orbit with a radius of 300 km. Once the orbiter reaches this orbit, the aeroshell that contains the lander is detached and sent into Venus's atmosphere. The lander performs a free falling atmospheric entry before being slowed down and detached from its heat shield by a parachute which is also used to control the attitude of the probe before the last part of free falling and landing. A system of 6 grid fins is used to control and maintain the attitude of the lander before the touch down of the lander, which occurs after about 1 hour and 26 minutes of descent at a velocity of about 6 m/s. Once on the Venusian surface, the operations of atmospheric and surface sampling collection starts: a liter of atmosphere is collected from the surface, while another liter will be collected during the ascent phase; on the other hand, two drills, one telescopic and the other attached to a mechanical arm, are used to acquire about 1 kg of surface samples from the top 10 cm and distributed over at least  $10$  m<sup>2</sup>. It takes about 69 minutes to complete this operations. In the meantime, the scientific payload instruments are turned on and start collecting data and images that are sent to Earth by the antennae of the communication system (two pair of high- and low- gain antennae). Once the samples

are collected and safely placed into the proper containers, the ascent phase starts: a zero-pressure natural-shaped balloon inflated with Helium is used to lift off a two-stage ascent rocket from the lander up to an altitude of about 51 km, where the first stage ignites and performs a ballistic trajectory to maneuver the rocket to the altitude of the orbiter's Venus orbit. Here, the first stage is detached while the second stage ignites in order to insert the rocket in orbit and perform the rendezvous with the orbiter. Once the rendezvous is done and the launch window for the Venus-to-Earth interplanetary transfer is open, the orbiter performs the maneuvers to return back to Earth and insert into a Earth's orbit where the samples container can be reached or detached to collect the samples and take them on Earth.

## 2.3 Scientific Goals and Objectives

Venus has been consistently identified as high-priority target for scientific exploration by the planetary science community in the past few years. In the latest Decadal Survey (*Visions and Voyages for Planetary Science in the Decade 2013-2022*, National Research Council, 2011), Venus was addressed as an *important object of study* in all three crosscutting themes (building new worlds, planetary habitats, and workings of solar systems) [35].

Exciting Venus research has been ongoing since 1961 with a brief stanstill during the '90s: 16 probes have been launched toward Venus by Russia between 1961 and 1983, including the only probes that ever successfully landed on the surface of the planet; 10 other missions were launched by NASA between 1962 and 2004, and, during the 2000s, 3 other missions by Japan and 1 by ESA were launched toward Venus [36].

The combination of spacecraft investigations and ground based observations conducted during all these missions, have collected a lot of data about the thick, dynamic and acid atmosphere (Fig. 2.1), about the global circulation characterized by superrotation of the upper clouds (from 48 to 70 km), the complex vortices at both poles and the vast basaltic plains on the surface.



Figure 2.1: Venus in visible and ultraviolet light as seen from the Mariner 10 flyby in 1974 (Courtesy NASA)

However, the detailed dynamics and composition of the Venusian atmosphere is still unknown, and since the atmosphere is more than an impediment to analyzing or even seeing the surface, very little is known about the local geology, except for the spectacular images of the surface we got from the Venera missions (Fig. 2.2), and even less about the interactions between the surface and the atmosphere. In this context characterized by

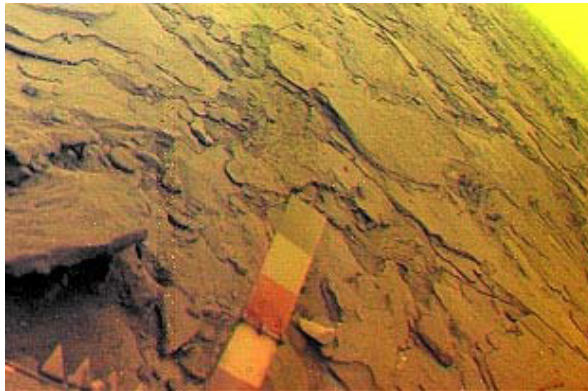


Figure 2.2: The basaltic plain of the Venera 14 landing site.

high interest and lack of knowledge about Venus, a list of scientific goals, objectives and investigations has been developed through an extended process that included meetings and workshops of the major representatives of the VEXAG community. Those are intended to address the priorities of the *Visions and Voyages* (National Research Council, 2011) Decadal Survey for 2013-2022 and to motivate future efforts.

In particular, three non-prioritized goals have been defined [35]:

- Understand Venus’s early evolution and possible habitability to constrain the evolution of Venus-sized (exo)planets.
- Understand composition and dynamics of Venus’s atmosphere.
- Understand the geologic history preserved on the Venusian surface and the present-day interactions between the surface and the atmosphere.

Each goal is supported by two objectives, which are summarized in Table 2.1.

This section describes the six objectives that support the scientific goals defined to be the reference for the future exploration missions to Venus and the investigations proposed by this thesis for each of those objectives will be described.

### 2.3.1 Goal 1: Understand Venus’s early evolution and possible habitability to constrain the evolution of Venus-sized (exo)planets

Similarly to Earth, Venus may have hosted seas and oceans of liquid water for billions of years [5]. However, during their history, the two planets may have followed different evolutionary pathways. That is why, since at the beginning they may have been so similar

Goal	Objective
1. Understand Venus’s early evolution and possible habitability to constrain the evolution of Venus-sized (exo)planets	A. Did Venus have temperate surface conditions and liquid water at early times?
	B. How does Venus elucidate possible pathways for planetary evolution in general?
2. Understand composition and dynamics of Venus’s atmosphere	A. What processes drive the global atmospheric dynamics of Venus?
	B. What processes determine the baseline and variations in Venus atmospheric composition and global and local radiative balance?
3. Understand the geologic history preserved on the Venusian surface and the present-day interactions between the surface and the atmosphere	A. What geologic processes have shaped the surface of Venus?
	B. How do the atmosphere and surface of Venus interact?

Table 2.1: VEXAG Goals and Objectives of Venus’s future exploration

and yet evolved to become so different, Venus represents the planet that most likely can show whether a Venus-sized exoplanet can sustain habitability and how planetary evolution can be changed by climate and environment more than any other.

**Objective 1A: Did Venus have temperate surface conditions and liquid water at early times?**

The amount of water that Venus received during its formation and history is still unknown. Standard models suggest that Earth and Venus received comparable amount of water, mostly from comets and bodies that had been formed in the vicinity of Jupiter [37]. Therefore, understanding whether once there were temperature surface conditions would represent a crucial information to define Venus evolutionary path and the habitability not only of ancient Venus, but also of Venus-sized exoplanets at present day, helping to improve our knowledge about the conditions that can sustain life on other planets.

**Objective 1B: How does Venus elucidate possible pathways for planetary evolution in general?**

Depicting an overall picture of Venus formation and evolution processes can not only tell how the potentially habitable systems are, but also how the planetary architecture (distance from the main star of the system, type of orbit, presence of other bodies in the system) can impact on the potential habitability of a planet. High number of examples of Venus-sized planets are being discovered all over the universe [38] and improving the information about the potential habitability on Venus can help to better select those to study for a deeper understanding of the systems that can host life.

### **2.3.2 Goal 2: Understand composition and dynamics of Venus’s atmosphere**

Additional detailed studies about the Venusian atmosphere can improve our understanding about climate change on Earth. Venus represents an extreme case of global warming, apparently very far from the Earth situation, however, understanding the composition and the dynamics of its atmosphere can help to learn more about climate change phenomena that are still poorly explained in the Earth’s climate system.

#### **Objective 2A: What processes drive the global atmospheric dynamics of Venus?**

A lot of fundamental atmospheric characteristics of Venus are still poorly understood: the clouds superrotation, the atmospheric thermal structure, the clouds composition and so on. Understanding such phenomena will be a milestone advance for the atmospheric sciences in general, and will provide tests of different behaviour in models of exoplanetary atmospheres.

#### **Objective 2B: What processes determine the baseline and variations in Venus atmospheric composition and global and local radiative balance?**

The Venusian atmosphere is a dynamical system and significant questions about the chemical, radiative and physical interactions of its constituents remain unsolved. All the information about the composition of Venus’s atmosphere are crucial not only to understand the dynamics and the evolution of the overall system, but also to be aware about any risks or constraints for future exploration missions to Venus.

### **2.3.3 Goal 3: Understand the geologic history preserved on the Venusian surface and the present-day interactions between the surface and the atmosphere**

Despite the detailed view of the Venusian surface provided by the Magellan and Venera data, there is still a lot of missing information related to its topography, geochemistry and mineralogy. In order to unveil the past of the Venusian history and understand the present of the planet, it is necessary to solve those many first-order questions that regard the geological formation and dynamics of Venus. With those data we will be able to constrain the history of volatiles, specially water, and provide a basis for comparisons of surface evolution on Earth and Mars.

#### **Objective 3A: What geologic processes have shaped the surface of Venus?**

Understanding the stratigraphic history of the geological events that shaped and still deform Venus’s surface, is crucial not only to characterize the evolution of the planet itself, but also to facilitate comparisons with other terrestrial planets. Moreover, the history of tectonic and volcanic activities, which are driven by processes in the Venus’s interior, is

useful to understand the coupling interactions between the surface and the atmosphere over the planet's history.

**Objective 3B: How do the atmosphere and surface of Venus interact?**

Near Venus's surface there are temperatures of about 470 °C and pressures of about 90 bars. Those conditions assure geologically rapid chemical reactions and available data apparently indicate that the composition of the deep atmosphere is not compatible with chemical equilibrium. However, significant uncertainties remain in the dynamics of the reactions that occur at the surface-atmosphere interface. An improved understanding of those interactions would give clues useful to constrain the outgassing history, the role of current and past volcanic activity and in general the evolution of both the atmospheric and surface systems over the years.

## 2.4 Mission Requirements

In order to accomplish the scientific goals and objectives seen in the previous section, a list of mission requirements has been detailed by Jet Propulsion Laboratory (NASA) and it is here reported:

- Return to Earth or Earth vicinity at least one kg of Venus regolith from top 10 cm.
- Return to Earth or Earth vicinity at least ten distinct samples distributed over at least 10  $m^2$ .
- Return to Earth or Earth vicinity samples distributed from the top 10 cm.
- Accommodate at least 50 kg of science payload to the surface of Venus that can return data for at least one Earth day, not related to the sample return science.
- Return to Earth or Earth vicinity at least one cubic liter of Venus atmosphere from the surface.
- Return to Earth or Earth vicinity at least one cubic liter of Venus atmosphere from an altitude of 40 km above the surface.

The goal of this thesis is to describe a preliminary design of a space mission to Venus that could accomplish the requirements just listed.



# Chapter 3

## Mission Main Phases

The following chapter gives an overview of the main phases and operations of the mission, with details for the calculations and the instruments used to define and characterize them.

### 3.1 Launch

Selecting a launch vehicle is always a crucial decision for any space mission and, since nowadays there is a wide choice of launchers, is not even an easy choice. A lot of countries has already developed launch vehicle in the past and are steadily advancing with their development, whereas more and more others are starting to design and build their own launcher with the hope of possessing one in the future and use it for business reasons. United States and Russia are by far the leaders of the field, however, countries such as China, are increasing their knowledge faster and faster and they might insert soon into the space launch vehicles market. This increasing offer of space launchers is justified by the increasing demand of sending payload into space by international customers and academic institution.

Due to the high variety of space missions that can be designed, every launch vehicle is very different from all the others. Therefore, the main criteria used to choose the proper launcher for a space mission are: cost, maximum payload mass and volume allowed, reliability, performance and availability. That is why, even if a country possesses a space launcher, it may choose the launcher of another country if it is cheaper than the one of its own. Moreover, more and more private companies, such as SpaceX and Stratolaunch are starting making their way into the space launchers market, so the availability of launch vehicles does not increase only thanks to national providers.

In this scenario of wide opportunities and choices, a list of possible launch vehicle for this mission has been developed and is reported below (Tab. 3.1):

In order to make the right choice, some criteria, such as price, maximum payload mass and volume available and reliability, have been used to evaluate all the launch vehicles reported in Table 3.1. As a result, the SpaceX Falcon 9 has been chosen for this mission, whose payload fairing is shown in Fig. 3.1.

Company	Launch Vehicle	Price	Max Payload to Low Earth Orbit [kg]	Max Payload to Geosynchronous Orbit [kg]
SpaceX	Falcon 9	\$ 62 M	22800	8300
	Falcon Heavy	\$ 90 M	63800	26700
	ATLAS 401	\$ 109 M	9797	4750
	ATLAS 401	\$ 109 M	9797	4750
	ATLAS 411	\$ 115 M	12150	5950
	ATLAS 431	\$ 130 M	15718	7700
United Launch Alliance (ULA)	ATLAS 501	\$ 120 M	8123	3775
	ATLAS 521	\$ 135 M	13490	6475
	ATLAS 541	\$ 145 M	17443	8290
	ATLAS 551	\$ 153 M	18814	8900
	DELTA IV M+ (5,2)	\$ 150 M	11060	5080
	DELTA IV M+ (5,4)	\$ 160 M	13730	6890
	Vulcan Centaur	In progress	17800	7400

Table 3.1: Launch Vehicles List

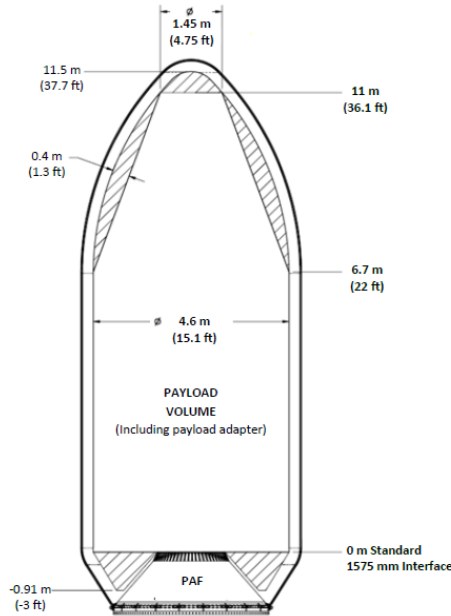


Figure 3.1: SpaceX Falcon fairing - Adopted from Ref. [39]

## 3.2 Interplanetary Travel

The method of patched conics is used to develop preliminary calculations about the spacecraft’s trajectory during the interplanetary travel from Earth to Venus. This method involves dividing the journey into three parts: the departure along a hyperbolic trajectory and relative to the Earth, the cruise ellipse relative to the Sun and the arrival hyperbolic trajectory relative to Venus. The use of this method is justified by calculating the radius of each planet’s sphere of influence and showing how small it is on the scale of the solar system.

Without derivation, the average dimension of the *SOI* of a planet can be computed

with the following equation [40]:

$$r_{SOI} = r_{planet} \left( \frac{m_{planet}}{m_{sun}} \right)^{0.4} \quad (3.1)$$

where  $r_{planet}$  is the distance between the particular planet and the Sun (not to be confused with the radius of the former), and  $m_{planet}$  and  $m_{sun}$  are the masses of the planet and the Sun, respectively. The resulting dimensions of the *SOI*'s for the planets in our Solar System are summarized in Table 3.2. It is clear that the size of any *SOI* is marginal

Planet	Sphere of Influence	
	[AU]	[% of average distance from Sun]
Mercury	0.008	0.2
Venus	0.004	0.6
Earth	0.006	0.6
Mars	0.004	0.3
Jupiter	0.322	6.2
Saturn	0.365	3.8
Uranus	0.346	1.8
Neptune	0.579	1.9
Pluto	0.021	0.1

Table 3.2: Dimensions of the *SOI* of the planets in our Solar System

compared to the size of our Solar System. Therefore, we can consider the heliocentric part of the transfer to (effectively) take place between the exact positions of the departure and target planets and the planetocentric part to take place on a local scale within the *SOI*. In particular, the  $\Delta V$  requirements are calculated matching the velocity of the spacecraft at the departure and arrival planet's sphere of influence with the one required to start the elliptical cruise phase and the one required to be captured by the target planet at the end of the cruise, respectively.

### 3.2.1 Interplanetary Hohmann Transfer

As can be seen from Table 3.3, the orbit of Venus lies very close to the Earth's orbital plane (the ecliptic plane) and both of the planets have small eccentricities as well. Therefore, we will assume that those orbits are both circular and coplanar, in order to simplify the beginning of our study of the interplanetary trajectory.

Planet	Orbit eccentricity	Inclination of orbit to the ecliptic plane
Venus	0.0067	3.39°
Earth	0.0167	0.00°

Table 3.3: Eccentricity and Inclination to the ecliptic plane



	Parameter	Expression	Calculations
$V_{dep}$	Heliocentric velocity of departure planet	$V_{dep} = \sqrt{\frac{\mu_S}{r_{dep}}}$	29.784 <i>km/s</i>
$V_{tar}$	Heliocentric velocity of target planet	$V_{tar} = \sqrt{\frac{\mu_S}{r_{tar}}}$	35.022 <i>km/s</i>
$V_{C0}$	Circular velocity around departure planet	$V_{C0} = \sqrt{\frac{\mu_{dep}}{r_0}}$	7.784 <i>km/s</i>
$V_{C3}$	Circular velocity around target planet	$V_{C3} = \sqrt{\frac{\mu_{tar}}{r_3}}$	7.152 <i>km/s</i>
$a_{tr}$	Semimajor axis of transfer orbit	$a_{tr} = \frac{r_{dep} + r_{tar}}{2}$	$1.29 \cdot 10^8$ <i>km</i>
$e_{tr}$	Eccentricity of transfer orbit	$e_{tr} = \frac{ r_{dep} - r_{tar} }{r_{dep} + r_{tar}}$	0.1606
$V_1$	Heliocentric velocity at departure position	$V_1 = \sqrt{\mu_S \left( \frac{2}{r_{dep}} - \frac{1}{a_{tr}} \right)}$	27.288 <i>km/s</i>
$V_2$	Heliocentric velocity at target position	$V_2 = \sqrt{\mu_S \left( \frac{2}{r_{tar}} - \frac{1}{a_{tr}} \right)}$	37.729 <i>km/s</i>
$V_{\infty,1}$	Excess Velocity at departure planet	$V_{\infty,1} =  V_1 - V_{dep} $	2.496 <i>km/s</i>
$V_{\infty,2}$	Excess Velocity at target planet	$V_{\infty,2} =  V_2 - V_{tar} $	2.707 <i>km/s</i>
$V_0$	Velocity at pericenter of hyperbola around departure planet	$V_0 = \sqrt{\frac{2\mu_{dep}}{r_0} + V_{\infty,1}^2}$	11.29 <i>km/s</i>
$V_3$	Velocity at pericenter of hyperbola around target planet	$V_3 = \sqrt{\frac{2\mu_{tar}}{r_3} + V_{\infty,2}^2}$	10.47 <i>km/s</i>
$\Delta V_0$	Maneuver at pericenter around departure planet	$\Delta V_0 =  V_0 - V_{C0} $	3.504 <i>km/s</i>
$\Delta V_3$	Maneuver at pericenter around target planet	$\Delta V_3 =  V_3 - V_{C3} $	3.318 <i>km/s</i>
$\Delta V_{Tot}$	<b>Total velocity change</b>	$\Delta V_{Tot} = \Delta V_0 + \Delta V_3$	<b>6.822 <i>km/s</i></b>
$T_{tr}$	<b>Transfer time</b>	$T_{tr} = \pi \sqrt{\frac{a_{tr}^3}{\mu_S}}$	<b>146.07 <i>days</i></b>

Table 3.4: Calculation of the interplanetary Hohmann transfer's characteristics

As can be seen from Table 3.6, the velocity at the periapsis of an elliptical orbit is higher than the velocity of a circular orbit with the radius equal to that periapsis radius. Therefore, elliptical departure and target orbits are suggested in order to save money and fuel. However, this work will still consider circular departure and arrival orbit and will leave the study of more optimized orbits to future researches.

### 3.2.2 Timing

The geometry of the problem is sketched in Figure 3.3 for the case in which we perform a trip to an inner planet and back, in this analysis, an Earth-Venus-Earth trip. During the time of the mission, the Earth is assumed to cover an angle  $\Delta\nu_E$ , whereas the

Parameter	Value	
$\mu_S = \mu_{Sun}$	$1.32712 \cdot 10^{11}$	$km^3/s^2$
$\mu_{dep} = \mu_{Earth}$	398600	$km^3/s^2$
$\mu_{tar} = \mu_{Venus}$	324859	$km^3/s^2$
$r_{Earth}$	6378.1	$km$
$r_{Venus}$	6051.8	$km$
$r_{dep} = r_{Earth\ Orbit}$	$1.496 \cdot 10^8$	$km$
$r_{tar} = r_{Venus\ Orbit}$	$1.082 \cdot 10^8$	$km$
<b><math>h_0</math></b>	<b>200</b>	<b><math>km</math></b>
<b><math>h_3</math></b>	<b>300</b>	<b><math>km</math></b>
$r_0$	6578	$km$
$r_3$	6351.8	$km$

Table 3.5: Data used for Hohmann calculations

	Periapsis altitude	200	$km$
	Apoapsis altitude	1000	$km$
Earth	Circular velocity at periapsis	7.784	$km/s$
	Velocity at periapsis of hyperbola	11.29	$km/s$
	Elliptical velocity at periapsis	8.004	$km/s$
	Maneuver at periapsis	3.284	$km/s$
	Periapsis altitude	300	$km$
	Apoapsis altitude	2000	$km$
Venus	Circular velocity at periapsis	7.152	$km/s$
	Velocity at periapsis of hyperbola	10.47	$km/s$
	Elliptical velocity at periapsis	7.562	$km/s$
	Maneuver at periapsis	2.908	$km/s$
	<b>Total velocity change</b>	6.192	$km/s$

Table 3.6: Calculation of the  $\Delta V$  using elliptical departure and target orbit

spacecraft covers an angle  $\Delta\nu_{spc}$ . In order to rendezvous at the Earth again at the end of the mission, the relation between the two angles must be the following:

$$\Delta\nu_E = \Delta\nu_{spc} + 2\pi W \quad (3.2)$$

where  $W$  is an integer number (which can be positive or negative). Without derivation, the fastest round trip to Venus following a dual-Hohmann transfer is achieved when  $W = -1$  (the case  $W = 0$  would require departure from Venus before even having arrived there). In addition, the total transfer time  $T$  can be expressed as the summation of two Hohmann transfer times  $T_H$  plus a stay time at the target planet  $T_S$ :

$$T = 2T_H + T_S \quad (3.3)$$

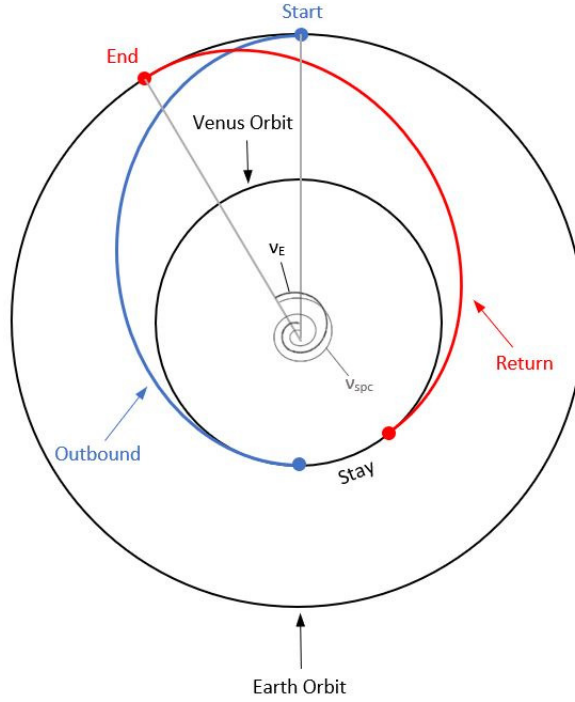


Figure 3.3: Geometry sketch

If the angular velocities of the Earth and Venus around the Sun are expressed as  $\omega_E$  and  $\omega_V$ , respectively, one can express the total angle  $\Delta\nu_E$  covered by the Earth as:

$$\begin{aligned}\Delta\nu_E &= \omega_E T = \Delta\nu_{spc} + 2\pi W \\ &= \pi + \omega_V T_S + \pi + 2\pi W\end{aligned}$$

(Any Hohmann transfer covers an angle of  $\pi$  radians;  $\omega_E$  and  $\omega_V$  are constant since we assume circular orbits).

By solving these equations, we get a solution for the total trip time  $T$  and the stay time  $T_S$ :

$$T = \frac{(W + 1)2\pi - 2\omega_V T_H}{\omega_E - \omega_V} \quad (3.4)$$

$$T_S = T - 2T_H = \frac{(W + 1)2\pi - 2\omega_E T_H}{\omega_E - \omega_V} \quad (3.5)$$

Obviously, the stay time has to be a positive number, so this condition defines the possible values for the parameter  $W$ . Clearly, the fastest round trip can be achieved when  $W$  is chosen such that the stay time is smallest. Table 3.7 gives the numerical values for a round trip from Earth to Venus.

Target	Angular motion [rad/s]	Hohmann transfer time [years]	Stay time [years]	Total trip time [years]
Venus	$3.236 \cdot 10^{-7}$	0.4002	1.279	2.078

Table 3.7: Hohmann round trip timing

### 3.2.3 Launch Windows

An interplanetary travel requires the spacecraft not only to intercept the target planet's orbit, but also to rendezvous with it when it does it. Therefore, the location of the target planet when the spacecraft leaves the departure planet's orbit must be such that the target planet arrives at the apse line of the elliptical transfer trajectory at the same time the spacecraft does.

Let's consider planet 1 and planet 2 inserted in circular orbits around the Sun, as shown in Figure 3.4.

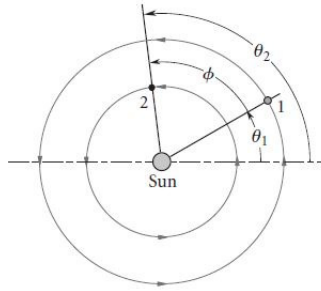


Figure 3.4: Planets in circular orbit around the Sun - Fig. 8.3 in Ref. [40]

We can choose a common apse line from which to measure the true anomaly  $\theta$ . Then, the true anomalies of planets 1 and 2, respectively, are

$$\theta_1 = \theta_{1_0} + n_1 t \quad (3.6)$$

$$\theta_2 = \theta_{2_0} + n_2 t \quad (3.7)$$

where  $n_1$  and  $n_2$  are the mean motions (angular velocities) of the planets and  $\theta_{1_0}$  and  $\theta_{2_0}$  are their true anomalies at time  $t = 0$ . Then, we can define the phase angle between the position vectors of the two planets as

$$\phi = \theta - \theta_1 \quad (3.8)$$

$\phi$  is the angular position of planet 2 relative to planet 1. Substituting Equations 3.6 and 3.7 into 3.8 we get

$$\phi = \phi_0 + (n_2 - n_1)t \quad (3.9)$$

$\phi_0$  is the phase angle at time zero;  $n_2 - n_1$  is the orbital angular velocity of planet 2 relative to planet 1: if the orbit of planet 2 lies inside that of planet 1, as in our case, then

$n_2 > n_1$ . Thus, the relative angular velocity  $n_2 - n_1$  is positive and the relative motion is counterclockwise.

Logically, the phase angle changes with time according to Equation 3.9. The time required for the phase angle to return to its initial value is called the synodic period (denoted as  $T_{syn}$ ), corresponding to a rotation of  $2\pi$  radians of the position vector of planet 2 with respect to planet 1. For our case (shown in Figure 3.4) in which the relative motion is counterclockwise,  $T_{syn}$  is the time required for  $\phi$  to change from  $\phi_0$  to  $\phi_0 - 2\pi$ .

From Equation 3.9 we have:

$$\phi_0 - 2\pi = \phi_0 + (n_2 - n_1)T_{syn}$$

so that

$$T_{syn} = \frac{2\pi}{|n_2 - n_1|} \tag{3.10}$$

Considering

$$n_1 = \frac{2\pi}{T_1} \quad n_2 = \frac{2\pi}{T_2}$$

Thus, in term of the orbital periods of the two planets,

$$T_{syn} = \frac{T_1 T_2}{|T_1 - T_2|} \tag{3.11}$$

Observe that  $T_{syn}$  is the orbital period of planet 2 relative to planet 1.

Obviously, in our case, planet 1 is represented by the Earth and planet 2 by Venus. So, following the equations just seen, we can compute

Synodic period [years]	Angular velocity difference [°/years]
1,5987	225,189

Table 3.8: Synodic period and Angular velocity difference

In order to calculate the launch opportunities, we refer to the positions of both Earth and Venus at January 1st 2000 12:00:00.000 UTC (J2000) in Table 3.9:

	Mean Longitude at J2000 [°]
Venus	100.464
Earth	181.979

Table 3.9: Mean longitude at J2000

Therefore, the angular difference between the two planets at J2000 is  $81.515^\circ$ .

Moreover, knowing Venus’s angular velocity and the duration of the Hohmann transfer, we can easily calculate the angle described by Venus during the Hohmann transfer, which is

234.187° and the angle between Earth and Venus needed at the departure time, -54.187°. With these values we can calculate the first launch opportunity before J2000:

$$\text{Leave date} = 2000 + \frac{(-54.187 - 81.515)}{225.189} = 1999,397$$

Therefore, knowing the value of the synodic period of Venus with respect to the Earth, we can calculate all the other launch opportunities (in Table 3.10 are reported only the dates after 2020). Similarly, adding the value of the duration of the Hohmann transfer to each leave date, we can obtain the related arrival date on Venus.

LEAVE FROM EARTH				ARRIVAL ON VENUS			
Leave Date	Day-Month	Year	Time	Arrival Date	Day-Month	Year	Time
2020.180	5-Mar	2020	17:21	2020.580	29-Jul	2020	21:26
2021.779	10-Oct	2021	9:12	2022.178	5-Mar	2022	7:16
2023.377	16-May	2023	19:02	2023.777	9-Oct	2023	23:06
2024.976	21-Dec	2024	10:52	2025.376	16-May	2025	8:57
2026.575	27-Jul	2026	20:43	2026.975	21-Dec	2026	12:47
2028.173	3-Mar	2028	6:33	2028.573	27-Jul	2028	10:37
2029.772	7-Oct	2029	22:23	2030.172	2-Mar	2030	20:27
2031.371	14-May	2031	8:14	2031.771	7-Oct	2031	12:18
2032.969	19-Dec	2032	00:04	2033.369	13-May	2033	22:08
<b>2034.568</b>	<b>25-Jul</b>	<b>2034</b>	<b>9:54</b>	<b>2034.968</b>	<b>18-Dec</b>	<b>2034</b>	<b>13:58</b>
2036.166	29-Feb	2036	19:44	2036.566	24-Jul	2036	23:49
2037.765	5-Oct	2037	11:35	2038.165	29-Feb	2038	9:39
2039.364	11-May	2039	21:25	2039.764	5-Oct	2039	1:29
2040.962	16-Dec	2040	13:15	2041.362	11-May	2041	11:20

Table 3.10: Launch windows

The time reference in Table 3.10 is UTC.

The date highlighted in bold is the one chosen for our analysis.

### 3.2.4 Planetary Departure

Generally, a space vehicle is inserted into an interplanetary trajectory from a circular parking orbit. The radius of this parking orbit equals the periaipse radius  $r_p$  of the departure hyperbola.

From the orbit formula (with  $e > 1$ )

$$r = \frac{h^2}{\mu} \frac{1}{1 + e \cos \theta} \quad (3.12)$$

we can clearly observe that the denominator goes to zero when  $\cos \theta = -1/e$ . We denote this value of true anomaly as

$$\theta_\infty = \cos^{-1}(-1/e) \quad (3.13)$$

From the geometry of the hyperbola, shown in Picture 3.5, we define the Turn Angle  $\delta$  as the angle between the two asymptotes. This is the angle that denotes the rotation of the velocity vector in order to follow the hyperbolic trajectory.

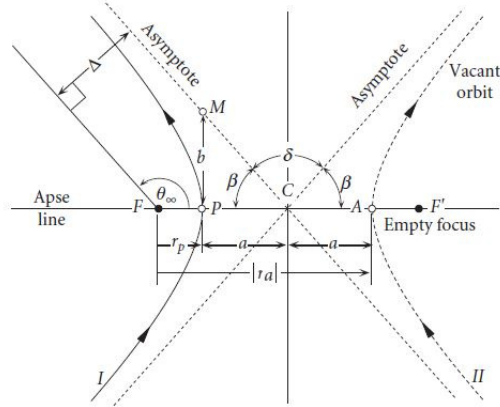


Figure 3.5: Geometry of a hyperbolic orbit sketch

Therefore, we can write

$$\begin{aligned}\frac{\delta}{2} &= \frac{180^\circ - 2\beta}{2} \\ \sin\left(\frac{\delta}{2}\right) &= \sin\left(\frac{180^\circ - 2\beta}{2}\right) \\ \sin\left(\frac{\delta}{2}\right) &= \sin(90^\circ - \beta) \\ \sin\left(\frac{\delta}{2}\right) &= \cos(\beta)\end{aligned}$$

And we can relate  $\beta$  to  $\theta_\infty$  as it follows:

$$\begin{aligned}\beta &= 180^\circ - \theta_\infty \\ \cos(\beta) &= -\cos(\theta_\infty) \\ \beta &= \cos^{-1}(1/e)\end{aligned}$$

Therefore, we obtain

$$\sin\left(\frac{\delta}{2}\right) = \frac{1}{e}$$

and finally

$$\delta = 2\sin^{-1}(1/e) \quad (3.14)$$

Therefore we need to determine the eccentricity of the hyperbola in order to evaluate the turning angle  $\delta/2$ . So, we can write

$$\xi = \frac{V^2}{2} - \frac{\mu}{r} = -\frac{\mu}{2a}$$

As for a hyperbola,  $r$  goes to  $\infty$ , therefore we will have

$$\frac{V_\infty^2}{2} - \frac{\mu}{r_\infty} = -\frac{\mu}{2a}$$

$$a = -\frac{2\mu}{2V_\infty^2} = -\frac{\mu}{V_\infty^2}$$

where

$$r_p = a(1 - e)$$

and, computing  $e$ , and substituting the expression for  $a$ , we will obtain

$$e = 1 - \frac{r_p}{a} = 1 + \frac{r_p V_\infty^2}{\mu}$$

We are able now to compute the main characteristics of the escape hyperbolic trajectory from Earth (the results are reported in Table 3.11).

Hyperbola - Departure Planet (Earth)	
Radius periapse $r_p$ [km]	6578
Semimajor axis $a$ [km]	-63973.64
Eccentricity $e$	1.1028
Turn angle $\delta$ [°]	130.12

Table 3.11: Hyperbola calculations - Earth

### 3.2.5 Arrival at Venus

Since our spacecraft travels from an outer planet to an inner one, its heliocentric approach velocity is greater in magnitude than that of Venus ( $V_2 > V_{tar}$ , as seen in Table 3.4) and the spacecraft must cross the *rear* portion of the sphere of influence, as shown in Figure 3.6.

Depending on the goal of the mission, the aiming radius of the approach hyperbola assumes different values: if the purpose is to impact the target planet, then the aiming radius  $\Delta$  must be such that the hyperbolic periapse  $r_p$  is equal to the radius of the planet. On the other hand, if the goal is to insert the spacecraft in orbit, then  $\Delta$  depends on the altitude of the target orbit. Lastly, if the goal is not to impact the planet nor to be inserted into orbit, then the spacecraft will simply go along a flyby trajectory, exiting the planet's *SOI* with the same relative speed  $V_\infty$  it entered, but with the velocity direction rotated through the turn angle  $\delta$ , given by Equation 3.14.

Without derivation, we can calculate the value of the aiming radius as it follows:

$$\Delta = r_p \sqrt{1 + \frac{2\mu}{r_p V_\infty^2}} \quad (3.15)$$

where  $\mu = \mu_{tar}$  and  $V_\infty = V_{\infty,2}$  (see Tables 3.4-3.5).

Similarly to the departure from Earth, we are now able to calculate the main characteristics of the capture hyperbolic trajectory.

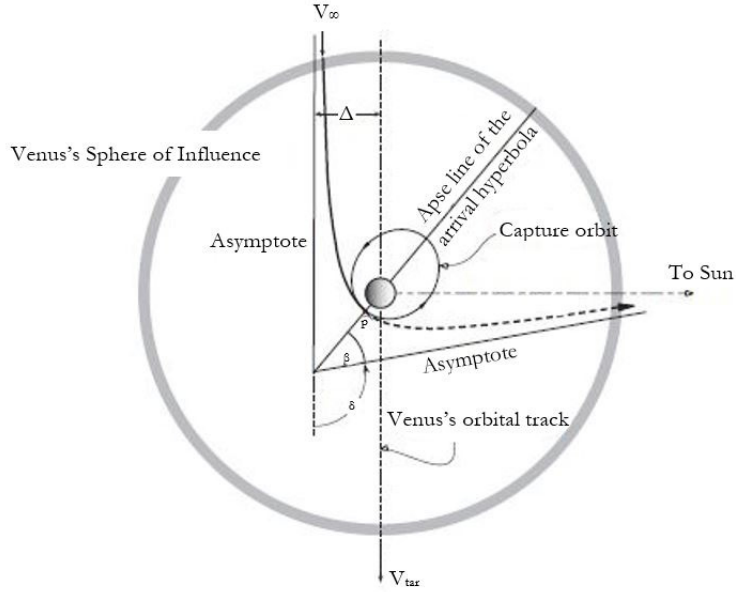


Figure 3.6: Arrival at Venus Sketch - Adopted from Figure 8.14 in Ref. [40]

Hyperbola - Arrival Planet (Venus)	
Radius periapse $r_p$ [km]	6351.8
Semimajor axis $a$ [km]	-44317.67
Eccentricity $e$	1.14
Aiming radius $\Delta$ [km]	24563.0
Turn angle $\delta$ [°]	122.0

Table 3.12: Hyperbola calculations - Venus

### 3.2.6 Implementation on STK

As we have seen in the previous sections, the Hohmann transfer, used to develop the preliminary calculations of the spacecraft trajectory from Earth to Venus, is very useful to obtain first results though is a bit inaccurate because of the assumptions made about the orbits involved. Therefore, in order to get more accurate results, STK has been used: inserting the results of the Hohmann transfer as first guesses inputs, the software calculates the trajectory without the assumptions previously made. Moreover, further analysis has been developed, performing an optimization of the maneuvers in terms of  $\Delta V$ . The final results are reported in Table 3.13 and sketched in Figure 3.7.

## 3.3 Descent and Landing

Once the spacecraft has reached the target orbit around Venus, it starts getting ready for the descent and landing phase. However, before going into details of those phases, it

Launch Date	25 July 2034 @ 9:54 AM UTCG
Arrival Date	18 December 2034 @ 1:58 PM UTCG
Trip Time	146 days
Total $\Delta V$ Required [km/s]	6.982

Table 3.13: Interplanetary transfer results obtained using STK

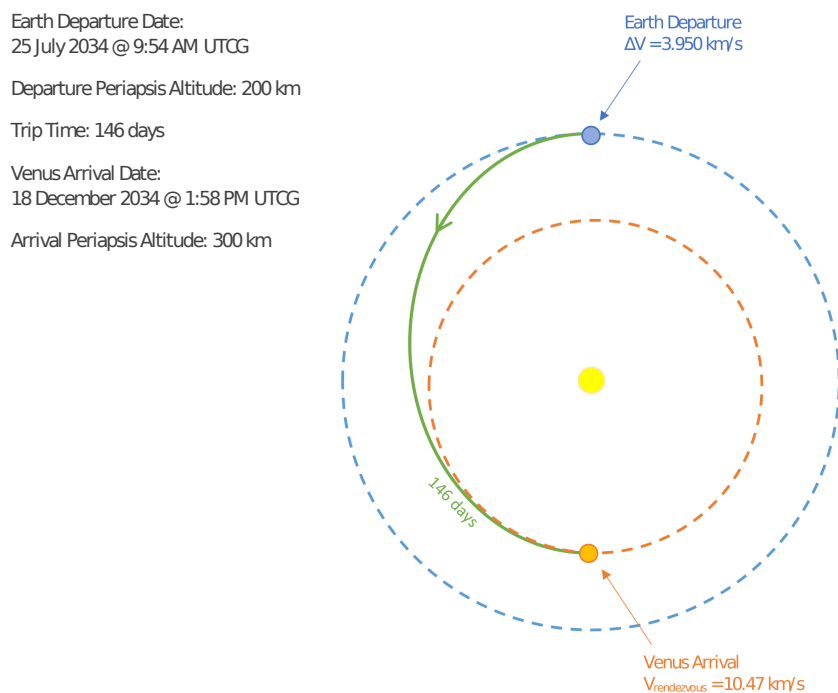


Figure 3.7: Interplanetary Trajectory Transfer to Venus Sketch

is important to understand how the landing site area has been identified. In fact, it is naturally crucial, before landing or descending into a planet's atmosphere, to know where the spacecraft should go in order to avoid unsafe sites or low scientific interests area.

### 3.3.1 Landing Site Selection

In order to choose the proper landing site on the Venusian surface, a list of requirements has been defined:

- Safety of the specific terrain

This is obviously the most important requirement for the selection of the landing site. Basing on past measurements and previous missions investigations, the potentially unsafe areas have been isolated.

As mentioned in Section 1.2.1, the Venusian surface is composed of a small number of terrain types: tectonized terrains, volcanic terrains and impact related terrain.

Each of them can then be divided into other subtypes (e.g. tectonized terrain - Tessera, volcanic terrain - Shield Plains)[34]. Among all these types and subtypes of terrains, the ones characterized by either obviously or potential enhanced roughness of the surface have been discarded, while the others have been selected for the next requirement analysis (Fig. 3.8).

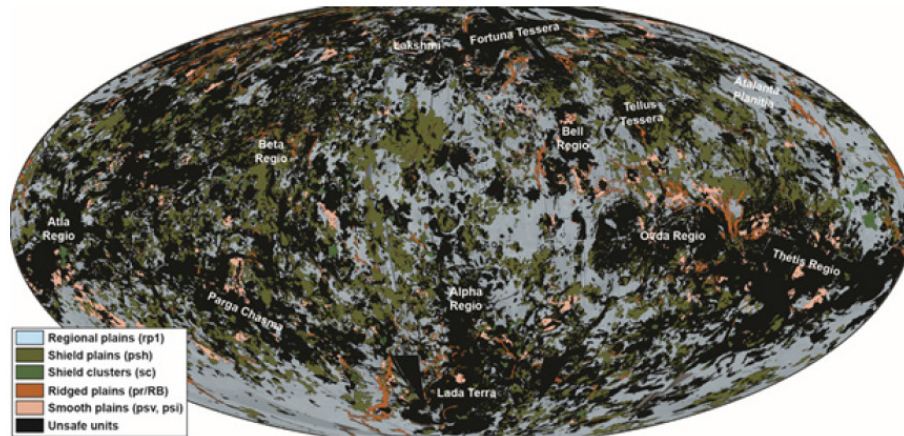


Figure 3.8: Geological Map of Venus - Unsafe units shown in black - Adopted from [34]

- Scientific interest level of the materials at the landing site  
The science interest level is based on the representativeness of the specific terrain that should address the scientific goals and objectives seen in Section 2.3. For example, units that overall occupy a small portion of the whole Venusian surface, are not useful to understand global dynamics or the composition of the planet and are, then, listed as low scientific priority units. Following this and similar criteria, the high interest priority units have been selected for the next requirement analysis (Fig. 3.9): shield plains (volcanic terrain), regional plains (volcanic terrain), smooth plains of impact origin (impact-related terrain). Please note that, as seen in Section 1.2.1, the tectonized terrains are not selected as high representative units, since they occupy only the 20% of the entire Venusian surface. On the other hand, the impact related terrains have been selected as high scientific interest units because they may give important information about the materials beneath the crust, even if they occupy only the 10% of the entire Venusian surface.
- Potential quality of the geochemical signal at the landing site  
After having applied the first two criteria, only three reliable units for landing sites are left: shield plains (volcanic terrain), regional plains (volcanic terrain), smooth plains of impact origin (impact-related terrain). The typical characteristic of the shield plains are abundant small volcanic constructions that probably received magma from the interior and fed small volcanic eruptions on the surface. This type of terrain may have a complex history because it originated from erupted lava and, as a consequence, its spectrum of composition may be equally complex. On the other hand, the smooth plains of impact origin appear to be characterized by a less complex geochemical target because they consist of well mixed, fine grained materials, though they may

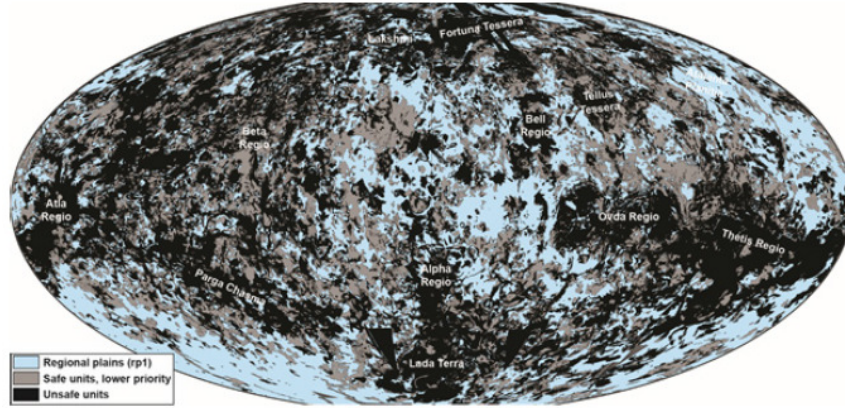
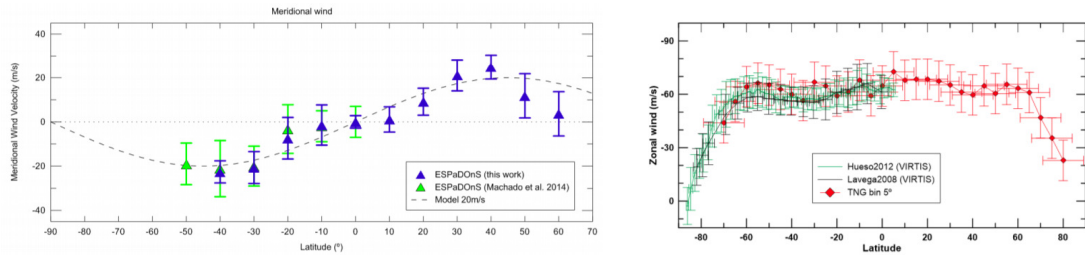


Figure 3.9: Geological Map of Venus - Lower scientific priorities units shown in gray - Adopted from [34]

have experienced chemical alteration due to the impact. Lastly, the regional plains represent a great candidate for geochemical analysis since they are characterized by uniform morphology everywhere on the Venusian surface (and that also means they probably originated in the same way) and they represent the most present type of terrain on Venus’s surface.

- Limitations due to orbital and ballistic restrictions  
 The last criterion used to select the proper landing site for the mission comes from the orbital and ballistic restrictions. In particular, high latitudes are avoided so that the inclination of the orbiter’s orbit does not have to be too high. Similarly, equatorial latitudes are not considered because of the strong winds (Fig. 3.10) they are characterized by and that may be a dangerous factor during the ascent phase.



(a) Meridional wind measured along both hemispheres at cloud top level (~70 km)

(b) Zonal wind measured at the bottom of the cloud layer (~48 km)

Figure 3.10: Zonal and Meridional winds - Adopted from Ref. [41]

### 3.3.2 Atmospheric Entry

The descent phase is divided into 3 subphases:

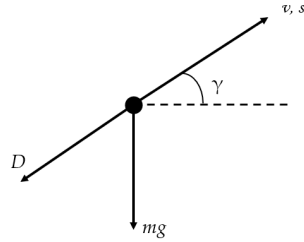
- Free falling from 300 km to 58 km  
During this phase the lander is encapsulated inside the aeroshell (Fig. 3.11), which is composed by a backshell and a heat shield.



Figure 3.11: CAD Model of the spacecraft encapsulated inside the aeroshell

The entry trajectory is calculated as a ballistic atmospheric entry based on density and altitude (no lift is included in the calculation).

Let  $s$  be the distance along the flight path,



then

$$\begin{aligned}\frac{dv}{dt} &= -g \sin \gamma - \frac{D}{m} \\ \frac{dv}{dt} &= \frac{dv}{ds} \frac{ds}{dt} = v \frac{dv}{ds} = \frac{1}{2} \frac{d(v^2)}{ds} \\ \frac{1}{2} \frac{d(v^2)}{ds} &= -g \sin \gamma - \frac{D}{m}\end{aligned}$$

Drag is defined as  $D = \frac{1}{2} \rho v^2 A c_D$  and we can write  $ds = \frac{dh}{\sin \gamma}$ , thus

$$\frac{\sin \gamma}{2} \frac{d(v^2)}{dh} = -g \sin \gamma - \frac{\rho v^2}{2m} A c_D$$

Considering an exponential expression for the atmospheric density

$$\rho = \rho_0 e^{-\frac{h}{h_s}}$$

where  $h_s$  is the scale height for Venus, which is  $h_s = 15.9$  km [43].  
Then

$$\frac{d\rho}{\rho_0} = e^{-\frac{h}{h_s}} \left( -\frac{dh}{h_s} \right) = \frac{\rho_0 e^{-\frac{h}{h_s}}}{\rho_0} \left( -\frac{dh}{h_s} \right) = \frac{\rho}{\rho_0} \left( -\frac{dh}{h_s} \right)$$

$$dh = -\frac{h_s}{\rho} d\rho$$

$$\frac{\sin\gamma}{2} \frac{d(v^2)}{dh} = -g \sin\gamma - \frac{\rho v^2}{2m} A_{cD}$$

$$\frac{\sin\gamma}{2} \frac{d(v^2)}{d\rho} \left( -\frac{\rho}{h_s} \right) = -g \sin\gamma - \frac{\rho v^2}{2} \frac{A_{cD}}{m}$$

$$\frac{d(v^2)}{d\rho} = \frac{2gh_s}{\rho} + \frac{h_s v^2}{\sin\gamma} \frac{A_{cD}}{m}$$

And, defining the Ballistic Coefficient ( $\beta$ ) as  $\beta = \frac{m}{c_{DA}}$  we obtain the equation of the motion of the spacecraft during the atmospheric entry:

$$\frac{d(v^2)}{d\rho} - \frac{h_s}{\beta \sin\gamma} v^2 = \frac{2gh_s}{\rho} \quad (3.16)$$

This equation can be solved using as input parameters the initial velocity, the entry angle  $\gamma$  and the ballistic coefficient  $\beta$  (the density is calculated using the Venus Global Reference Atmospheric Model [44]), as seen in Tab. 3.14.

Initial Altitude [km]	300
Initial Velocity [km/s]	7.151
Entry Angle [°]	15
Ballistic Coefficient [ $kg/m^2$ ]	219.95

Table 3.14: Atmospheric Entry Input Parameters

- Falling with parachute from 58 km to 45 km  
Once the spacecraft has passed the atmospheric region characterized by strong winds and has been decelerated by the dense and thick atmosphere to a velocity such that a parachute can be jettisoned and opened, the heat shield is detached from the lander and the rest of the aeroshell. The parachute is needed not only to separate the heat shield from the lander, but also to stabilize its trajectory during the last part of the descent. Therefore, the parachute is designed to generate enough deceleration so that the heat shield, once detached, goes away separately from the lander and the rest of

the aeroshell. In particular, it must be able to generate a  $4 \text{ m/s}^2$  deceleration higher than the deceleration of the heat shield once detached. The parachute used for this mission is an annular parachute because it can be opened at high velocity and provides great stabilization of the trajectory during the descent.

Therefore, in order to design the parachute, it is firstly necessary to calculate the deceleration of the heat shield due to the detachment and then to determine the surface area of the parachute needed to generate a  $4 \text{ m/s}^2$  deceleration higher.

After the first free falling phase from 300 km to 58 km, the velocity of the aeroshell is  $72.48 \text{ m/s}$  and the atmospheric density is equal to  $0.5825 \text{ kg/m}^3$ , so that the Mach number is equal to 0.3 (which is a value low enough to use an annular parachute). The properties of the heat shield needed for these calculations are summarized in Table 3.15.

Heat Shield Diameter [m]	3.5
Heat Shield Mass [kg]	144
Heat Shield $c_D$	1.05

Table 3.15: Heat Shield Main Properties - From Ref. [45] [46]

Thus, the drag acting on the heat shield can be computed with Eq. 3.17.

$$D = \frac{1}{2} \rho v^2 A c_D \quad (3.17)$$

and results to be

$$D_{HeatShield} = 15457 \text{ N}$$

Then, the deceleration of the heat shield due to the detachment can be calculated with Eq. 3.18.

$$a = g - \frac{D}{m} \quad (3.18)$$

and results to be

$$a_{HeatShield} = -98.64 \text{ m/s}^2$$

Then, it is possible to evaluate the deceleration the parachute must generate to separate from the heat shield.

$$a_{Lander} = a_{HeatShield} - 4 = -102.64 \text{ m/s}^2$$

Thus, the drag acting on the parachute must be

$$D_{Parachute} + D_{Lander} = m_{Lander} \cdot (g - a_{Lander})$$

$$D_{Parachute} = m_{Lander} \cdot (g - a_{Lander}) - D_{Lander}$$

where  $D_{Lander}$  is calculated using Eq. 3.17 and substituting with the main properties of the lander, summarized in Table 3.16. Thus, the drag the parachute must provide

Lander Diameter [m]	3.5
Lander Mass [kg]	1771
Lander $c_D$	1.12

Table 3.16: Lander Main Properties

results to be

$$D_{Parachute} = 156760 \text{ N}$$

From this value is, then, possible to evaluate the area and the radius of the annular parachute

$$A_{Parachute} = 120.53 \text{ m}^2$$

$$r_{Parachute} = 6.19 \text{ m}$$

- Free Falling from 45 km to 0 km

The final part of the descent consists of a free falling of the lander detached from the backshell and the parachute. Since the Venusian atmosphere is so dense and thick, the lander is naturally decelerated before landing without any need of a parachute that carries the lander to the surface. Moreover, as seen in Section 1.2.4, the deep atmosphere is characterized by very harsh conditions: at 45 km there is a temperature of about  $110^\circ$ , a pressure that is almost twice the pressure at sea level on Earth and going down toward the surface, those parameters increase more and more, making a possible parachute design very complex. Therefore, as mentioned before, at about 45 km of altitude, the lander is supposed to detach from the backshell and the parachute, free falling to the surface. However, since it is very important for the lander to land properly on the surface, a set of 6 grid fins controls the attitude of the lander during this part of the descent.

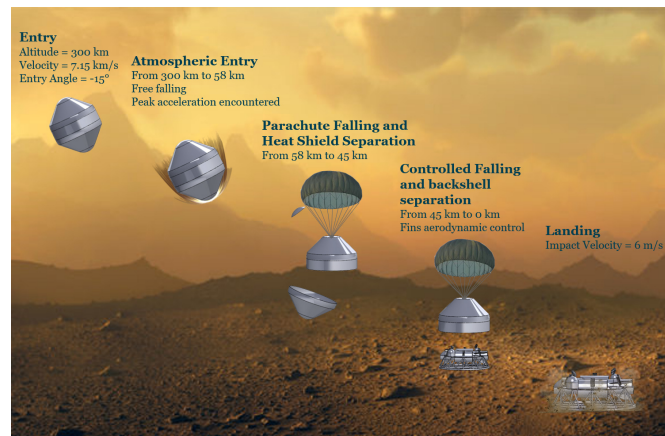


Figure 3.12: Descent Phase Summary

The total time of descent results to be 1 hour and 26 minutes.

In Fig. 3.13 is represented a summary of the descent phase with information about altitude and time, whereas Fig. 3.14 shows the velocity of the spacecraft over time during the descent.

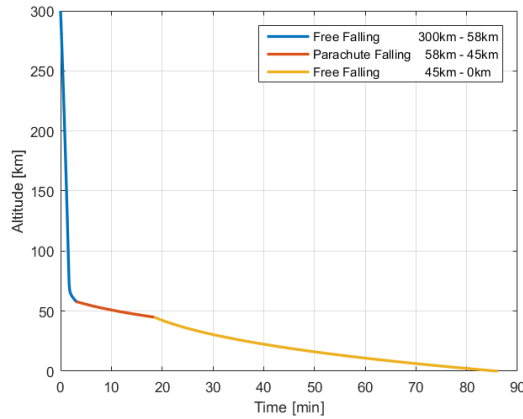


Figure 3.13: Landing Probe Descent - Altitude vs Time

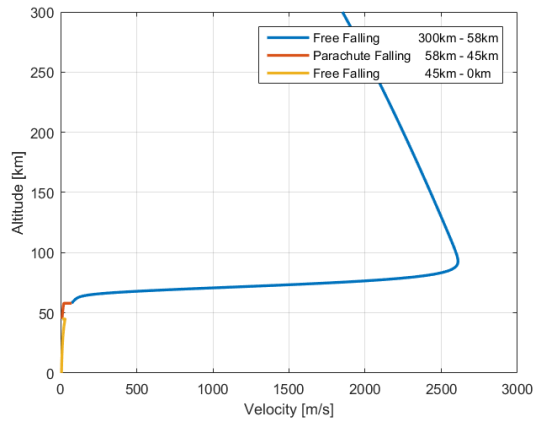


Figure 3.14: Landing Probe Descent - Altitude vs Velocity

### 3.3.3 Landing Phase

The landing phase comes right after the final subphase of the descent. The lander is free falling and its attitude is being controlled by a set of grid fins. The dense and thick deep Venusian atmosphere is such that the lander's velocity during the free falling does not reach too high values: the final velocity of the lander is calculated to be

$$V_{impact} = 6.002m/s$$

Then, the impact ring of the lander is designed to withstand the crash and provide a safe landing.

### 3.4 Surface Operations

Once the spacecraft has safely reached the surface, the operative phase starts. The surface operations concern the samples collection activity and the activation of all the scientific instruments and the subsystems of the spacecraft.

- Two drills are supposed to collect the soil samples from the Venusian surface. One is attached to a mechanical arm, so it can collect samples over a surface of at least  $10\text{ m}^2$  (as required by NASA-JPL, see Section 2.4); while the other is a telescopic drill, which helps the previously mentioned one to collect at least 1 kg of Venusian regolith (as required by NASA-JPL). Every samples is then transferred into the proper container through a pneumatic transfer system.
- The atmospheric collection system consists of two 1-liter-cylinders where the Venusian atmosphere is sucked thanks to a moving piston and the higher environmental pressure. One liter atmospheric sample is collected on the surface, whereas another one liter atmospheric sample is collected during the ascent phase.
- The scientific payload consists of a set of scientific instruments located inside two pressure vessels (details will be described later on). These instruments are supposed to turn on once on the surface and operate for at least 24 hours (see Section 2.4). They are connected to the communication system so that they can send to Earth and to the orbiter all the data and information collected.
- The power system, which consists of a set of High Temperature-resilient And Long-Life (HiTALL) batteries, provides the energy required by all the instruments and subsystems of the spacecraft.
- The communication system, which consists of 2 high-gain antennae and 2 low-gain antennae, transmists data and information to the orbiter and to the terrestrial ground stations.
- A 24 Hours Consumable-based Cooling System is supposed to rejects both the heat generated by the instruments of the lander and the heat leaks that income from the external environment. This system consists of 2 pressure vessels and a network of vapor tubes and valves that allow the working fluid to circulate inside the structure and to vent in the external environment.

After having collected the soil and atmospheric samples on the surface, the ascent phase starts. However, the scientific instruments and subsystems designed to work for at least 24 hours, stay on the surface and keep sending data and information about the Venusian environment to the orbiter.

## 3.5 Ascent, Rendezvous with the Orbiter and Return to Earth

The ascent phase starts once the operations of sample collection on the surface are completed. It involves the so called Venus ascent vehicle, which basically includes a balloon and a rocket. The former is designed to carry the rocket to an altitude where the environmental conditions are less harsh so that the rocket can perform the maneuvers to reach the target altitude and rendezvous with the orbiter. On the other hand, the rocket contains the samples collected on the surface and during the ascent (please note that the second sample of Venusian atmosphere is collected during the balloon ascent at an altitude of about 40 km, as required from NASA-JPL, Section 2.4) and is supposed to carry them to orbit.

The balloon, inflated with Helium, is basically a zero-pressure natural-shaped balloon (details will be given later on), which is designed to carry the ascent rocket exploiting the buoyant force. The expression *zero-pressure* balloon is due to the fact that the pressure difference between the external atmosphere and the lifting gas is essentially zero at a certain level in the gas throughout flight. These type of balloon is open at the bottom and presents open ducts hanging from the sides that allow gas to escape and to prevent the pressure inside the balloon from increase too much during gas expansion as the balloon rises above Venus's surface. In order to provide enough lift to get off and reach the target altitude to the balloon, a measured (calculated) amount of Helium is put into the balloon at the surface. During the balloon's ascent, the gas inside it expands because the atmospheric pressure surrounding the balloon drops. The main advantage of a zero-pressure balloon with respect to other types of balloon (e.g. superpressure balloons) is the opportunity to vent out the gas: in fact, in the case of a close system, such as the superpressure balloon, the excess gas would exert excessive pressure on the balloon skin and ultimately can cause it to rupture. Therefore, thanks to the open ducts, zero-pressure balloons minimize the pressure on the film of the balloon so that it is possible to realize large balloons composed of thin and lightweight films [47].

The balloon trajectory analysis has been performed solving second order differential equations for the position of the ascent vehicle. As a result, the ascent time of flight for the balloon to reach the target altitude of 51 km above Venus's surface is calculated to be about 5 hours and 31 minutes.

Once the balloon has reached the target altitude, the rocket perform the first of several maneuvers to reach the orbiter's orbit and detaches from the balloon. The rocket is basically a two-stage solid rocket and its propellant is made of Hydroxyl-terminated polybutadiene (HTPB) mixed with Aluminum and Ammonium Perchlorate. Each stage corresponds to a maneuver: the first stage performs the first burn of the rocket at the altitude of about 51 km, while the second stage performs the second burn of the rocket, which is needed to circularize the trajectory and insert in orbit at the altitude of about 300 km.

Once in orbit, the rocket performs the maneuvers to rendezvous with the orbiter and then, the entire system waits for the next launch window before travelling to Earth.

In Figure 3.15 the summary of the ascent phase is shown with the main information about each sublevels of the phase.

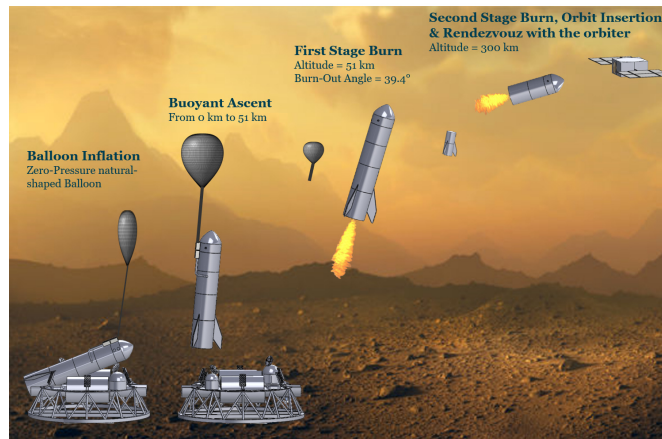


Figure 3.15: Ascent Phase Summary

# Chapter 4

## Systems and Subsystems

This chapter describes a Design Reference Mission that is supposed to implement the phases developed and seen in Chapter 3. The main purpose of the Design Reference Mission is to quantify the resources and the components needed to implement the proposed Venus sample return mission via a recommended mission architecture. Of particular interest are the subsystems of the lander, the total landing mass and the design of the Venus ascent vehicle. It is important to underline that the Design Reference Mission described here is not intended to be the final choice of the Venus sample return mission: it is an example mission concept that both achieves the mission requirements and covers a large variety of the scientific goals related to the Venus science research, and provides enough engineering definition for first-order estimations of the needed resources. The level of detail for the proposed Design Reference Mission is uneven, with some elements having received advanced design and analysis work (e.g Venus ascent vehicle) and other elements not advanced beyond the rough concept stage (e.g the orbiter).

Following the phases seen in Chapter 3, the subsystems description will include 3 of the main components of the spacecraft: the entry probe, the lander and the ascent vehicle.

This chapter provides not only the technological description and details of each designed part, but also the most important equations and derivations used to design them, in order to give a global overview of the entire work and provide the opportunity to the reader to understand and, possibly, figure out tips or suggestions useful to improve the precision and the reliability of the proposed mission concept or to inspire future works.

### 4.1 Venus Entry Aeroshell

The Venus Entry Aeroshell is basically the vehicle supposed to perform the detachment from the orbiter and the atmospheric entry and descent on Venus. It consists of an external shell (that includes a heat shield and a backshell) that contains the parachute, the lander and the drag plate. As seen in Section 3.3.2, the parachute is designed so that the heat shield can detach and separate from the rest of the entry probe during the descent. The Venus Entry Aeroshell's goal is to protect the lander and all its components during the descent phase from heat, pressure, acceleration peaks and possible debris created by drag

during the atmospheric entry. Moreover, thanks to the heat shield, the aeroshell absorbs the resulting friction and decelerates the spacecraft during the descent. The aeroshell is a key component in a safe descent and, then landing, of the spacecraft in the Venusian atmosphere.

#### 4.1.1 Heat Shield

The heat shield of the entry probe is basically represented by the so called NASA HEEET (Heat Shield for Extreme Environment Technology). It consists of a dual layer structure composed of a higher density all-carbon fiber wave surface which is exposed to entry environment and is designed to manage recession, and a lower density, lower thermal conductivity layer of blended carbon/phenolic yarn, which is designed to manage heat loads. These two layers are integrally woven together so that they are mechanically interlocked and not bonded, and are then infused with a mid-density phenolic resin [48].

The recession layer's material thickness is 1.5 cm, while the insulating layer's one is 3.8 cm so that the total thickness is 5.3 cm. The diameter of the structure is 3.5 m and the unmarginated mass is estimated to be 210 kg [46], as shown in Table 4.1.

Base Diameter [m]	3.5
Sphere-Cone Angle [°]	45
<b>Heat Shield Mass [kg]</b>	<b>210</b>

Table 4.1: Heat Shield Properties

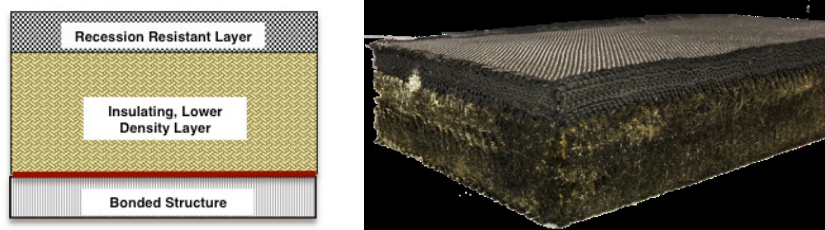


Figure 4.1: Heat Shield for Extreme Entry Environment Technology layers - Adopted from Ref. [49]

Since the Technology Readiness Level is 6, this type of heat shield can be part of preliminary design proposals, and that is why, since this technology seems to be very promising, it has been chosen as heat shield for this mission.

The structure is composed of *tiles* and *gap filler* (Fig. 4.2); the gap filler between tiles performs two primary functions: it provides structural relief for all load cases (thanks to a relatively high compliance of gap filler compared to acreage tiles) and it provides an aerothermally robust joint, *aerothermally monolithic seam* (thanks to very thin adhesive widths between gap filler and acreage tiles). In particular, there are 12 outer radial gap fillers, 12 outer tiles, 6 inner circumferential gap fillers, 6 inner radial gap fillers, 6 inner tiles and 6 outer circumferential gap fillers (Fig. 4.3).

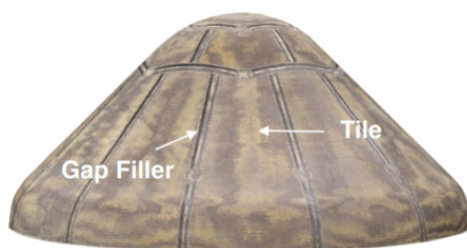
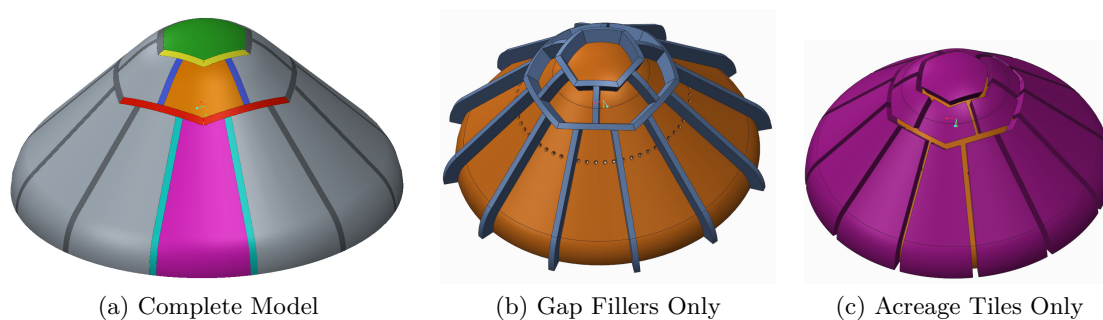


Figure 4.2: Heat Shield for Extreme Entry Environment Technology configuration - Adopted from Ref. [49]



Tile Type	Tile Color	Tile Quantity for 1x Tile Set
Nose Cap	Green	1
Inner Circumferential Gap Filler	Yellow	6
Inner Radial Gap Filler	Blue	6
Inner Tile	Orange	6
Outer Circumferential Gap Filler	Red	6
Outer Radial Gap Filler	Cyan	12
Outer Tile	Purple	12

Figure 4.3: Heat Shield for Extreme Entry Environment Technology model - Adopted from Ref. [49]

Lastly, it is important to underline that the NASA HEEET heat shield is being designed precisely for Venus landing mission, thus the structure is being tested in order to withstand atmospheric entries on Venus. To date, the HEEET materials have been tested to conditions of  $\sim 6000 \text{ W/cm}^2$  heat flux and 5 atmospheres of pressure and have shown excellent performance.

### 4.1.2 Backshell

As mentioned in Section 4.1.1 the aeroshell of the entry probe includes a backshell which is used to enclose the lander and protect it from the external environment. The backshell consists of a PICA (Phenolic Impregnated Carbon Ablator) structure with the same diameter and similar shape to the heat shield. The backshell is designed in order to jettison the parachute at a certain altitude, therefore is equipped with a drogue whose purpose is to pull

the parachute out during the descent. Besides the parachute and the drogue mechanism, the backshell contains electronics, batteries and an Inertial Measurements Unit (IMU) in order to release the parachute properly and to measure the attitude and orientation of the backshell itself during the descent.

An outer layer of graphite epoxy is used to protect the structure from the sulfuric acid environment. The density of the backshell's material is  $270 \text{ kg/m}^3$ , therefore it is possible to evaluate the mass of the component after having calculated the volume (Table 4.2).

PICA Density [ $\text{kg/m}^3$ ]	270
Graphite Epoxy Density [ $\text{kg/m}^3$ ]	1550
Outer Coating Volume [ $\text{m}^3$ ]	0.02522
Outer Coating Mass [kg]	39.1
Backshell Volume [ $\text{m}^3$ ]	0.5646
Backshell Mass [kg]	152.4
<b>Total Backshell Mass [kg]</b>	<b>191.5</b>

Table 4.2: Backshell Properties

The CAD model of the backshell is shown in Figure 4.4.

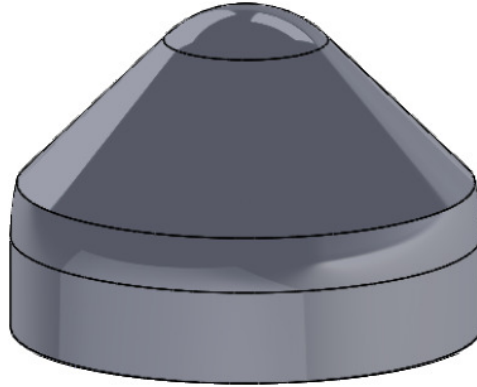


Figure 4.4: Backshell CAD Model

### 4.1.3 Parachute

As mentioned in Section 4.1.2, the Backshell contains the parachute designed to slow the entry probe down in order to detach the heat shield from the rest of the aeroshell. The parachute is located at the apex of the backshell and is connected to a drogue which is supposed to help pulling it out for a proper release. The parachute is also supposed to stabilize the entry trajectory before the last part of free falling and the landing. The type of the parachute chosen for the mission is the *annular parachute* because it is the one with the highest drag coefficients related to the canopy surface area of all known parachute types [50] and it provides a great stabilization of the trajectory, with low average angle

of oscillation, which is important since the parachute working environment is still quite windy (average windspeed between 58 and 45 km of altitude  $\sim 50$  m/s).

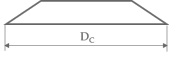
Type	Plan	Profile	Drag Coeff $c_{D0}$	Average angle of oscillation [°]
Annular			0.85 ÷ 0.95	< 0.6

Table 4.3: Annular Parachute Properties

As mentioned previously, the parachute is supposed to be deployed at about 58 km of altitude and carry the entry probe down to an altitude of about 45 km. As seen in Section 3.3.2, the parachute has been designed in order to create enough deceleration to the backshell and the lander in order to separate from the heat shield (which is being decelerated as well due to the detachment from the lander).

The parachute’s materials need to exhibit not only high specific strength, but also good thermal mechanical properties in order to withstand the environmental temperatures that ranges between 3 °C (at 58 km of altitude) and 107 °C (at 45 km of altitude) [44]. A list of possible materials that can be used for the parachute film is presented in Table 4.4 along with some of their properties.

Material	Density	Max Service Temperature [°C]	Min Service Temperature [°C]	Tensile Strength [MPa]
Kapton	1420	400	-269	231
Mylar	1390	200	-250	186
Kevlar	1440	177	- 196	3000

Table 4.4: Parachute Film Materials

Kapton® is obtained synthesizing an aromatic dianhydride with an aromatic diamine. It is characterized by excellent chemical resistance: there are no known organic solvents that can affect the film. Moreover, it can be used either at low and high temperatures since its maximum service temperature is around 400°. On the other hand, Kevlar displays higher tensile strength but lower thermal properties, which are more desirable for this application. Lastly, Mylar has better thermal properties than Kevlar, however, its density and tensile strength are both lower than the Kapton’s ones. Therefore, the chosen parachute material is Kapton: its low density and good thermal properties makes it the most suitable material for this application. However, since it is characterized by low tensile strength, a load-carrying net is added around the parachute. Fibers that can be used for the netting are reported in Table 4.5.

Spectra and Carbon both have poor thermal properties and lower tensile strength than PBO, that is why this one has been chose for the load-carrying net around the parachute.

Material	Density	Max Service Temperature [°C]	Tensile Strength [MPa]
PBO	1560	500	5800
Spectra	970	150	3000
Carbon	1800	300	3790

Table 4.5: Parachute Fiber Materials

Analysis of the performances of Kapton film (chosen to construct the parachute) and the PBO fiber (chosen for the load-carrying net around the parachute) at different temperatures is reported in Table 4.6. The PBO fiber is characterized by great thermal properties so

Temperature [°C]	Kapton film [MPa]	PBO fiber [Mpa]
20	231	5800
100	162	4730
200	139	3630
300	77	2540
400	55	2080

Table 4.6: Tensile Strength Analysis of Kapton and PBO

that it presents high performances even at very high temperatures, while the Kapton film displays enough strength since it is not the load carrying material.

As seen in Section 3.3.2, the design of the parachute basically depends on the mass of the carried lander and backshell, on the entry speed and the deceleration needed to separate from the heat shield. As a result, a 6.19 m radius parachute is needed. The final dimensions of the parachute are presented in Figure 4.5, whereas the masses of the parachute are reported in Table 4.7.

Component	Size [ $m^2$ ]	Mass [Kg]
Film (Kapton, $32.7 \text{ g}/m^2$ )	287.5	11.4
Fiber (PBO, $24 \text{ g}/m$ )	-	4.4
<b>Total</b>		<b>15.8</b>

Table 4.7: Final Parachute Materials and Masses

#### 4.1.4 Aerodynamic Grid Fins

Grid fins are a type of aerodynamic flight control surfaces. They have been chosen for the proposed mission instead of solid surfaces because of the thick and dense atmosphere of

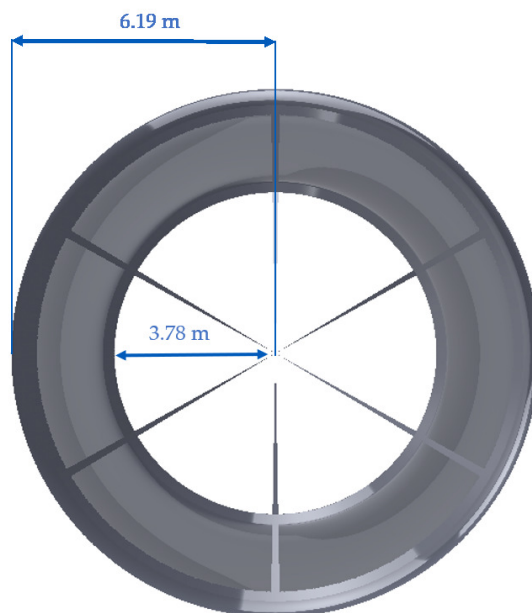


Figure 4.5: Annular Parachute Final Dimensions

Venus. In fact, not only solid surfaces would be less precise in controlling the trajectory of the lander during the descent, but also they would be more exposed to fractures or breaks. Therefore, a set of 6 independent grid fins have been chosen to actively control the lander's descent toward the Venusian surface. Those fins are made of Waspaloy, which is a nickel-based, age hardenable superalloy with excellent high temperature strength developed for the handling of sulfuric acid environments. The main properties of this material are listed in Table 4.8.

Material	Density [ $kg/m^3$ ]	Max Service Temperature [ $^{\circ}C$ ]	Tensile Strength [MPa]	Young Modulus [GPa]
Waspaloy	8190	650	1276	213

Table 4.8: Waspaloy Main Properties

The grid fins provide not only the attitude control of the lander during the descent, but also the trajectory monitoring before landing, in order to avoid complicated-landing areas. They are attached to the main frame of the lander and they are the only moving parts of the entire landing structure.

A CAD model of a single grid fin is presented in Figure 4.6, whereas the total mass of the complete set is shown in Table 4.9.

Component	Unit Mass [kg]	Quantity	Total Mass [kg]
Grid Fin	4.04	6	<b>24.24</b>

Table 4.9: Grid Fins Total Mass



Figure 4.6: Single Grid Fin CAD Model

## 4.2 Venus Lander

This section describes the various components of the Venus lander, specifically the subsystems it consists of, the mass and the materials of each component and the techniques used for sample collection. An impact structure that consists of a ring, legs and a frame is designed to provide a safe landing to all the systems. A thermal protection system, that includes insulating layers and a cooling system, provides both protection and proactive action against the high temperatures on the Venusian surface. Thanks to this one, the scientific instruments, charged by a set of high-temperature resilient batteries, gather data and information about Venus's environment while the communication system sends all these valuable information to the orbiter around Venus and the ground stations on Earth. A set of two different drills is designed to collect enough soil samples to accomplish the NASA requirements seen in Section 2.4 while a samples handling system inside the ascent rocket provides the protection to the collected material in order to guarantee its integrity until the end of the mission. Similarly, an atmospheric samples collection system is designed to collect and preserve portion of the Venusian atmosphere.

The lander represents the system that has to provide not only a safe landing to the entire structure, but also to keep operational every subsystems on the Venusian surface guaranteeing a suitable working environment for at least 24 hours, as seen in Section 2.4. Therefore, it is equipped with pressure vessels that host the components of all the subsystems and are designed to survive and work properly for at least one Earth day.

The lander is designed to fit inside the heat shield and to have a low center of mass in order to avoid rotation of the structure during the descent.

The lander is mostly made of is Ti-6Al-4V, because of its high performances even at high

temperatures.

Figure 4.7 shows the CAD model of the lander designed for the proposed mission.

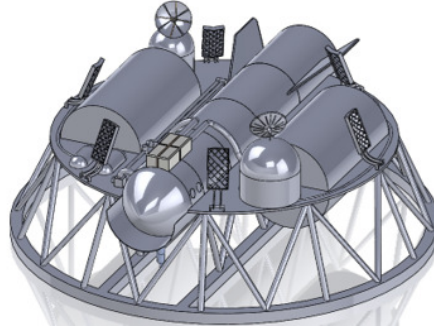


Figure 4.7: Lander CAD Model

The Venus Lander is mainly constituted of two large cylindrical tanks, two scientific payload vessels and the ascent rocket attached to a titanium platform. The two big pressure vessels host the helium needed to inflate the ascent balloon. Attached to the frame are also a robotic arm with the drill on top and a telescopic drill. Those are connected to the rocket casing so that the samples are directly inserted into the sample capsules. An impact ring and legs attached to the main platform support the lander and provide a safe landing on the Venusian surface.

### 4.2.1 Platform

The platform of the lander is basically represented by a titanium frame that is designed to contain all the components of the lander. In particular, the biggest component is the ascent vehicle and the platform is shaped so that it can keep the rocket steady and locked during all the mission phases. Similarly, room for the pressure vessels and the tanks are designed. Moreover, every connection between the components of the lander is constructed so that it is attached to the frame in order to have no moving parts except for the grid fins, as seen in Section 4.1.4. The platform is made of Ti-6Al-4V, which is a high strength-to-weight ratio titanium alloy characterized by excellent corrosion resistance (Table 4.10 presents the main properties of the material).

Material	Density [ $kg/m^3$ ]	Young Modulus [GPa]	Ultimate Tensile Strength [MPa]	Strength to Density Ratio (*1000)
Titanium Alloy Grade 5 (Ti-6Al-4V)	4430	133	950	214

Table 4.10: Titanium Alloy Grade 5 (Ti-6Al-4V) Main Properties

The Ti-6Al-4V platform is designed to withstand the maximum loads that occur during the Venus entry phase of the mission. The estimated 15- to 20-g deceleration peaks create transverse loads on the platform whose thickness is sized in order to provide a safe descent

to the lander and the components within it. The bending moment is calculated using the force at the center of the frame, and the distance from the center to the extremity of the structure. Moreover, the maximum load is computed from the deceleration peaks so that the platform can be designed to be thick enough to withstand the forces during the descent. The outer diameter of the platform is equal to 1.43 m and the required thickness is calculated to be 1.01 cm. Therefore, the total mass of the structure is 335.48 kg. Figure 4.8 shows the CAD model of the so designed platform.

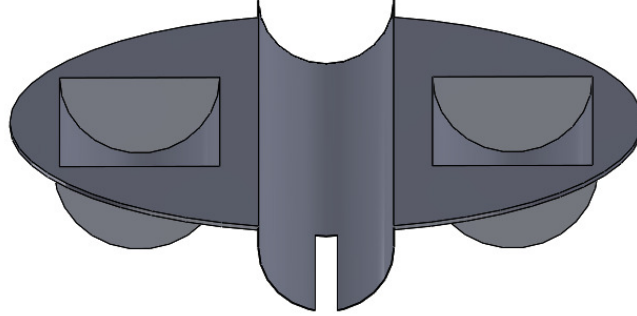


Figure 4.8: Platform CAD Model

From Figure 4.8, it is clear where the helium tanks and the ascent rocket are located. In particular, from the shape of the structure it can be immediately seen that the ascent rocket is equipped with fins used to control the ascent trajectory during the flight.

### 4.2.2 Helium Tanks

Mentioned in Section 4.2.1, the helium tanks are the containers of the gas used to lift off the ascent vehicle from the Venusian surface. Those pressure vessels must withstand the harsh conditions present on Venus's surface and keep the contained gas pressurized in order to be used properly by the balloon. Since the success of the mission depends mostly on the return of planetary materials from the Venusian surface, these components, together with the ascent vehicle, are the most important ones of the lander. Therefore, the tanks not only are designed to be pressurized and robust enough to withstand to  $\Delta P$  between the interior and the external environment, but are also protected with insulating and sulfuric acid protecting layers.

The size of the two Helium tanks starts with an initial volume estimation based on the perfect gas law (Eq. 4.1).

$$P \cdot V = m \cdot R \cdot T \quad (4.1)$$

where  $P$  is the pressure ([Pa]),  $V$  represents the volume ( $[kg/m^3]$ ),  $m$  represents the mass of the gas ([kg]),  $R$  is the Helium specific gas constant (2077.1 [J/(kg K)]) and  $T$  is the temperature ([K]).

An internal temperature and pressure of 250 K and 30 MPa respectively are used for this analysis.

Therefore, using Equation 4.1, a resulting volume of  $0.912 m^3$  is calculated. This calculation depends on the preliminary estimation of the mass of Helium needed by the balloon in order

to provide enough lift to ascend from the surface and reach the target altitude carrying the ascent rocket (see Section 4.3.1). This volume is the total one necessary for the mission and it is divided between two tanks. The two-tank system is useful not only to avoid an enormous pressure vessel, but also to create lander symmetry. In order to understand what shape fits best in the lander, two types of pressure vessels have been considered: cylindric and spheric ones. Therefore, calculations about their dimensions have been developed and a final comparison has been made. The reference volume is the one calculated before using Equation 4.1.

As for the two spheric tanks, the minimum radius of each vessel is calculated to be

$$r = \sqrt[3]{\frac{V}{\frac{4}{3}\pi}} = 0.478 \text{ m}$$

On the other hand, in order to determine the dimensions of the potential cylindric tanks, an analysis of the various geometric combinations has been developed (Table 4.11).

Vessel Radius [m]	Vessel Length [m]
0.3	1.614
0.35	1.186
0.4	0.908
0.45	0.717
0.5	0.581

Table 4.11: Helium Cylindric Tanks Geometry and Mass Combinations

Since the available space on the platform is limited (Figure 4.9), the configuration that fits best in the platform has been chosen.

In particular, it is immediately clear that the spherical tanks are bigger than the available space on the platform, therefore the cylindric configuration is selected. Then, similarly, the analysis of the size of the cylindric tanks geometry combinations (Table 4.11) has been performed so that the chosen configuration can fit on the platform. The resulting configuration is characterized by the values of the dimensions presented in Table 4.12.

Single Tank Radius [m]	Single Tank Length [m]
0.35	1.186

Table 4.12: Dimensions of the Helium Tanks

Once the configuration of the Helium tanks has been defined, the analysis of the thickness of the wall and the head end of the pressure vessel has been developed.

The membrane stresses acting on vessels of revolution, including those characterized by complex geometry, can be evaluated using the equations of statics as long as they are loaded in a rotationally symmetrical manner [51].

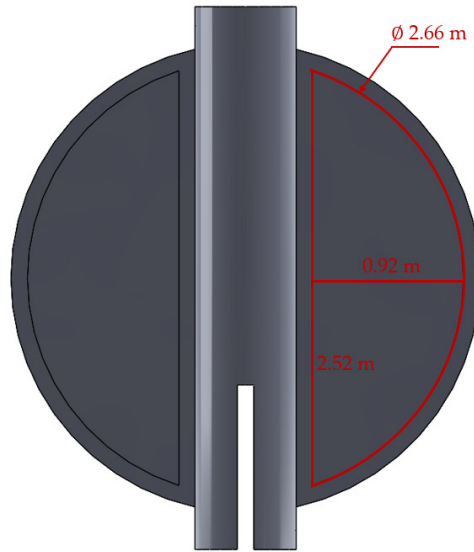


Figure 4.9: Available Space for the Helium Tanks on the Platform

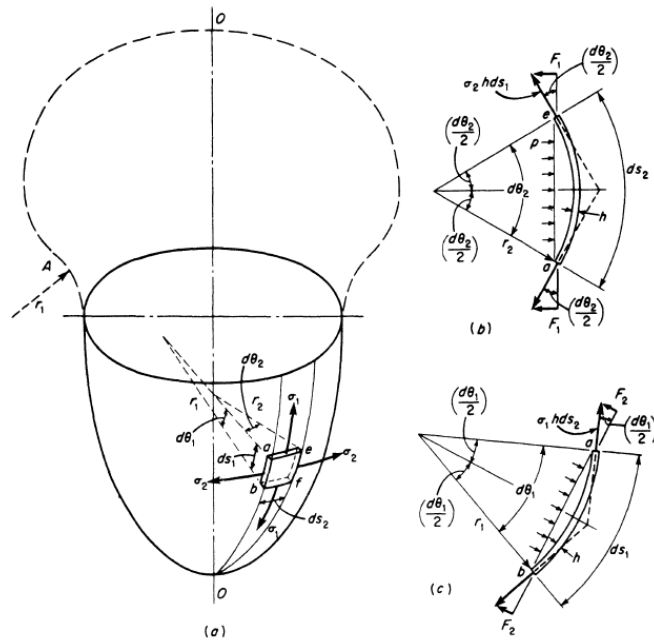


Figure 4.10: Membrane Stresses in Vessels - Adopted from Ref. [51], page 21

Referring to Figure 4.10 (a), the total forces acting on the side of the element are  $\sigma_1 h ds_2$  and  $\sigma_2 h ds_1$ . The force  $\sigma_2 h ds_1$  has a component along the normal direction to the element (b) of

$$2F_1 = 2\sigma_2 h ds_1 \sin\left(\frac{d\theta_2}{2}\right) \quad (4.2)$$

and similarly, the force  $\sigma_1 dhs_2$  has a component along the normal direction to the element (c) of

$$2F_2 = 2\sigma_1 hds_2 \sin\left(\frac{d\theta_1}{2}\right) \quad (4.3)$$

The pressure force normal to the element is

$$P = p \left[ 2r_1 \sin\left(\frac{d\theta_1}{2}\right) \right] \left[ 2r_2 \sin\left(\frac{d\theta_2}{2}\right) \right] \quad (4.4)$$

which is equilibrated by the sum of the normal membrane component forces (from Eq. 4.2-4.3):

$$2\sigma_2 hds_1 \sin\left(\frac{d\theta_2}{2}\right) + 2\sigma_1 hds_2 \sin\left(\frac{d\theta_1}{2}\right) = p \left[ 2r_1 \sin\left(\frac{d\theta_1}{2}\right) \right] \left[ 2r_2 \sin\left(\frac{d\theta_2}{2}\right) \right]$$

since

$$\sin\left(\frac{d\theta_1}{2}\right) = \frac{ds_1}{2r_1} \quad \sin\left(\frac{d\theta_2}{2}\right) = \frac{ds_2}{2r_2}$$

then

$$\frac{\sigma_1}{r_1} + \frac{\sigma_2}{r_2} = \frac{p}{h} \quad (4.5)$$

The Equation 4.5 can be obtained more directly by noting in Eqs. 4.2, 4.3, 4.4 that for small angles the tangent and the sine are equal to the respective angle in radians, and that the chord is equal to the arc.

In the case of a cylindric vessel under internal pressure  $p$  the hoop radius  $r_2$  is equal to the radius of the vessel, whereas the longitudinal radius  $r_1 = \infty$  and each is constant throughtout the cylinder. Thus, substituting those values into Equation 4.5 we obtain

$$\frac{\sigma_1}{\infty} + \frac{\sigma_2}{r_2} = \frac{p}{h}$$

Thus,

$$\sigma_2 = \frac{pr}{h} \quad (4.6)$$

where  $\sigma_2$  represents the hoop stress and  $h$  the thickness of the vessel.

On the other hand, the longitudinal stress can be obtained by equating the longitudinal forces producing extension to the total pressure force on the cross section of the cylindrical vessel

$$\sigma_1 2\pi r h = p\pi r^2$$

Thus,

$$\sigma_1 = \frac{pr}{2h} \quad (4.7)$$

where  $\sigma_1$  is the longitudinal stress and  $h$  the thickness of the vessel.

In order to design the thickness of the vessel, the Ultimate Tensile Strength corrected by a safety factor of 1.5 (or the Yield Tensile Strength if lower) has been used as maximum allowable stress value of the structure. Then, an analysis of the combination of the materials and the resulting thicknesses and masses has been developed (Table 4.13).

Material	Density [ $kg/m^3$ ]	Tank Thickness Required [mm]	Single Tank Mass [kg]	Total Mass [kg]
Maraging Steel	8000	8	169	338
A-286 Iron-based Alloy	7920	38	831	1663
D6 AC Steel	7780	11	219	438
Titanium Alloy Grade 5 (Ti-6Al-4V)	4430	17	196	392
Graphite Epoxy	1550	11	43	86

Table 4.13: Helium Cylindric Tanks Materials, Thickness and Mass Combinations

Among the possible materials, Maraging steels (from *martensitic* and *aging*) are iron alloys known for being characterized by very high strength and toughness without losing ductility. Their principal alloying element is represented by nickel.

Type A-286 Iron-based Alloy is a superalloy useful for applications that require high strength and corrosion resistance up to 704 °C. It is an austenitic iron-based material that can be age hardened to a high level of strength.

D6 AC Steel is a medium-carbon alloy primarily developed for high strength structural applications.

Titanium Alloy Grade 5 (Ti-6Al-4V) is an alloy characterized by high strength-to-weight ratio and excellent corrosion resistance.

Lastly, Graphite/Epoxy is being used increasingly in space applications because of its good mechanical properties (high strength-to-weight ratio) and near-zero coefficient of thermal expansion.

Therefore, in order to maximize the performance and minimize the mass, Graphite composite with an epoxy resin matrix has been chosen for constructing the Helium tanks even though is the most expensive material among those seen in Table 4.13. Graphite epoxy is also characterized by corrosion resistance against sulfuric acid which is crucial for surviving on the Venusian surface.

The characteristics of the so designed Helium tanks are presented in Table 4.14.

Material	Tank Radius [m]	Tank Length [m]	Single Tank Mass [kg]	Total Mass [kg]
Graphite Epoxy	0.35	1.186	43	86

Table 4.14: Material, Dimensions and Masses of the designed Helium Tanks

As previously mentioned, the Helium tanks are attached to the lander which is shaped in order to house them properly. A sketch of the CAD model which shows the location of the

Helium tanks is presented in Figure 4.11.

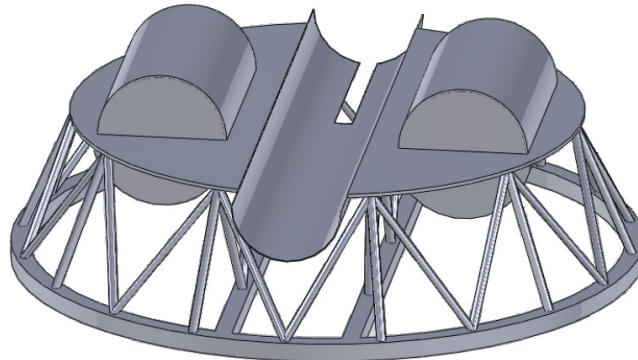


Figure 4.11: Helium Tanks Location - CAD Model

### 4.2.3 Landing Ring

The landing ring is the structural component that is designed to protect the entire lander system during the landing phase, providing a safe touchdown on the Venusian surface and absorbing the crash energy due to the impact. The goal is to use lightweight high-strength resilient materials in order to maximize the performance and minimize the mass. That is why both the impact ring and the legs are made of crushable honeycomb aluminum core material such as Plascore CrushLite™. This material is certified to specific crush strengths for energy absorption applications. It is designed to provide reliable and consistent energy absorption in almost any environment, yielding at a constant force [52]. Its main features include:

- Predictable energy absorption properties
- High crush strength-to-weight ratio
- Efficient constant force crush curve
- Wide range of strengths available
- Crush stroke in excess of 70%
- Excellent moisture and corrosion resistance
- Elevated use temperatures

In the aerospace applications, it improves crashworthiness protection in seating, or acts as a single event shock absorber for impact protection without adding significant weight.

In order to ensure a safe landing, given its impact velocity and momentum, the amount of energy absorbing material is determined based on the kinetic energy that characterized the lander before touchdown. As a requirement for a safe landing, the 100% of the kinetic energy must be absorbed by the impact structure and its materials. Thus, knowing the

impact velocity (calculated in Section 3.3.3), the total kinetic energy is calculated using Equation 4.8.

$$E = \frac{1}{2}mV^2 \quad (4.8)$$

Then, the thickness of crushable honeycomb is estimated using Equation 4.9.

$$IE = \sigma AS \quad (4.9)$$

where  $IE$  is the impact energy (equal to the total kinetic energy of the lander),  $\sigma$  is the crush strength of the material the impact ring is made of,  $A$  is the area of the crushing surface and the stroke  $S$  is based on the thickness of the crushable honeycomb.

Every single leg of the landing structure is, then, designed using Equation 4.10 [53] in order to absorb an additional 25% of the impact energy.

$$r_{Leg} = \sqrt{0.25 \cdot \frac{\frac{1}{2}m_{tot}V_{impact}^2}{\pi\sigma_{leg}\Sigma s}} \quad (4.10)$$

where  $r_{leg}$  is the radius of the honeycomb material in a single leg,  $m_{tot}$  is the total mass of the lander,  $V_{impact}$  is the lander's terminal velocity,  $\sigma_{leg}$  is the crush strength of the honeycomb-based material in a leg, and  $\Sigma s$  represents the total stroke of all the legs of the structure.

In particular, different configurations of Plascore CrushLite exist (see Figure 4.12), therefore the configuration with enough crush strength and foil thickness has been considered. As a result, 5 mm of Plascore Honeycomb is required for the impact ring and a radius of 8 mm is needed for every leg. Another 2 mm of Titanium Grade 5 (Ti-6Al-4V) is used to support the honeycomb material and provide a stable attachment to the legs of the structure which are covered by a 2 mm layer of Titanium Grade 5 (Ti-6Al-4V) as well. Moreover, the Titanium cover is used to protect from the sulfuric acid environment of Venus. The total mass of the system is then estimated as a sum of the masses of ring and legs (Table 4.15).

Component	Mass
Landing Ring	397.8
Legs	7.9
<b>Total Mass</b>	<b>405.71</b>

Table 4.15: Landing Ring and Legs Masses

A sketch of the CAD model of the landing ring is shown in Figure 4.11.

#### 4.2.4 Scientific Payload

As seen in Section 2.4, a generic 50 kg of scientific payload is asked to be accommodate to the Venusian surface. However, in order to give a more complete system design, an analysis of the main objectives of the Venus science community has been performed and a list of

Plascore Honeycomb Designation					Crush Properties		
Nominal Density lbs/ft <sup>3</sup>	Cell Size (Inch)	Foil Gauge (Inch)	Available in Perforated	Foil Alloy	Crush Strength <sup>1</sup> (psi)	Standard Crush Tolerance (+/- psi)	Minimum Stroke <sup>2</sup> (%)
0.6	3/4	.0007	+	5052	7.5	2.5	70
1.0	1	.002	+	3003	10	2	70
1.2	1	.003	+	3003	25	5	70
1.0	3/8	.0007	+	5052	25	5	70
1.0	3/8	.0007	+	5056	35	5	70
1.6	3/8	.001	+	5052	45	4.5	70
1.8	3/4	.003	+	3003	45	4.5	70
1.6	1/4	.0007	+	5056	50	5	70
2.0	3/16	.0007	+	5052	75	7.5	70
2.3	3/8	.0015	+	5052	80	8	70
2.3	1/4	.001	+	5052	90	9	70
2.3	1/4	.001	+	5056	100	10	70
3.0	3/8	.002	+	5052	120	12	70
3.6	3/8	.003	+	3003	120	12	70
3.1	1/8	.0007	+	5052	130	13	70
3.4	1/4	.0015	+	5052	140	14	70
3.1	1/8	.0007	+	5056	170	17	70
3.7	3/8	.0025		5052	180	18	70
4.2	3/8	.003		5052	210	21	70
4.3	1/4	.002	+	5052	230	23	70
5.2	1/4	.003	+	3003	245	24.5	70
4.5	1/8	.001	+	5052	275	27.5	70
4.5	1/8	.001	+	5056	320	32	70
5.2	1/4	.0025		5052	330	33	70
5.4	3/8	.004		5052	350	35	70
5.7	3/16	.002	+	5052	380	38	70
6.0	1/4	.003		5052	420	42	70
5.7	3/16	.002	+	5056	440	44	70
6.1	1/8	.0015	+	5052	450	45	70
6.1	1/8	.0015	+	5056	535	53.5	70
8.1	1/8	.002	+	5052	700	70	70
8.1	1/8	FC	+	5052	750	75	70

<sup>1</sup> Crush Strength  
<sup>2</sup> Minimum Stroke  
 Tested per ASTM D726



Figure 4.12: Plascore CrushLite Configurations - From Ref. [54]

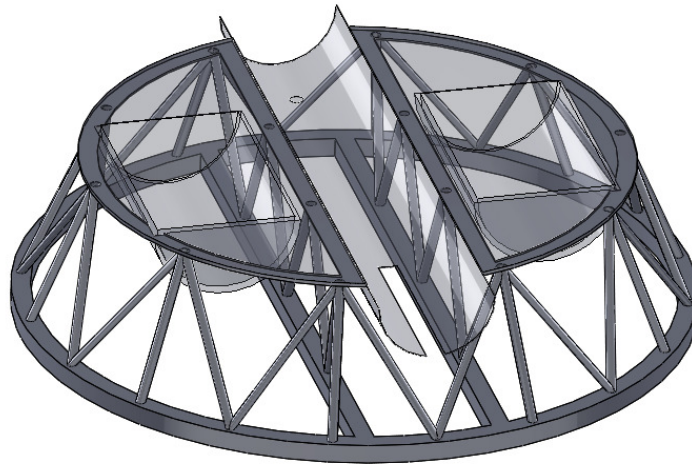


Figure 4.13: Landing Ring and Legs CAD Model

three crucial goals defined by the VEXAG community has been considered as a reference for the selection of the scientific instruments the lander is equipped with (see Section 2.3). The next paragraph provides details about the selected scientific instruments for addressing those goals and objectives, whereas the following one presents the design process followed

to develop the vessels used to contain those instruments.

### Scientific Instruments

The list of the selected scientific instruments for the proposed mission is presented:

- Neutral Mass Spectrometer (NMS)  
The Neutral Mass Spectrometer is intended to provide *in situ* measurements of isotopes of noble gas and ratios of the mixing gases. It includes 3 modules: an ion source that converts the molecules of the gas samples into ions; an analyzer of the mass that sorts the resulting ions by mass using electromagnetic fields; and a detector capable of quantifying the presence of each ion. The gas sample is collected through inlet ports located at the bottom of the pressure vessel and put into a reservoir inside the instrument. A picture of an existing Neutral Mass Spectrometer is shown in Figure 4.14.

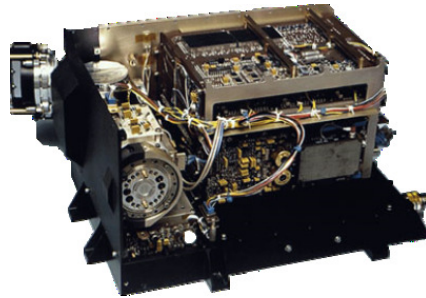


Figure 4.14: Neutral Mass Spectrometer - Courtesy NASA

- Tunable Laser Spectrometer (TLS)  
The Tunable Laser Spectrometer (TLS) is intended to measure trace of gases, including isotopes, especially of sulfur and hydrogen-based species such as the ratio of Deuterium/Hydrogen (D/H) inside the atmosphere. This type of instrument is capable of making high precision measurements thanks to its ability to scan at very high resolution ( $0.0001 \text{ cm}^{-1}$ ) over targeted spectral lines without those interferences that can influence the measurements of mass spectrometers.
- Raman/Laser Induced Breakdown Spectrometer (LIBS)  
This type of spectrometer provides measurements of the mineralogy and the elemental chemistry of the rocks on the Venusian surface. It utilizes a single laser to illuminates the object of interest and a single telescope to determine the vibrational modes of the same laser by observing the scattered return (the shift of the Raman wavelength). The instruments uses a view window on the side of the vessel in order to access to the observed area.

- **Magnetometer Sensors**

Magnetometer Sensors are used to verify or disprove the belief that Venus does not have a magnetic field since little data has been acquired in this area. This instrument is asked to determine the direction, the strength and the relative change of the magnetic field of Venus. A resolution requirement of a few nano-Tesla is needed in order to provide all the information required to address the questions about the Venusian magnetic field. The instrument is inside the payload vessel and does not need a boom. The sensors need an electronic box that can be allocated to a free position inside the pressure vessel.
- **Atmospheric Structure Investigation (ASI)**

This package consists of temperature and pressure sensors, and instruments such as anemometers and accelerometers. The package is designed in order to characterize the properties of the Venusian atmosphere (T, dT, P, E,  $\omega$ , H). The measurements performed by the instruments of the package collect data not only once on the surface, but also during the landing phase in order to get information about the vertical structure of the atmosphere as well. The sensors need to be located on the outside of the payload pressure vessel in order to work properly.
- **Camera System**

This package consists of 4 Panoramic Cameras, 1 Close Range Camera, 1 Descent Imager and 2 Data Compression Units (DCU). The goal of the system is to document all the phases of the mission from the detachment of the entry vehicle from the orbiter until the end of the life of the instruments on the surface. Currently, there is no regional synoptic image of the surface of Venus at visible or near-infrared wavelengths. A substantial new view of Venus' geology can be obtained by the successful acquisition of image data from a lander as it descends to the surface, something that has not been done in any previous Venus mission. Such data can be used to establish correlations with SAR images and identify additional units or clarify units and unit boundaries to determine stratigraphic relationships. Once on the surface, the panoramic imagers enable geologic investigations and the characterization of possible variability in rock types. The Close Range Camera is used to show the movements and the work of instruments and mechanisms such as the mechanical arm and the two drills. Each camera is placed inside the payload pressure vessel so that its Field Of View is not obstructed by anything and differs from the FOV of other imagers. The electronics box is placed in close proximity to all the cameras in order to minimize the length of the connecting wires.
- **Seismometer**

A Seismometer is an instrument used to measure the direction, intensity and duration of earthquakes detecting the actual movement of the ground. A seismometer basically measures the three vectors of the displacement field as a function of time caused by the passage of seismic waves. This instrument provides characterization of the current activity of Venus and the interior of the planet.
- **Life Detection Microscope**

The Life Detection Microscope is designed to search for possible *cells* in the regolith on

the Venusian surface, investigating regolith and dust particles through high-resolution images. In particular, this instruments detects organic compound that have the characteristic features of the terrestrial ones: life on Earth is characterized by cells, so the Life Detection Microscope is designed to search for them on the Venusian surface. The instrument is able to detect and characterize organic compounds by using a combination of fluorescent dyes.

The list of the properties, dimensions, mass and power needed by each instrument is presented in Table 4.16.

Scientific Instrument	Dimensions [mm]	Unit Mass [kg]	Quantity	Tot Mass [kg]	Power Needed [W]
Neutral Mass Spectrometer	260x160x190	11	1	11	50
Tunable Laser Spectrometer	250x100x100	5	1	5	17
Raman LIBS	300x300x300	13	1	13	80
Magnetometer Sensors	150x150x150	3	1	3	-
Electronic Box	70x30x30	3	1	3	7
Panoramic Camera	80x80x60	1	4	4	
Close Range Camera	80x80x60	1	1	1	12
Descent Imager	80x80x60	2	1	2	
Data Compression Unit	100x120x80	1.5	2	3	
Atmospheric Structure Investigation (ASI)	80x80x160	2	1	2	3.2
Seismometer	30x30x30	1	1	1	5
Life Detection Microscope	6.3 $dm^3$	7	1	7	30
<b>TOT</b>				<b>52</b>	<b>204.2</b>

Table 4.16: Scientific Payload Properties

As shown in that Table, the total mass results to be higher than 50 kg, therefore the

mission requirement related to the scientific payload (see Section 2.4) has been satisfied.

### Payload Containers

In order to protect the scientific payload from the external environment, two different Payload Containers have been designed. Each of them is different from the other since it is sized depending on the dimensions of the instruments inside it. Not only these containers are pressurized, but also they are covered by insulating layers and connected to the cooling system so that the system can adjust the internal conditions depending on the external factors acting on them.

As mentioned in the previous section, the instruments contained inside these pressure vessels are located so that their FOVs are not obstructed by anything; similarly, the pressure vessels are placed on the lander so that the same requirement is satisfied.

The working conditions the payload containers provide to the scientific instruments consist of 1.2 atm of pressure and 70 °C of temperature.

Each pressure vessel is made of Titanium Ti-6Al-4V because of its high strength even at high temperatures and its good acid resistance and is covered by insulating layers (see Section 4.2.5).

The Payload containers' shape has been determined in order to have the maximum optimization in terms of space and material needed to construct them. A sketch of the two payload containers on the lander is shown in Figure 4.15.

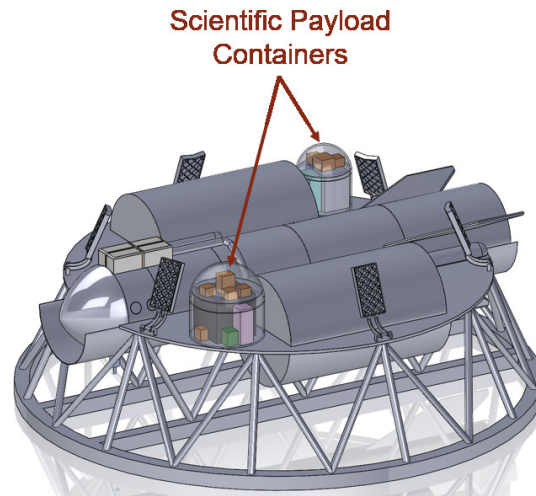


Figure 4.15: Payload Containers CAD Model

Structural analysis of the scientific payload containers has been performed in order to design the thickness and determine the mass of each pressure vessel. A cylindrical shape with hemispheric head has been designed and the properties of each container are presented in Table 4.17.

As mentioned before, each of the pressure vessel is made of Titanium Grade 5 (Ti-6Al-4V). The minimum thickness required is estimated using Equation 4.5. The masses of each so designed container is presented in Table 4.18.

	Container 1	Container 2
Internal Radius [mm]	240	175
Cylindrical Height [mm]	250	250
Internal Volume [ $m^3$ ]	0.0742	0.0353
Minimum Thickness Required [mm]	11	10

Table 4.17: Scientific Payload Containers Dimensions

	Container 1	Container 2
Mass [kg]	37.25	21.55

Table 4.18: Scientific Payload Containers Masses

### 4.2.5 Thermal Protection System

As seen in Section 1.2, the Venusian surface presents a unique thermal environment. The temperature is around 470 °C and the pressure is about 93 bar. The operational temperature limits of the electronics and the avionics of the lander of the proposed mission range between -20 °C and 70 °C. As mentioned in Section 4.2.4, each pressure vessel presents a 1.2 atm pressure, and natural convection is considered to take place in the interior of the vessels. The thermal strategy to protect the lander from the external heat and to dissipate the heat loads coming from the electronic instruments is to use not only insulating layers that cover each sensible part of the lander, but also to use a cooling system that keeps the operational conditions inside it.

#### Insulating Layers

The insulation layers provide the reduction of heat transfer between the Venusian environment and the components of the lander. The outer layers of the Thermal Protection System consist of:

- AZ-93 Paint  
AZ-93 Paint is developed by the company AZ Technology and is an inorganic white thermal control paint used on spacecrafts and satellites exposed to the effects of the space environment. This coating has already been tested and used extensively in space and it resulted to maintain its properties extremely well. It is characterized by low solar absorptance and high thermal emittance (see Table 4.19).
- Aerogel  
Aerogel is a material derived from a gel in which a gas has replaced the liquid component of the gel. The obtained material is ultralight, porous, synthetic and characterized by extremely low density and thermal conductivity [56]. The liquid part of the gel is extracted through supercritical drying in order to make it dry slowly

	Solar Absorptance	Infrared Emittance
AZ-93 Paint	0.122	0.916

Table 4.19: AZ-93 Paint Main Properties [55]

without collapsing the solid matrix of the gel due to capillary action, as it would happen through conventional evaporation. The name *Aerogel* refers to the fact that this material is made from gel and not to the fact that it has similar properties to gels. In fact, Aerogels are solid, rigid and dry materials. However, they are often referred as *friable* material, because they shatter like glass under high pressure even though they are very strong from a structural point of view.

Aerogel is basically formed by a solid network that contains air pockets, where the air represents the 99.8% of the entire material. As a result, the material is lightweight and has low thermal conductivity: not only it inhibits conduction because it is mostly composed of gas, but also it is good convective inhibitor because air cannot flow through the lattice. Main properties of Aerogel are presented in Table 4.20.

	Density [ $kg/m^3$ ]	Specific Surface Area [ $m^2/g$ ]	Max Operating Temperature [ $^{\circ}C$ ]	Thermal Conductivity [ $W/mK$ ]
Silica Aerogel	5 ÷ 20	500 ÷ 800	650	0.016 ÷ 0.03

Table 4.20: Aerogel Main Properties [56]

- Titanium Grade 5 (Ti-6Al-4V)  
As mentioned in the previous sections, the lander is mostly made of Titanium Grade 5 (Ti-6Al-4V). This is one of the most used alloys in the Titanium industry. As suggested by the text in brackets, it is composed of 90% Titanium, 6% Aluminum and 4% Vanadium. As seen from Table 4.10, it has very high tensile strength, low thermal conductivity, high modulus of elasticity, high corrosion resistance and good weldability. This is the main layer of every component of the lander and the thermal protection system is basically designed to protect this layer as the most important from the structural point of view.
- Teflon  
An internal layer of Teflon (PTFE) is designed in order to lower the heat leaks coming from the external environment and to retain the sulfuric acid typical of the Venusian atmosphere. Teflon, in fact, is able to retain the sulfuric acid even at high temperature. Teflon is a synthetic fluoropolymer of tetrafluoroethylene with excellent acid resistant properties and high melting temperature (around 327  $^{\circ}C$ ). Even if the temperature on the Venusian surface is higher than the maximum one Teflon is able to sustain, its use is justified by locating it as the most internal layer of the Thermal Protection System. Therefore, not only it can protect from the sulfuric acid infiltrations and the heat leaks (it is characterized by low thermal conductivity as well) the

interior of the pressure vessel where it is used, but also, it is cooled and kept to a sustainable temperature by the cooling system.

Table 4.21 presents the main properties of Teflon.

	Density [ $kg/m^3$ ]	Melting Temperature [°C]	Max Operating Temperature [°C]	Thermal Conductivity [W/mK]
Teflon (PTFE)	2200	327	270	0.25

Table 4.21: Teflon (PTFE) Main Properties

After having defined the properties of the insulating layers that compose the Thermal Protection System, a thermal analysis of the heat rate from the external environment toward the pressure vessels has been performed. A sketch of the problem is shown in Figure 4.16.

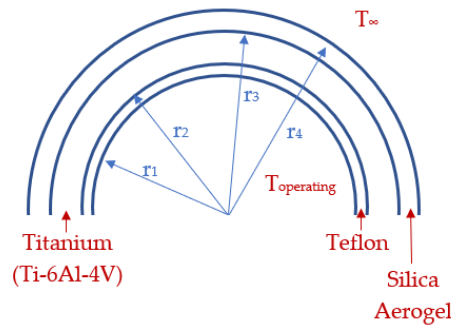


Figure 4.16: Insulating Layers Sketch

The analysis has been performed referring to a thermal resistance diagram, as shown in Figure 4.17.

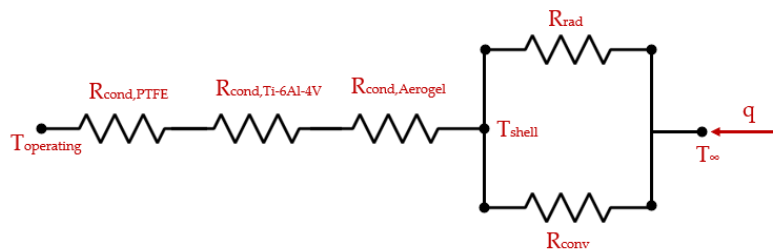


Figure 4.17: Thermal Resistance Diagram of Lander Pressure Vessels

where

$$q = \frac{T_{\infty} - T_{operating}}{R_{cond,PTFE} + R_{cond,Ti-6Al-4V} + R_{cond,Aerogel} + \frac{R_{conv} \cdot R_{rad}}{R_{conv} + R_{rad}}}$$

$$R_{conv} = \frac{1}{4\pi r_3^2 h}$$

$$h_{conv} = 274 \frac{W}{m^2 K}$$

$$R_{rad} = \frac{1}{4\pi r_3^2 h_{rad}}$$

$$h_{rad} = \epsilon \sigma (T_{\infty}^2 + T_{operating}^2) (T_{\infty} + T_{operating})$$

$$R_{cond} = \frac{1}{4\pi k} \left( \frac{1}{r_i} - \frac{1}{r_{i+1}} \right)$$

Then, the thickness of each layer has been estimated and the results are presented in Table 4.22.

Layer	Thickness [mm]
Teflon PTFE	25
Ti-6Al-4V	11
Aerogel	22

Table 4.22: Insulating Layers Thicknesses

## Cooling System

The cooling system used for the proposed mission is represented by an already existing strategy based on venting consumable fluids into an environment which is characterized by higher pressure than the vapor pressure related to the temperature of the pressure vessel interior. The technology has been developed by Advanced Cooling Technologies, Inc. (see Ref. [57]).

Figure 4.18 shows the refrigerating system based on the mentioned venting concept, which can be divided into two main parts: a venting-based cooling system designed to reject the heat loads from the interior of the pressure vessel and a heat guarding system that manages the heat leaks that come from the external environment.

This venting-based cooling system includes two pressurized vessels: a two-phase working fluid is contained in the primary vessel, where the vapor is mixed with a pressurized gas (Helium in this case) that comes from the secondary vessel and serves as pressurizer. Two valves are used to control the pressure and the temperature of the system and a venting valve is used to control the venting of the consumable fluid and its recharging.

The system works in cycles (Figure 4.19):

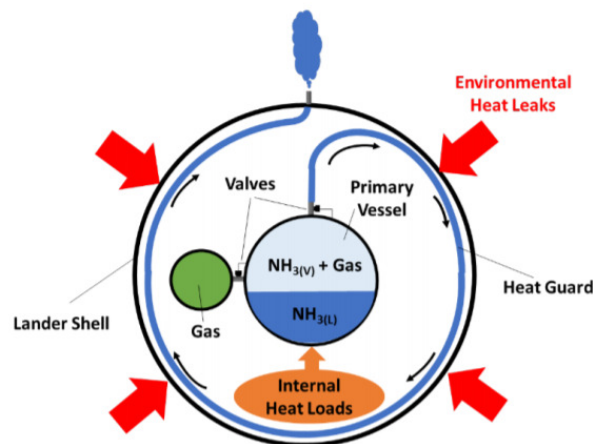


Figure 4.18: Thermal Management System Concept - Ref. [57]

- **Heat Acquisition**  
The heat load coming from the instruments and the heat leaks from the external environment make the liquid working fluid to vaporize inside the primary vessel. As a result, the density of the vapor and the total pressure within that vessel increase.
- **Venting**  
The temperature of the primary vessel starts increasing and when it reaches the set point, as a consequence, the total pressure within the vessel is higher than the Venus ambient and the venting valve is opened. The mixture of fluid composed by the consumable working fluid and the compressed gas is ejected and that causes the total pressure to decrease making room for compressed gas that charges the vessel.
- **Gas Recharging and Evaporative Cooling**  
As mentioned before, the pressurized gas recharges the primary vessel thanks to the opening of the valve that divides the secondary vessel and the primary one: in fact, as the pressure inside the primary vessel decreases, and the fluid mixture is ejected, the valve opens and the compressed gas at higher pressure flows inside the primary vessel inducing the liquid working fluid to evaporate and the total pressure to increase. Once the internal pressure reaches the set point, the valve closes and the cycle starts again.

An important design parameter of the system is the set temperature of the primary vessel (in this case  $\sim 70$  °C), because it determines the amount of sensible heat capacity the fluid mixture is able to absorb while flowing within the payload pressure vessel before being vented away.

The study conducted by Advanced Cooling Technologies, Inc. (ACT) tested 24 hours consumable-based cooling system for Venus lander using different combinations of working fluid and pressurizing gas. The most effective is represented by Ammonia as working fluid and Helium as pressurizing gas: a total mass of 18 kg (4.5 kg of Ammonia and 13.5 kg of Helium) is required to reject 150 W of heat loads coming from electronic instruments and

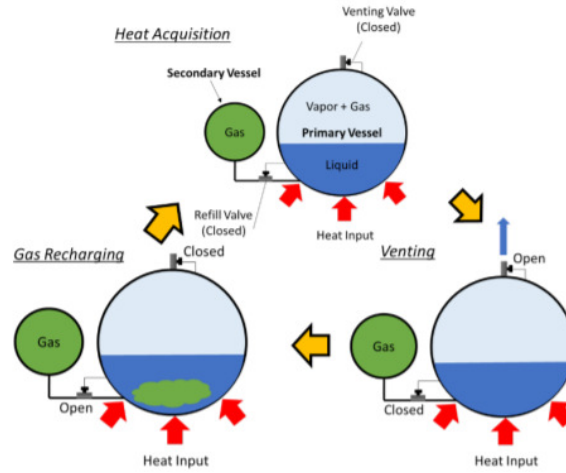


Figure 4.19: Cooling System Cycles - Ref. [57]

keep a 112 cm-diameter vessel internal temperature at 70 °C for 24 hour by venting in the 93 bar Venusian atmosphere [57].

Therefore, basing on the dimensions of the payload vessel of the lander, an estimation of the amount of Ammonia and Helium required for the proposed mission has been developed and the results are reported in Table 4.23. Lastly, a structural design of the Ammonia and

	Payload Container 1	Payload Container 2
Set Temperature [°C]		70
Environment Temperature [°C]		470
Environment Pressure [bar]		93
Venting Pressure [bar]		97
Vessel Internal Diameter [cm]	48	35
Ammonia Required	2.71	1.83
Helium Required	1.14	0.91

Table 4.23: Insulating Layers Thicknesses

Helium tanks has been developed: the volume of those containers and their thicknesses (using Eqs. 4.2-4.5) have been estimated as well as their masses, as presented in Table 4.24.

## 4.2.6 Mechanisms

The lander’s primary mechanisms are those responsible for the soil and atmospheric samples collection. These mechanisms serve to collect, store and organize the samples. In particular, two different drills, one telescopic and another attached to a mechanical arm are designed to collect from the Venusian surface enough samples in order to satisfy the mission requirements seen in Section 2.4, while the atmosphere is collected inside cylindrical containers thanks to piston-based mechanical actuators. All the samples are, then,

Component	Internal Volume [ $m^3$ ]	Tank Thickness [mm]	Tank Mass [kg]
Ammonia Tank 1	0.0004	4	2.17
Ammonia Tank 2	0.0003	4	1.72
Helium Tank 1	0.0006	7	3.06
Helium Tank 2	0.0005	6	2.61
<b>TOT Mass</b>			<b>9.56</b>

Table 4.24: Ammonia and Helium Cooling System Tanks

kept inside proper capsules that can withstand the temperatures and the pressures (the conditions in general) of both the Venusian and the space environment.

The two drills used for the proposed mission are both produced by Honeybee Robotics and differ from the type of function of the samples: in particular, the telescopic drill operates with a discrete function with the target of collecting 10 different samples with a total depth of penetration of at least 10 cm, whereas the drill attached to the robotic arm operates with a continuous function collecting 20 different samples with a depth of 5 cm for each penetration.

The drills consist of rotary-percussive rock sampling drills with high temperature (HT) electromagnetic actuator (Figure 4.20) and are powered by 2 brushless DC motors. This type of drill has already been successfully dynamometer tested to operate at Venus surface temperature ( $\sim 470$  °C) [58].

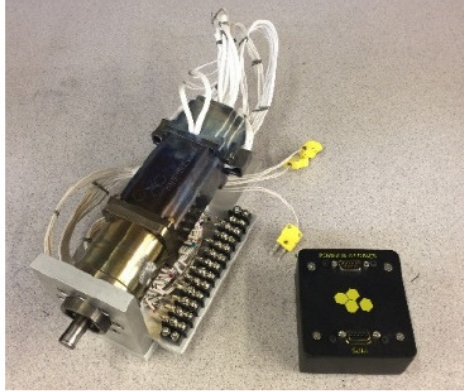


Figure 4.20: Honeybee HT actuator with remote (i.e., room temperature) interface electronics - Ref. [58]

Both the drills are connected to the samples handling capsules through a pneumatic system which is designed to transfer the drill cutting to the proper container thanks to the hollow interior of the drill (Figure 4.21).

Basing on the specifications of the Honeybee Robotics developed drills, the total number of samples collected by each drill and the estimated time of operations have been determined in order to design the movements of the mechanical arm so that the mission requirements that concern the soil samples collection are satisfied (Table 4.25).

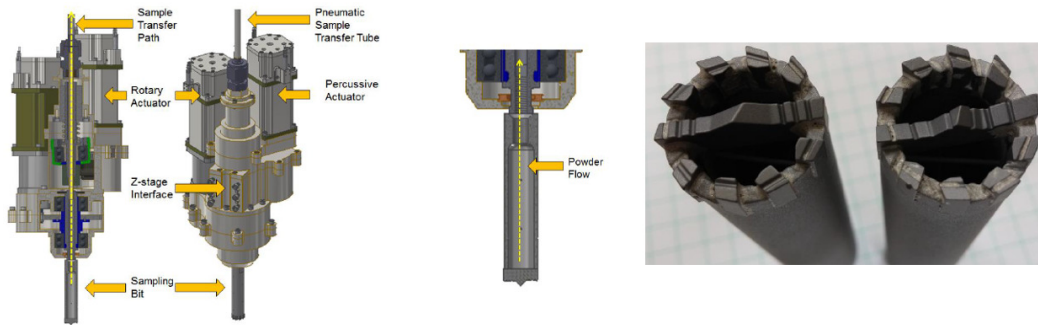


Figure 4.21: Sketches of the Pneumatic Transfer System Concept - Ref. [59]

	Robotic Arm Drill	Telescopic Drill
Number of Collected Samples	20	10
Depth of each Penetration [cm]	5	1
Type of Sunction of each Penetration	Continuous	Discrete
Mass of each Sample [g]	26	48.5
Total Mass Collected [g]	520	485
Rate of Penetration [cm/min]	1.45	0.4
Total Drilling Time [min]	69	25

Table 4.25: Samples Drilling Performances

### Mechanical Arm Drill

As seen in Section 2.4, the soil samples collection requirements include:

- Return to Earth or Earth vicinity at least one kg of Venus regolith from top 10 cm.
- Return to Earth or Earth vicinity at least ten distinct samples distributed over at least 10  $m^2$ .
- Return to Earth or Earth vicinity samples distributed from the top 10 cm.

In order to collect samples distributed over at least 10  $m^2$ , it is clear that either a set of multiple fixed drills or a mechanism that allows a drill to move is needed. However, fixed drills may not be the best solution because the orientation of the lander after the descending and landing phase may be different from the expected one because of non-uniformity of the surface or even because of small masses of regolith. That is why, it is important to provide the lander with a moving drill. In particular, the mechanical arm is designed in order to cover an area of at least 10  $m^2$ , to be robust enough to carry the drill and to be made of a material with excellent thermal and sulfuric acid resistance properties. That is why, even if much denser than Titanium, Waspaloy has been used to design the mechanical arm (see Section 4.1.4 as well as Table 4.8).

The mechanical arm is composed of multiple rods and joints that allow them to rotate in order to move the drill over the Venusian surface. In particular, the arm consists of two

main rods, whose length is 1.26 m (Figure 4.22), that are able to draw a  $204^\circ$  angle with a maximum radius of 1.36 m. The mass of the mechanical arm has been estimated, basing on the developed CAD model and the properties of the material it is made of (Table 4.26).

Component	Total Mass [kg]
Mechanical Arm	21.76

Table 4.26: Mechanical Arm Estimated Mass

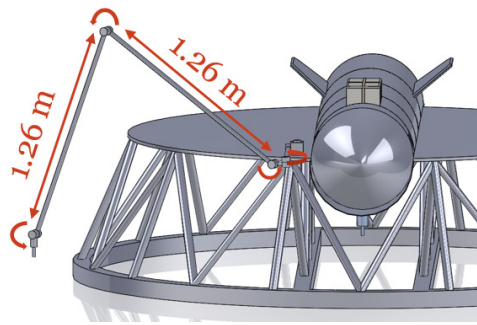


Figure 4.22: Detail of the Mechanical Arm Rods

As mentioned in the previous section, the mechanical arm drill is designed to collect 20 samples from the Venusian surface. A total area of  $10.25 \text{ m}^2$  is covered by the mechanical arm and the proposed samples location over this area are shown in Figure 4.23.

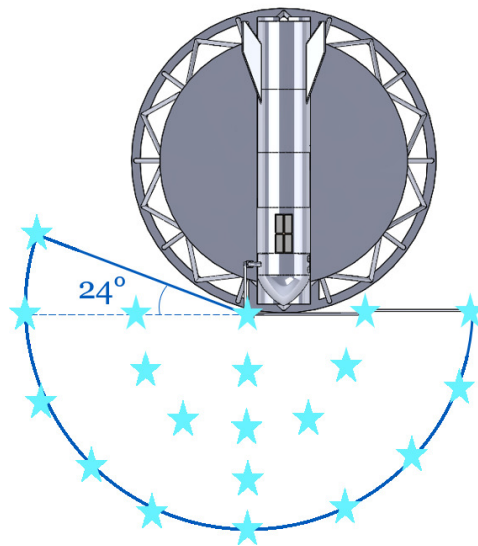


Figure 4.23: Sketch of the Collected Soil Samples Locations

### Telescopic Drill

The telescopic drill is located under the upper stage of the Venus Ascent Rocket and is directly connected through valves to the payload room inside it. A telescopic drill is needed because the drill needs to move along the Z-axis during the penetration and because the drill must be *compressed* during all the mission phases in order not to be damaged during the journey toward the Venusian surface. As mentioned before, the minimum required mass of soil samples to be collected is 1 kg, which is too much for a single drill, and that is why the telescopic drill is added to the lander: it helps the drill attached to the mechanical arm to collect enough samples to satisfy the mission requirements (see Section 2.4). As mentioned before, the telescopic drill is developed by Honeybee Robotics and differs from the drill attached to the mechanical arm for the type of suction: in fact, the telescopic drill is designed to collect a total amount of 10 samples from the top 10 cm of the Venusian surface (each 10 different penetrations characterized by 1 cm depth), whereas the mechanical arm drill performs 20 different penetrations (each characterized by 5 cm depth each) with a continuous suction each. Figure 4.24 shows the telescopic drill in its two configurations: compressed and extended.

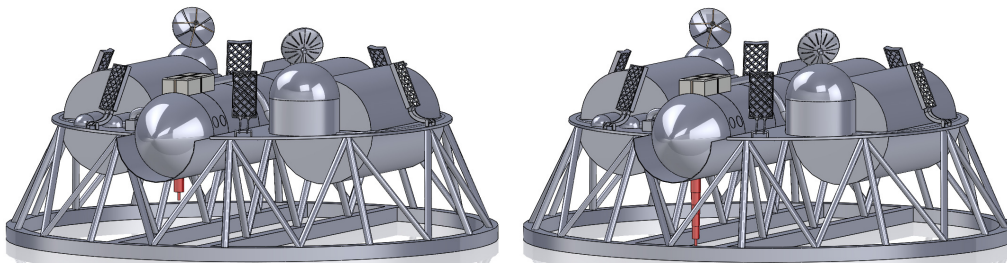


Figure 4.24: Telescopic Drill Compressed (left) and Extended (right)

### Atmospheric Samples Collecting System

The Atmospheric Samples Collecting System is designed to collect 1 cubic liter of Venus atmosphere from the surface and 1 cubic liter of Venus atmosphere from an altitude of about 40 km above the surface. The former is logically collected once the lander has reached the Venusian surface and the operative phase has started, while the latter is collected during the ascent phase. In particular, the cubic liter of atmosphere from an altitude of 40 km could be collected during the descent phase, however, the atmosphere that surrounds the lander during the descent phase may be chemically modified because of the velocity and the friction of the falling lander (as seen from Section 3, the parachute is detached at 45 km of altitude above the Venusian surface). That is why, the system is designed to collect the atmospheric sample during the ascent phase, when the velocity of the ascent rocket carried by the ascending balloon is low and the atmosphere is not contaminated for sure by the motion of the lander.

The atmospheric sample collecting system basically consists of two cylindric capsule equipped with a moving piston that helps the suction of the atmosphere: the movement of the piston inside the cylindrical container opens the valve that divide the capsule from the external

environment and the atmosphere starts flowing towards the cylindrical container. Once the piston arrives at the end of its path, the valve closes and the atmospheric sample is kept inside the capsule. An actuator (the piston) is needed to mechanically open and close the valve in order to control the flow of air. Figure 4.25 shows the piston that operates inside the capsule.

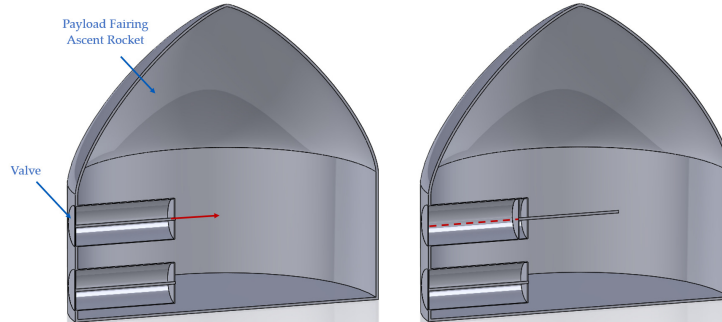


Figure 4.25: Sketches of the Atmospheric Collecting System Concept

### Samples Containers

The sample containers are represented by the capsules that are designed in order to keep the collected samples safe and intact. Two different types of capsules have been designed: the soil samples capsules and the atmospheric samples capsules. The former are cylindrical, attached to a samples handling rotating system that allows to separate them and to put the planetary material into the proper capsule. This system is rigid so that the integrity of each sample is guaranteed and a stable acquisition can be performed. Thanks to the pneumatic system that connects the drills to the capsules and to a set of valves that control the flow of materials, the samples are, then, collected separately without any contaminations. As seen from Table 4.25, the samples collected by the two drills are different and that is why the respective capsules are different as well. In Table 4.27 are presented the characteristics of the soil samples capsules.

	Telescopic Drill	Mechanical Arm Drill
Single Sample Density [ $kg/m^3$ ]	2700	2700
Single Sample Mass [g]	48.5	26
Single Sample Volume [ $m^3$ ]	$1.80 \cdot 10^{-5}$	$9.63 \cdot 10^{-6}$
Cylindrical Capsule Height [mm]	80	50
Cylindrical Capsule Radius [mm]	9	8
Number of Capsules	10	20

Table 4.27: Soil Samples Capsules Properties

As mentioned previously, the sample collecting system is designed in order to separate each soil sample from the others. A handling rotating system allows a stable collection without

contaminations between the various samples. Figure 4.26 shows a proposed concept for the samples handling system.

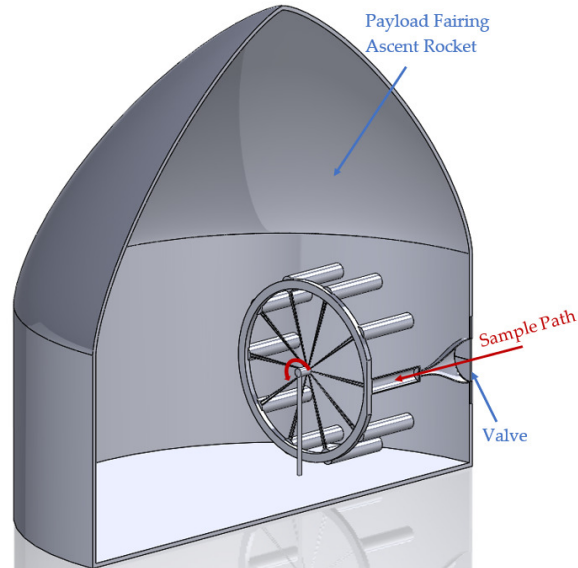


Figure 4.26: Soil Samples Handling System Concept

In particular, while the drill is cutting and the powder is collected, the higher pressure of the Venusian environment pushes the sample and opens the valve, so that the planetary material flows toward the capsule. On the other hand, while the mechanical arm moves and there is no material flowing inside the pneumatic system, the valve is closed and the system rotates so that the next sample is pushed toward an empty capsule.

The other type of capsules are those designed to keep safe and intact the atmospheric samples. As seen from Section 2.4, they have to contain at least 1 cubic liter of Venusian atmosphere each. The CAD model of these containers has already been shown in Figure 4.25 and have been designed so that the internal volume is equal to 1 cubic liter. As for the atmospheric samples there is no need to design a handling system supposed to separate the samples, because two different capsules with two different valves have been designed. The characteristics of the atmospheric samples containers are summarized in Table 4.28. The thickness of these capsules must withstand the difference of pressure between the internal part and the external environment.

### 4.2.7 Communication System

The antennae the landing vehicle is equipped with are used not only to send the data collected by the scientific instruments, but also to send information about the spacecraft health to Earth. The lander is in direct contact with Earth while it is in line of sight with the terrestrial ground stations. Otherwise, the orbiter relays data from the lander to Earth. The antennae on the lander must remain functional for at least 24 hours. In order to monitor the spacecraft during all phases of the mission, NASA's Deep Space Network (DSN) is used. It is important to underline that the mission is mostly autonomous, even

	Atmospheric Sample at 0 km	Atmospheric Sample at 40 km
Sample Density [ $kg/m^3$ ]	66.35	4.30
Volume Required [ $m^3$ ]	0.001	0.001
Cylindrical Capsule Height [mm]	200	200
Cylindrical Capsule Radius [mm]	40	40
Number of Capsules	1	1

Table 4.28: Atmospheric Samples Capsules Properties

the rendezvous between the ascent vehicle and the orbiter: digital cameras and omnidirectional S-band antennae are designed in order to provide the data required for an autonomous rendezvous.

Two steerable high-gain antennae and two low-gain antennae are located on the lander (Figure 4.27) and connected to those instruments that transmit data.

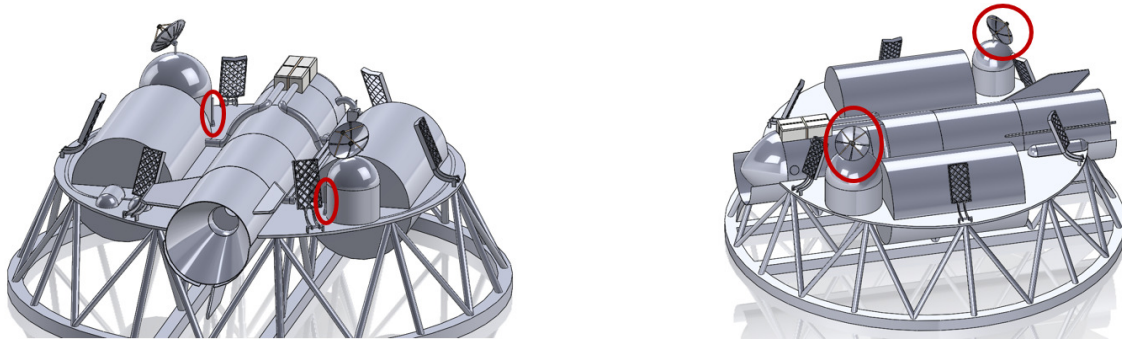


Figure 4.27: Low-Gain Antennae (Left) and High-Gain Antennae (Right) Locations

The steerable High-Gain Antennae use an X-band signal and a frequency around 80 GHz so that NASA's Deep Space Network (which is basically the monitoring agent on Earth during the entire mission) can pick up the data. They require 60 W of power so that they can operate.

#### 4.2.8 Power System

Power generation on Venus surface is almost impractical due to the harsh conditions that may damage or even cause failure to any active or moving parts. Moreover, since the thick and dense Venusian atmosphere is an obstacle for the sunlight, the use of solar panels in order to generate power is impractical. Therefore, primary batteries represent the most reliable choice for a lander power supply. The number and the mass of the batteries depend on the power requirements of the instruments, the electronics and the avionics of the lander. In particular, a set of battery is required for each payload vessel an additional one is needed by the ascent vehicle in order to perform all the designed operations and maneuvers. As seen in Section 2.4, the scientific payload is asked to be operational for at least one Earth day. Thus, the scientific instruments must be supplied by the batteries for at

least 24 hours. On the other hand, the batteries needed by the rocket and the balloon (e.g. for the deployment system) must operate for the time of descending, samples collection and ascending, which is around 8 hours.

However, none of the state of art batteries are capable of being operational for extended durations on the Venusian surface. Even using considerable insulation, the existing batteries could support the lander for a maximum time of a few hours (that was the case of the Russian Venera series and Vega 2 landers). High Temperature-resilient And Long-Life (Hi-TALL) primary batteries are used for the proposed mission. Based on Li-Si anode,  $FeS_2$  cathode and Alkali metal halide eutectic electrolyte, these batteries are supposed to be inherently stable in environments with up to 500 °C temperature, high  $CO_2$  concentration and 93 bar pressure. These batteries are currently being developed by NASA-JPL [60] and their performance target are summarized in Table 4.29.

	Gen-1 Batteries	Gen-2 Batteries
Performance Target	100 Wh/kg	150 Wh/kg
Operational Life at 500 °C	15 days	30 days
High Capacity Anode	Li-Si	Li-rich formulation
High Energy Cathode	$FeS_2$ or $CoS_2$	$FePS_3$ or $CoPS_3$
Electrolyte (500 °C)	Alkali Metal Halide Eutectic	All Li-ternary eutectic

Table 4.29: HiTall Batteries Target Performances - Ref. [60]

In order to determine the quantity of batteries needed by the lander, a power budget of all the scientific instruments and the electronics of every component has been performed. In particular, the drilling system, which includes a mechanical arm, the attached drill and a telescopic drill, operates for 69 minutes, as seen from Section 4.2.6, while the scientific instruments and the related subsystems operate for at least 24 hours. Tables 4.30 to 4.34 present the power budget each component of the landing vehicle.

Instrument	Power [W]	Time of Operations [hr]	Power Required [W · hr]
Telescopic Drill	180	0.417	75
Robotic Arm	30	1.15	34.5
Mechanical Arm Drill	210	1.15	241.5
<b>TOT</b>			<b>351</b>

Table 4.30: Drills Power Budget

Basing on the properties of the chosen batteries (seen in Table 4.29), the masses of the batteries needed by each component have been estimated and are presented in Table 4.35.

Instrument	Power [W]	Time of Operations [hr]	Power Required [W · hr]
Tunable Laser Spectrometer	17	24	408
Raman LIBS	80	24	1920
ASI	3.2	24	76.8
Camera System	12	24	288
Seismometer	5	24	120
Computer	5.5	24	132
<b>TOT</b>			<b>2944.8</b>

Table 4.31: Scientific Payload (Container 1) Power Budget

Instrument	Power [W]	Time of Operations [hr]	Power Required [W · hr]
Neutral Mass Spectrometer	50	24	1200
Magnetometer System	7	24	168
Camera System	12	24	288
Life Detection Microscope	30	24	720
Computer	5.5	24	132
<b>TOT</b>			<b>2508</b>

Table 4.32: Scientific Payload (Container 2) Power Budget

As a result almost 70 kg of HiTALL batteries are needed.

It is important to underline that those batteries are located inside the proper pressure vessel: those used by the scientific payload are contained inside the payload containers, those used by the ascent vehicle are contained inside the payload fairing of the ascent rocket and so on.

Instrument	Unit Power [W]	Quantity	Tot Power [W]	Time of Operations [hr]	Power Required [W · hr]
HGA Antenna	60	2	120	24	2880
LGA Antenna	35	2	70	24	1680
<b>TOT</b>			<b>4560</b>		

Table 4.33: Communication System Power Budget

Instrument	Unit Power [W]	Quantity	Tot Power [W]	Time of Operations [hr]	Power Required [W · hr]
Computer	5.5	1	5.5	6	33
ADCS Sensors	4	8	64	6	192
Ignition	2	2	4	-	-
<b>TOT</b>			<b>225</b>		

Table 4.34: Ascent Vehicle Power Budget

Component	Battery Mass Needed [kg]
Drills	2.34
Scientific Payload 1	19.63
Scientific Payload 2	16.72
Communication System	30.4
Ascent Vehicle	1.50
<b>TOT</b>	<b>69.6</b>

Table 4.35: Batteries Mass Budget

## 4.3 Venus Ascent Vehicle

The Venus Ascent Vehicle is composed of all those components of the lander that are designed to ascend from the Venusian surface in order to carry the collected samples on orbit. In particular, it includes an ascending balloon and the Venus Ascent Rocket.

As seen from Section 3.5, the Venus Ascent Vehicle is lifted off from the Venusian surface thanks to a Helium inflated balloon that is designed to carry the ascent rocket up to an altitude of about 51 km above Venus’s surface. Here, the environmental conditions are much less harsh than on the surface so the rocket can perform the maneuver to reach the altitude of the orbiting vehicle in order to perform the rendezvous with it: in fact the conditions of temperature and pressure on the Venusian surface are too tough for a rocket to perform a burn.

This section describes the calculations and the preliminary estimations made in order to design an ascent vehicle that can successfully carry the collected samples up on orbit to

rendevous with the orbiter and return back to Earth.

### 4.3.1 Venus Ascent Balloon

As mentioned in Section 1.2, the environmental conditions of the Venusian atmosphere are unique and very harsh. However, goal of this research has been to try to take advantage of those conditions in designing the various strategies to successfully satisfy the mission requirements. Therefore, the high-temperature, pressure and density Venusian atmosphere that does not allow a rocket to perform any burns is exploited to develop an alternative concept: a balloon that uses the buoyant force to lift off from Venus surface, could possibly carry the rocket up to an altitude where the pressure, temperature and density are lower so that it can perform the maneuver to reach the orbiting vehicle's altitude.

The preliminary design of the proposed ascending balloon included different steps:

- Requirements Definition

First of all, it is necessary to determine the goals and the targets of the ascending balloon. Obviously, it must be able to withstand the environmental conditions, such as the 470 °C temperature, 93 bar pressure, sulfuric acid concentrations and high windspeed. Then, it is important to define which is the most suitable altitude for the balloon to reach. In fact, the higher it is and the stronger are the winds and the higher is the sulfuric acid concentration in the atmosphere (Figure 4.28), the heavier is the lifting gas, the bigger is the balloon and so on; on the other hand, though, the higher is the balloon target altitude and the lower is the mass of propellant needed by the rocket, the lower are pressure and temperature and the lighter is the rocket. Therefore, a trade-off analysis must be performed (we will see it later on) in order to better quantify those pros and cons and determine the best choice for the proposed mission.

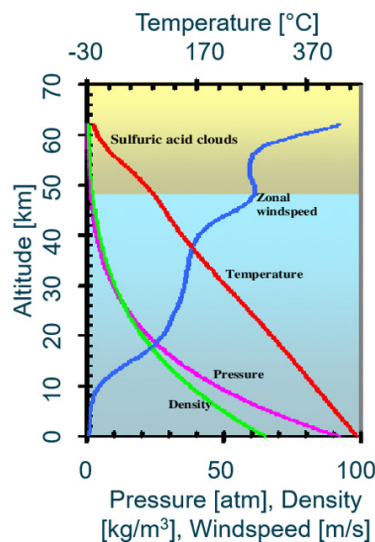


Figure 4.28: Venus's Atmosphere Overview

- Balloon Type Definition

The second task of the balloon designed for the proposed mission concerns the definition of the type of balloon. In particular, among all the standard balloon types (e.g. superpressure, zero pressure, weather, hot air balloon), two concepts could possibly be suitable for this mission: the superpressure balloon and the zero-pressure balloon. The former, has been used in the Soviet Vega program to fly in the Venusian atmosphere; this is basically a sealed, constant volume balloon where the balloon changes pressure instead of volume; it is filled with a measured amount of gas which creates sufficient free lift to reach the desired altitude. On the other hand, the zero pressure balloon is open at the bottom and have open ducts hanging from the sides so the gas is allowed to escape in order to prevent the pressure inside the balloon from building up during gas expansion as the balloon rises above Venus's surface; as the balloon rises, the gas inside it expands because the atmospheric pressure surrounding the balloon drops. The main advantage of a zero-pressure balloon with respect to a superpressure balloon is the opportunity to vent out the gas: in the case of superpressure balloon (which is a closed system), in fact, the excess gas would determine excessive pressure acting directly on the skin of the balloon that can ultimately cause it to rupture. Therefore, thanks to the open ducts that allow the gas in excess to escape, zero-pressure balloons minimize the pressure acting on the film and make possible the realization of large balloons constructed from thin and lightweight films. That is why a zero pressure balloon has been chosen for the proposed mission.

- Balloon Materials Definition

The list of the requirements for the ascending balloon is directly "translated" into a list of properties the material the balloon is made of must be characterized by. Those include Low gas permeability, Acceptable pinhole seaming, Acceptable fabrication and folding, Toughness in tear resistance, High specific strength, Resistance to sulfuric acid, Maintenance of mechanical properties at high altitude.

Finding a single material that could be used to produce balloon film that can satisfy all the balloon requirements is nearly impossible. That is why, in addition to the balloon film, other protecting layer are added so that the balloon can withstand the environmental conditions of the Venusian atmosphere during the ascent.

As for the balloon film material, a list of possible solutions is presented in Table 4.36.

Comparing the data it becomes clear that the best option for the balloon film material is represented by Zylon (PBO). This is a synthetic polymer invented and developed by SRI International during the 1980s and is produced by Toyobo Corporation. It has already been used for high-altitude balloon science due to its low weight, high tensile strength and thermal properties. PBO is characterized by a rigid-rod molecular structure (Figure 4.29) that provides the material the strength and stiffness of a composite with no interface problems between the fiber and the matrix.

Zylon does not have a melting temperature nor a glass transition temperature and it is characterized by a high resistance to corrosive chemicals. Figure 4.30 shows how strength and temperature of PBO change with temperature.

As seen from Section 1.2, the temperature on the Venusian surface is around 470 °C, so Figure 4.30 shows that PBO retains about 28% of strength and 36% of modulus

Material	Tensile Strength [MPa]	Specific Strength [kN·m/kg]	Max Working Temperature [°C]
Zylon	5800	3766	650
P-Aramid (HM)	2800	1931	550
PBI	400	285.7	550
M-Aramid	650	471.1	400
Teflon	23	10.45	260
Kevlar	3600	2500	180
Vectran	2900	2071	160
HDPE	3500	3608	150

Table 4.36: Potential Balloon Film Materials - Ref. [62], [61]

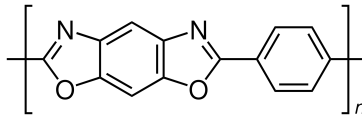


Figure 4.29: PBO Chemical Structure

at a nearly 100 °C higher temperature than that on Venus surface. However, a single film layer of PBO would not be sufficient for the balloon to withstand the harsh conditions of the Venusian environment. In particular, sulfuric acid tests performed on PBO films have shown how profound are the effects on the mechanical properties of the material due to the corrosive environment: it loses nearly 75% of its strength. That is why, additional protecting layers have been designed in order to keep the balloon film operational. The best choice for corrosive protection is represented by a noble metal coating; however, this has a high thermal conductivity, therefore, a heat transmission protective layer needs to be applied as well. On the other hand, Fluoropolymers have satisfactory acid resistance properties, but are characterized by poor heat resistance. A list of possible corrosive protection layer is listed in Table 4.37.

The best option is represented by metal coatings. In particular, gold provide excellent corrosive protection for less mass than titanium. The problems with metal coatings are related to the difficulty to adhere to the balloon materials and to the high thermal conductivity coefficient. Basing on the information from Ref. [64], physical vapor disposition process can be used to bond the protective metal layer onto the surface of the balloon material underneath. Therefore, gold has been chosen to be the most external layer of the balloon. Other two layers are applied: one, made of superwool, that provides heat transmission protection and the other made of aluminum that is used to reduce the lifting gas permeability of the balloon. The resulting configuration along with the thickness properties of each layer is presented in Figure 4.31.

- Potential Lifting Gases

In order to select the best choice among all the possible lifting gases the balloon can

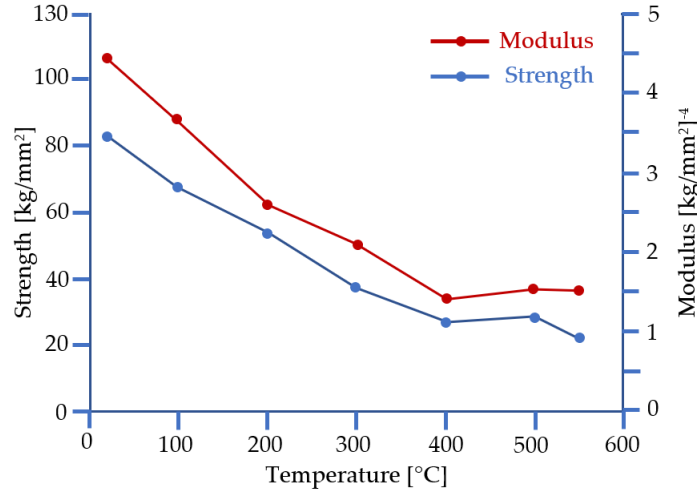


Figure 4.30: Strength and Modulus versus Temperature - Ref. [63]

Material	Density [ $kg/m^3$ ]	Coating Mass [ $g/m^2$ ]	Thermal Conductivity [ $W/(m K)$ ]	Max Operating Temperature [°C]
PFA	2150	27	0.25	260
PTFE	2200	27.5	0.25	260
Gold	19300	2.32	310	-
Titanium	4500	2.35	17.5	600

Table 4.37: Potential Corrosive Protection Materials

use to ascend from the Venusian surface, estimations about the balloon size, the balloon mass and the lifting gas mass have been performed and after having compared the results, the most suitable option has been selected. In particular, three gases have been chosen as potential ones because of their light mass and lower density than the external Venusian atmosphere: Hydrogen, Helium and Ammonia.

Hydrogen is the lightest existing gas and, because of that, it seems to be the most suitable gas for lifting. Moreover, it can be produced in large quantities by electrolysis of water. However, there are some disadvantages related to the use of Hydrogen: it is flammable and, since it is characterized by small molecular size, it can easily diffuse through many materials causing the quick deflation of the balloon.

Helium is the second lightest existing gas and, because of that, it represents an attractive solution for lifting as well. The most important advantage is that this gas is noncombustible. While, the disadvantages in using Helium are related to the cost (it is expensive) and the same diffusion problem of Hydrogen (Helium has a small molecular size).

Lastly, Ammonia, which is sometimes used for weather balloons. It is very cheap to obtain and easily transportable. However, it is relatively heavy and can damage many metals and plastics.



Figure 4.31: Balloon Layers Specifications

The analysis and the comparisons of the performances of those three potential lifting gases will be shown later on.

- Balloon Shape Definition

After having defined the balloon type, another important task concerns the definition of the shape of the balloon. In particular, two different configurations have been selected as potential ones: spherical shape and natural shape.

The spherical shape is the most efficient in terms of used surface area for a given volume. However, the concerns for the Spherical Shape Balloon are the film stresses occurring during deployment and partial inflation, and the maintenance of the spherical shape during the ascent.

The natural shape concept is based on the fact that all the tensions in the balloon film is carried in the meridional direction and the circumferential stress is assumed to be zero. A Natural Shape Balloon can be partially inflated and automatically changes its shape depending on the altitude (Figure 4.32). That is why this concept is preferred than the spherical one or the other shapes to design the proposed ascending balloon.

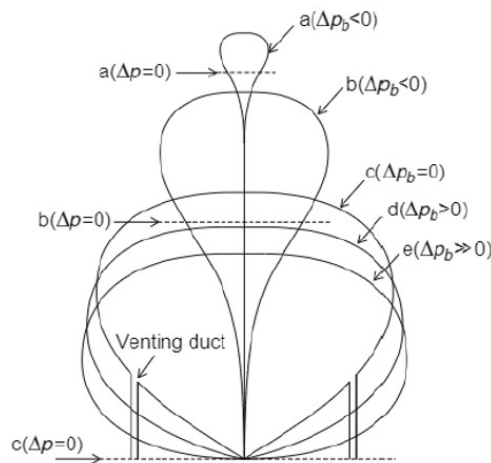


Figure 4.32: Natural Shape Balloon Evolution During the Ascent - Ref. [47]

- Balloon Design

After having selected the materials and the properties of the ascending balloon, the

design itself has been developed. In particular, as mentioned before, an important design parameter is represented by the target altitude the balloon must reach, which corresponds to the altitude of the first burn of the Venus Ascent Rocket. In order to make this decision, a trade off between the variation of the balloon and the rocket performances and the disadvantages due to the environmental conditions of the Venusian atmosphere has been performed. As it can be seen from Figure 4.33, the lifting gas mass and the size of the balloon needed to reach an altitude above 50 km increase exponentially with the altitude (Figure 4.33 presents the results with Helium as the lifting gas, however the calculations have been performed for Hydrogen and Ammonia as well, and have shown similar results).

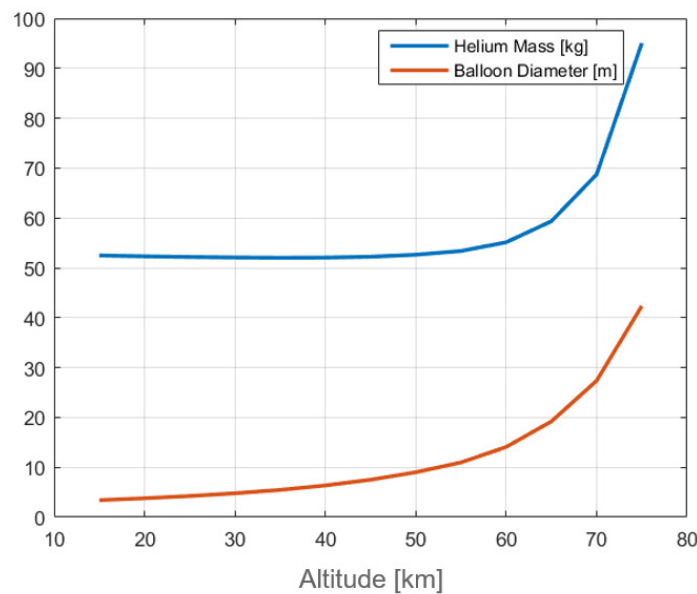


Figure 4.33: Balloon Characteristics vs Altitude

Another important parameter in order to better select the proper target altitude for the balloon are related to the propellant required by the rocket in order to perform the impulse at that altitude. In the range of the first 80 km above the Venusian surface, the parameter that mostly influences the amount of propellant needed by the rocket is represented by the drag losses. In fact, as seen from Section 1.2, the density of the atmosphere on Venus surface is 50 times higher than that on Earth at the sea level. Therefore, the drag losses in terms of additional  $\Delta V$  the rocket would need have been estimated with respect to the altitude above the Venusian surface and the results are presented in Figure 4.34.

Lastly, it is important to take into account the variations of the properties of Venus atmosphere with respect to the altitude above the surface. In fact the higher is the altitude and the stronger are the winds, the lower is the altitude and the higher are pressure and temperature and so on. Figure 4.35 shows the variation of the average windspeed versus the altitude within the Venusian atmosphere while the variations

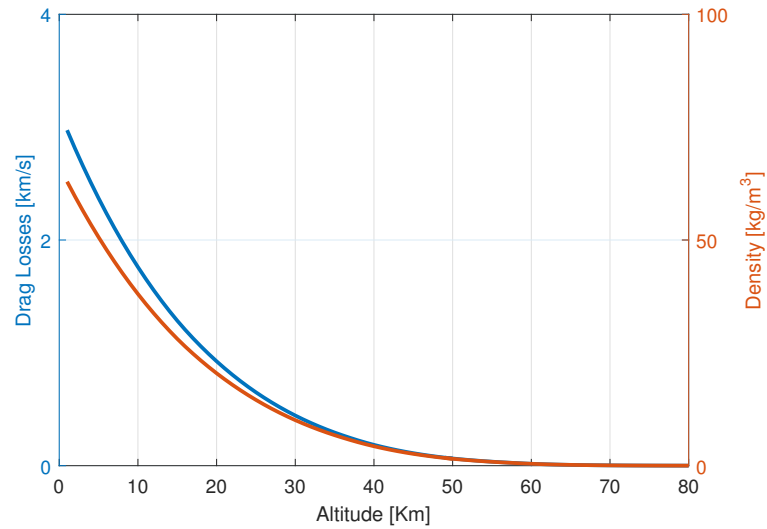


Figure 4.34: Drag Losses and Atmospheric Density vs Altitude

of pressure and temperature, according to the Venus Global Reference Atmospheric Model [44] are presented in Figure 4.36.

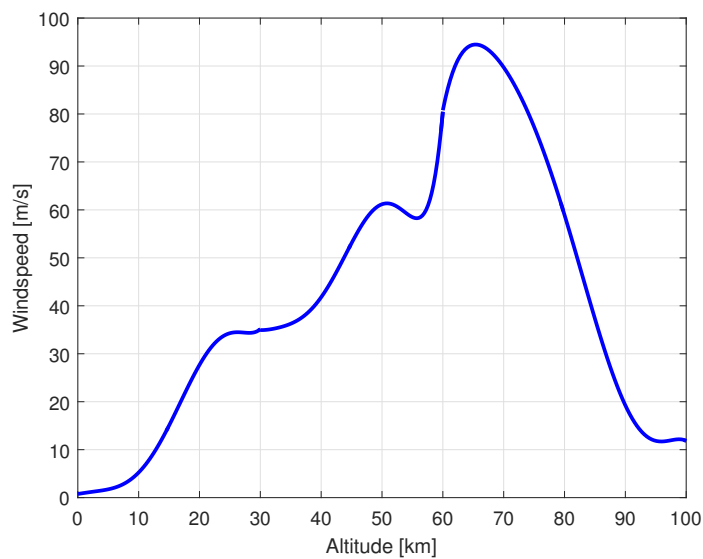


Figure 4.35: Average windspeed versus altitude within the Venus atmosphere - Ref. [65]

Comparing all these results and taking into account the presence of sulfuric acid within the Venusian atmosphere (as Seen from Figure 4.28), which is better to avoid with the balloon, a range of possible suitable target altitude for the balloon has been identified between 50 and 52 km of altitude above the Venusian surface. In particular, specifications of the atmospheric parameters and the sizing of both the balloon and

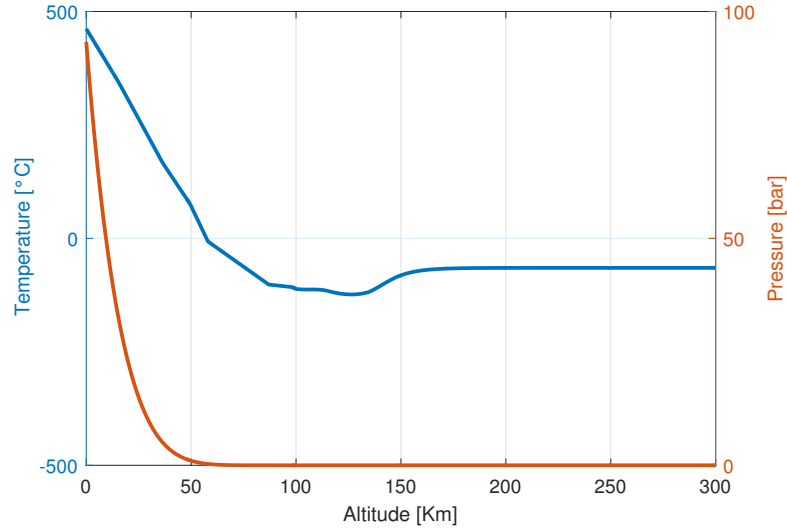


Figure 4.36: Temperature and Pressure versus altitude within the Venus atmosphere

the rocket for those target altitude are presented in Table 4.38.

Target Altitude [km]	Pressure [Pa]	Temperature [°C]	Rocket Mass [kg]	Helium Mass [kg]	Balloon Mass [kg]	Balloon Ideal Radius [m]
50	100510	71.02	498.1	52.5	20.3	4.42
51	87673	61.3	497.7	52.7	21.9	4.59
52	76170	51.59	497.2	52.9	23.6	4.76

Table 4.38: Balloon Potential Target Altitudes

All these results considered, a balloon target altitude of 51 km has been selected for the proposed mission, so that the rocket can perform the impulse maneuver in a environment with not-too-low pressure and the balloon mass and size are not too high.

The results presented so far have concerned only helium as the lifting gas, however, as mentioned previously, a comparison between the mass of gas needed, the size and the mass of the balloon has been performed considering all the three potential lifting gas listed previously: Hydrogen, Helium and Ammonia (Helium resulted to be the best choice, that is why the results reported so far concern Helium only).

The sizing of the balloon has been done in iterative steps calculating the mass to be lifted, the target altitude to be reached, the balloon film thickness and the resulting dimension and mass of the balloon itself. The main equations used for the analysis are basically represented by the buoyancy force (Eq. 4.11) and the ideal gas law (Eq. 4.12).

$$b_g = (\rho_a - \rho_g)g \quad (4.11)$$

$$PV = MRT \quad (4.12)$$

where  $b_g$  represents the effective buoyancy force per unit volume (the net upward force) that is generated by the difference between the density of the lifting gas inside the balloon and the surrounding atmosphere.

Together with these equations, it is necessary to have the expressions of the variations of atmospheric pressure, temperature and density with the altitude above the Venusian surface (Figure 4.37).

Model of Venusian Atmosphere, 0 to 100 km		
Geopotential Altitude, h (km')	Molecular-Scale Temperature, T <sub>M</sub> (K)	Pressure, P (Pa)
(-3)-15.5	735.00 - 7.63 × h	9332000 × [735.000 / (735.000 - 7.63 × h)] (46.353 / -7.63)
15.5-36.5	748.02 - 8.47 × h	3214540 × [616.735 / (616.735 - 8.47 × (h - 15.5))] (46.353 / -8.47)
36.5-49.5	691.08 - 6.91 × h	499392 × [438.865 / (438.865 - 6.91 × (h - 36.5))] (46.353 / -6.91)
49.5-58	830.175 - 9.72 × h	107458 × [349.035 / (349.035 - 9.72 × (h - 49.5))] (46.353 / -9.72)
58-87	456.4735 - 3.27687 × h	29634.9 × [266.415 / (266.415 - 3.27687 × (h - 58))] (46.353 / -3.27687)
87-98.3745	214.8174 - 0.499214 × h	57.7754 × [171.386 / (171.386 - 0.499214 × (h - 87))] (46.353 / -0.499214)
Density, ρ (kg/m <sup>3</sup> ) = P/(RT <sub>M</sub> ) Speed of sound, C (m/s) = (γRT <sub>M</sub> ) <sup>1/2</sup>		
Specific gas constant, R = 191.357 J/kg-K Specific heat ratio, γ = -8.175E-10 T <sub>M</sub> <sup>3</sup> + 0.000001665 T <sub>M</sub> <sup>2</sup> - 0.001233 T <sub>M</sub> + 1.5336		

Figure 4.37: Model of Venusian Atmosphere, 0 to 100 km - Ref. [66]

Initial size estimates for the balloon sizing have been made using the mass of the rocket alone. Then, iterations that include the mass of the balloon as well as the one of the lifting gas have been performed in order to update at every cycle the design parameters of the balloon. The mass of the lifting gas required to reach 51 km of altitude have been calculated for Hydrogen, Helium and Ammonia (Table 4.39) as well as the dimensions of the balloon at the target altitude (Figure 4.38).

Lifting Gas	Lifting Gas Mass Required [kg]	Balloon Mass [kg]
Hydrogen	24.5	21.1
Helium	52.7	22.0
Ammonia	424	41.2

Table 4.39: Balloon Potential Target Altitudes

As it can be clearly seen by those estimations, Ammonia results to be too heavy for the mission, while Hydrogen and Helium does not differ too much in terms of dimensions of the balloon. However, as mentioned before, Hydrogen is difficult to handle because it is flammable and its molecules are characterized by smaller size than the

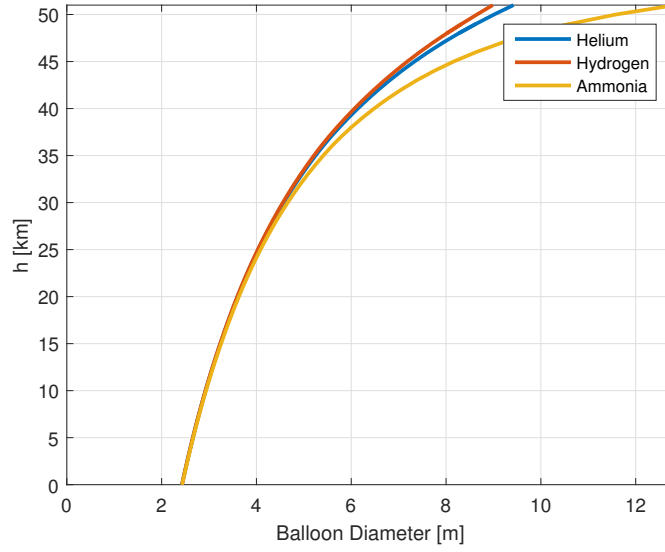


Figure 4.38: Balloon Diameters with different Lifting Gases Comparison

Helium one so there is an existing risk of losing gas during the ascent because of a non perfect permeability of the balloon materials. Thus, even if Hydrogen is lighter than Helium, the latter has been chose for the proposed mission.

Other two tasks have been performed in the design of the ascending balloon: the determination of the evolution of the balloon shape during its ascent and the estimations of the time of flight and other parameter related to its trajectory during the ascent.

A MATLAB spreadsheet model has been developed in order to evaluate the evolution of the shape of the balloon during its ascent. Figure 4.39 shows the so calculated shape of the balloon at the target altitude of 51 km above the Venusian surface, whereas Figure 4.40 presents the evolution of the natural-shape balloon during the ascent.

- Balloon Ascent Trajectory

As mentioned before, the last task of the balloon design concerns the calculations of some parameters related to its trajectory, such as the time of flight and the average rate of ascent. In order to perform this study, the equations that describe the vertical motion of a zero pressure balloon have been derived. In particular, when a balloon ascends in still air (free lift is positive), the equation for motion in the vertical direction can be written as follows

$$\left(m_g \tilde{M} \tilde{T}_g\right) + F_z = 0 \quad (4.13)$$

where  $m_g$  is the lifting gas mass,  $\tilde{M}$  is the molecular weight of the lifting gas of interest (Helium in this case),  $T_g$  is the temperature of the lifting gas,  $m_t$  represents the total balloon system mass (including the lifting gas mass) and  $F_z$  is the net force in the vertical position.

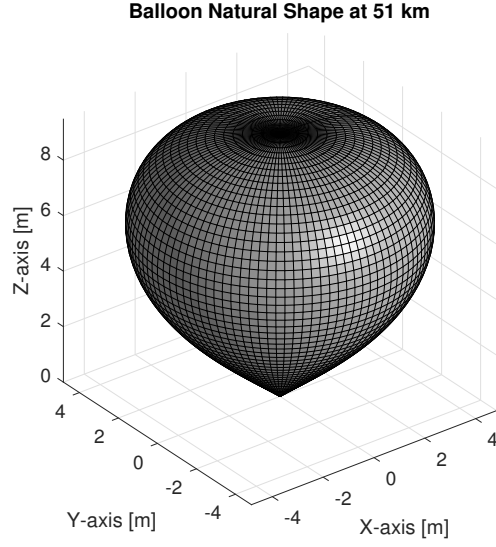


Figure 4.39: Balloon Shape at the target altitude of 51 km above the Venusian surface

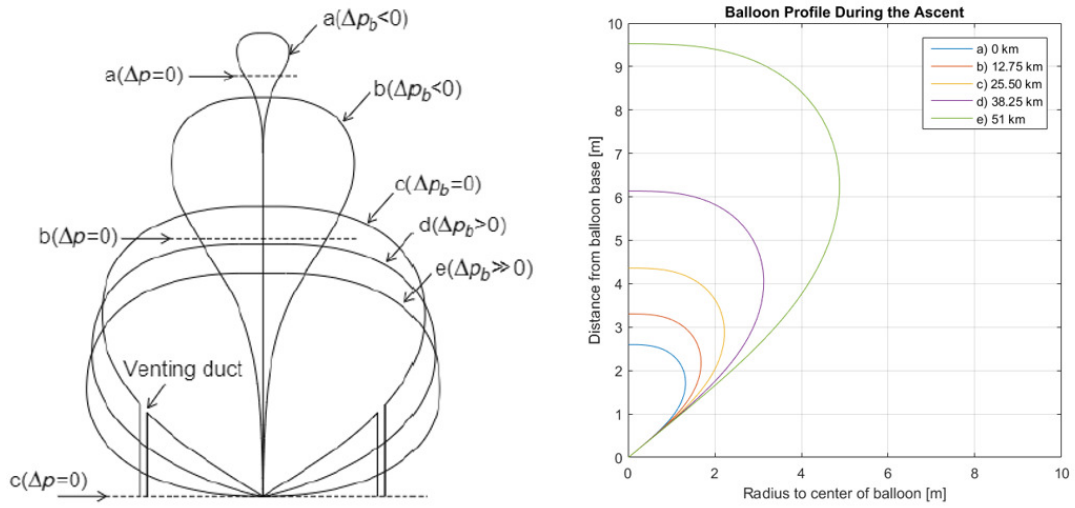


Figure 4.40: Balloon Profile During the Ascent

If we make use of the expression

$$V_b = m_g \frac{\tilde{M}\tilde{T}_g}{\rho_a} \tag{4.14}$$

the balloon's average rate of ascent is given by the following expression (which takes into account the drag force as well)

$$v_{bz}^2 = 2 \frac{m_g \tilde{M}\tilde{T}_g - m_t}{\rho_a C_D A_b} g \tag{4.15}$$

And using this parameter assuming a constant rate of ascent, the time for the balloon to reach the target altitude of 51 km above the surface has been estimated. The results are presented in Table 4.40.

Lifting Gas	Average Rate of Ascent [m/s]	Total Time of Ascent [hrs]
Helium	2.57	5.51

Table 4.40: Balloon Ascent Characteristics

Lastly, using the data related to the variations of the average windspeed with the altitude (Figure 4.35, Ref. [65]), the vertical motion of the balloon has been evaluated with and without the influence of the winds. The results are presented in Figure 4.41.

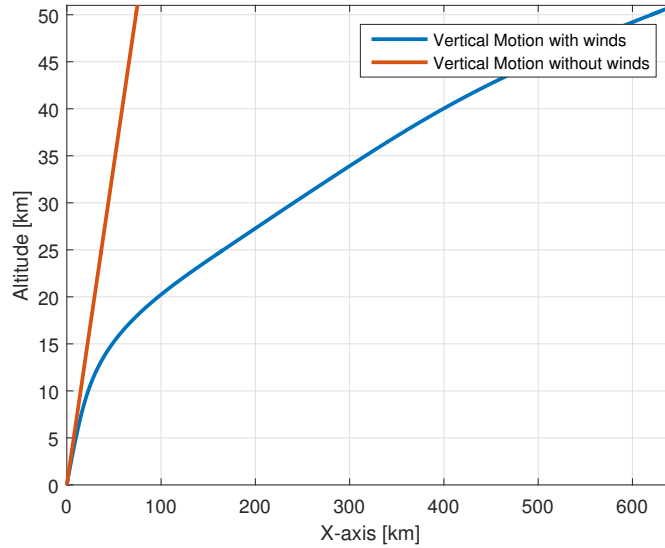


Figure 4.41: Balloon Vertical Motion

Therefore, a complete design of the balloon supposed to carry the ascent rocket with the collected samples to a target altitude of 51 km above the Venusian surface has been performed. Helium has been chosen as lifting gas due to its light molecular weight and its noncombustible properties. The final balloon configuration is characterized by a natural shape zero pressure balloon with three layers (gold, superwool and aluminum) used to protect the thin balloon film made of PBO. The balloon weights about 22 kg and has a radius of 4.6 m at its maximum extension (reached at the target altitude of 51 km above the Venusian surface). The total mass of lifting gas required to reach the target altitude is around 50 kg of Helium. The total time of ascent is around 5 hour and 30 minutes with an average rate of ascent of about 2.57 m/s.

Table 4.41 summarizes the final balloon specifications determined through the whole balloon design process described before.

Lifting Gas	Helium
Required Mass of Lifting Gas [kg]	52.7
Balloon Film Material	Zylon (PBO)
Balloon Mass [kg]	22.0
Balloon Radius at 51 km [m]	4.59
Average Rate of Ascent [m/s]	2.57
Total Time of Ascent [hrs]	5.51

Table 4.41: Final Balloon Specifications

### 4.3.2 Venus Ascent Rocket

The section that follows concerns the studies and the analyses developed in order to obtain a preliminary design of the potential Venus Ascent Rocket.

In general, arriving upon an optimized Venus Ascent Rocket design complete with all relevant masses and performance values requires an iterative approach between the evaluation of the subsystems performances and 3-DOFs or 6-DOFs numerical analysis (which can involve the trajectory, the aerodynamics, the engine dynamics, etc.) of the vehicle; in this chapter the process is simplified by treating the ascent problem as a two-burn transfer from the altitude reached with the Venus Ascent Balloon to the desired orbit. Due to the high thrust and short burn times, this assumption can be considered as quite valid.

The study of the Venus Ascent Rocket includes important aspects that must be taken under consideration in order to develop a functional design that is able to successfully fulfill the very delicate phase related to the carrying of collected samples to the orbiting vehicle's orbit, lifting off from the Venusian surface. Therefore, the Venus Ascent Rocket represents a crucial component in the proposed sample return mission and must be characterized by a compact shape where its systems and subsystems (structure, avionics, propellant, thrusters, nozzles) match and work together correctly so that the tasks of this phase can be successfully completed. That is why the research (that is described in this chapter) involved the types of propulsion systems (solids, liquids, hybrids and gelled), the trajectory design, the motor casing and the nozzles preliminary analysis, the insulating materials and the casing structure, the nosecone shapes and so on.

The entire work related to the Venus Ascent Rocket for the proposed mission can be divided into two main categories: the rocket trajectory design and the design of the rocket itself. The former has included the evaluation of the mass of propellant needed, the flying path followed by the rocket along with the preliminary evaluation of all the parameters of the ballistic trajectory. While, on the other hand, the design of the rocket itself included the definition of the casing and insulating materials, the nosecone shape, the nozzles design as well as the evaluation of a preliminary mass budget and the dimensions of the rocket. However, before going into details of this work, an important consideration must be made. In fact, before designing a rocket and its trajectory, it is crucial to understand which type of propulsion the rocket will use. As mentioned before, researches and studies have been conducted in order to understand how and why choose a type of propulsion instead of another.

- Solid Propulsion

In case of solid propulsion, the Venus Ascent Rocket must be at least a two-stages rocket because, since each stage can ignites just one time and cannot be restarted multiple times, a mono-propellant configuration would not be able to perform two impulses, but just one. And since, the best strategy in order to insert into the orbiting vehicle's orbit is to perform a first maneuver that allows the rocket to reach the target altitude and a second burn that circularizes the trajectory and insert the rocket on orbit, the monopropellant configuration does not represent the best solution for the proposed mission. Moreover, the monopropellant design is characterized by lower performances than the more-than-one stage configurations and presents a bigger structure that does not ensure good balance to the entire vehicle.

The advantages of a solid propulsion system are related to the simplicity and the reliability due to the use of a motor made of a single element and fewer parts that compose the entire system. On the other hand, solid propellants are very expensive to produce and require considerable labor and time to assemble [67] and are characterized by limited  $I_{sp}$  with respect of other types of propulsion system.

- Liquid Propulsion

The liquid propulsion represents the most efficient type of propulsion system. Moreover, it is characterized by a high level of control and is cheaper than solid propulsion. The ignition can be stopped and restarted and the specific impulse is higher than the one of solid propellants. However, there are some important disadvantages related to this type of propulsion. First of all, they are characterized by relatively high values of minimum allowable flight temperature and could suffer the high temperature of the Venusian surface during the operative phase of samples collection. Because of this issue, liquid propulsion has not been taken under consideration for the design of the Venus Ascent Rocket for the proposed mission. By the way, other issues in using the liquid propulsion are related to its complexity due to the presence of fuel tanks, pumps and injection nozzles.

- Hybrid propulsion

The hybrid propulsion typically includes a solid fuel and a liquid oxidizer. This is an interesting concept that presents high efficiency, simplicity and moderate cost. However, has drawbacks due to limitation in  $I_{sp}$  and performances and has no known flight experience, being a very immature technology compared to the liquid or solid propulsions [67].

All these studies considered, the solid propulsion has been selected for the Venus Ascent Rocket of the proposed mission, because, even if less efficient and more expensive than the other configurations, it presents fewer parts, lower complexity and higher reliability for the harsh environmental conditions of the Venusian environment. In particular, a two-stages configuration has been designed for the rocket so that each stage corresponds to a different maneuver, since the solid propulsion can be ignited just one time and cannot be stopped and restarted. The two maneuvers the rocket is designed to perform basically consist of a first impulse that allows the Venus Ascent Rocket to reach the orbiting vehicle's altitude and a second burn that circularizes the trajectory in order to insert in the target orbit. Table 4.42 summarizes the properties and the data of the target orbit the Venus Ascent Rocket is designed to insert into.

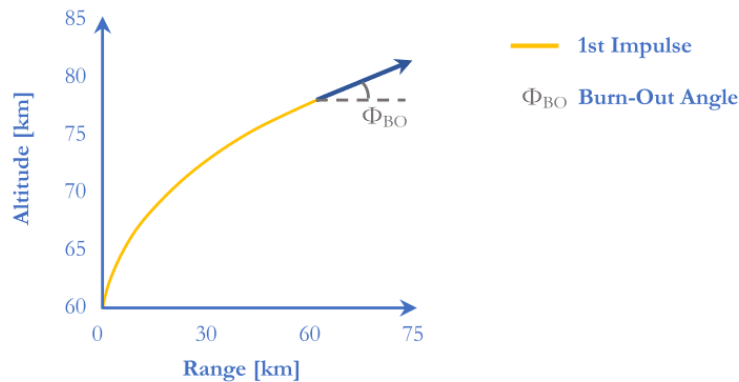
Orbit Type	Circular
Orbit Radius [km]	300
Orbit Inclination [°]	25

Table 4.42: Venus Ascent Rocket Target Orbit

## Trajectory Design

As seen in Section 3, the Venus Ascent Rocket is designed to be lifted off and carried up to an altitude of 51 km above the Venusian surface by the Venus Ascent Balloon, where it performs the first of two maneuvers in order to reach the orbiting vehicle’s orbit. Most of the total  $\Delta V$  required by the rocket is represented by the velocity necessary for the first impulse, leaving only a small burn to the second burn used to circularize the trajectory and insert on orbit.

Two different and extreme situations can be realized by the rocket: it is possible to perform a Hohmann transfer that launches the vehicle with a  $0^\circ$  elevation and reaches the orbit  $180^\circ$  later or the rocket can launch vertically to the desired altitude and then perform a  $90^\circ$  turn to reach the circular orbital velocity. Otherwise, launch angles between  $0^\circ$  and  $90^\circ$  lead to intermediate ascent trajectory profiles with various  $\Delta V$  split between the two stages distributions. The angle that determines the path-to-orbit is the flight path angle at the burn out of the first stage, as shown in Figure 4.42. This angle is designated  $\phi_{BO}$  and is what determines the total  $\Delta V$  as well as the  $\Delta V$  split between the two stages of the rocket.

Figure 4.42: Definition of Burn Out Angle  $\phi_{BO}$ 

In order to calculate the  $\Delta V$  required by the rocket to get to the target orbit, we need to determine the velocity necessary (in an inertial reference frame) from the 51 km altitude above the Venusian surface where the Venus Ascent Rocket performs its first burn. This,

of course, depends on  $\phi_{BO}$ :

$$\Delta V_{1,rel} = \sqrt{\frac{2(V_C^2 - V_0^2)}{\left[\left(\frac{V_C}{V_0}\right)^2 \cos(\phi_{BO})\right]^2 - 1}} \quad (4.16)$$

where  $V_C$  and  $V_0$  are the circular velocities at altitude  $h$  and  $h_{BO}$ , respectively:

$$V_C = \sqrt{\frac{\mu_V}{r_V + h}} \quad V_C = \sqrt{\frac{\mu_V}{r_V + h_{BO}}}$$

and  $r_V$  is the radius of Venus.

Since the Venus Ascent Rocket lifts off from the surface of Venus carried by the Venus Ascent Balloon, the velocity derived from the rotation of Venus must be taken into account. In particular, since a sidereal day on Venus lasts 2802 *hrs* (Ref. [43]), we can easily evaluate Venus's rotational Velocity and the westward velocity at the lift off site on the surface

$$\omega_V = \frac{2\pi}{2802 \cdot 3600} = 6.229 \cdot 10^{-7} \text{ rad/s}$$

$$V_{venus} = \omega_V r_V \cdot \cos(Lat) = 0.0038 \text{ km/s}$$

where *Lat* is the latitude of the lift off site.

The *SEZ* reference frame is used to represent the inertial velocity vector, so we can calculate each component as it follows (Eq.(4.17)-(4.18)-(4.19)):

$$V_S = -\Delta V_{1,rel} \cos(\phi_{BO}) \cos(Az) \quad (4.17)$$

$$V_E = \Delta V_{1,rel} \cos(\phi_{BO}) \sin(Az) - V_{venus} \quad (4.18)$$

$$V_Z = \Delta V_{1,rel} \sin(\phi_{BO}) \quad (4.19)$$

where *Az* represents the azimuth needed to achieve the desired orbit inclination  $i$  from the lift off latitude and can be calculated by

$$Az = \arcsin[\cos(i) \cdot \cos(Lat)]$$

Note that in Eq.(4.18) the contribution of  $V_{venus}$  is removed from  $V_E$ .

Therefore, the magnitude of the ideal impulsive change of velocity  $\Delta V$  required at the burn-out altitude is given by

$$\Delta V_{1,id} = \sqrt{V_S^2 + V_E^2 + V_Z^2}$$

On the other hand, the  $\Delta V$  needed to circularize the trajectory and to insert in the desired orbit after the coast phase is given by the difference between the horizontal component of the Venus Ascent Rocket velocity and the circular velocity the the given altitude,  $V_C$ :

$$\Delta V_2 = V_C - \Delta V_1 \frac{r_V + h_{BO}}{r_V + h_{BO} + h} \cos(\phi_{BO}) \quad (4.20)$$

As said before, Eq.(4.20) assumes a circular final orbit. So if required, any orbit may be targeted by replacing  $V_C$  with the velocity needed at that point in the orbit.

Therefore, we can evaluate the ideal (minimum)  $\Delta V$  required to insert into the desired orbit for a given  $\phi_{BO}$ :

$$\Delta V_{tot,id} = \Delta V_{1,id} + \Delta V_2$$

After having determined the equations and the expressions useful to estimate the first and the second  $\Delta V$  required to reach an insert into the target orbit, an estimation of the losses in terms of  $\Delta V$  needs to be performed.

Losses can be divided into 2 main categories:

- Gravity Losses

The gravitational loss is generally due to the finite nature of a rocket impulse. It is a function of the impulse time ( $t_b$ ) and is basically equal to the magnitude of the thrust needed to oppose the effect of gravity during the burn. In particular, the duration of the impulse can be estimated by

$$t_b = I_{sp}g \frac{M_{prop}}{T} \quad (4.21)$$

where  $I_{sp}$  represents the specific impulse,  $g$  is the gravitational acceleration,  $M_{prop}$  is the mass of the propellant used during the impulse and  $T$  is the magnitude of the thrust.

The losses due to gravity in terms of  $\Delta V$  is then given by [68]

$$\Delta V_{GL} = gt_b \sin(\phi_{BO}) \quad (4.22)$$

where  $t_b$  represents the time of the rocket burn and  $\phi_{BO}$  is the flight path angle at the first stage burnout. The longer are the burns and/or the more vertical is the ascent and the larger are the gravity losses.

- Drag Losses

In order to calculate the actual drag losses, a detailed knowledge of the Venus Ascent Rocket geometry, drag coefficients versus Mach number, atmospheric models, etc need to be possessed, However, since the Venusian atmosphere above 51 km of altitude is quite thin, the drag represents only a small fraction of the total  $\Delta V$  losses to get to orbit. In general, drag losses increase with increasing velocity and lower burnout angles. Therefore, lower burnout angles not only carry higher first stage velocities but also mean travelling at a shallower angle and staying in longer in the atmosphere. The drag losses can be estimated using equation 4.23.

$$\Delta V_{DL} = \frac{\rho C_D V^2 t_b A}{2M_{rocket} \sin \phi_{BO}} \quad (4.23)$$

where  $\rho$  is the atmospheric density,  $C_D$  is the drag coefficient,  $V$  represents the velocity at the end of the impulse,  $t_b$  is the time of the burn,  $A$  is the cross sectional area of the rocket,  $M_{rocket}$  represents the total mass of the rocket and  $\phi_{BO}$  is the burnout angle.

Those losses are typically characteristic of the first stage burn, because the second impulse generally has a zero flight path angle (i.e. horizontal) throughout its duration and occurs above the atmosphere, avoiding drag losses as well. That is why, the  $\Delta V$  required by the second stage is estimated simply by using Eq. 4.20, whereas the total  $\Delta V$  for the first stage is given by

$$\Delta V_1 = \Delta V_{1,id} + \Delta V_{GL} + \Delta V_{DL} \quad (4.24)$$

The resulting losses versus the burnout angle of the first stage have been estimated and are reported in Figure 4.43.

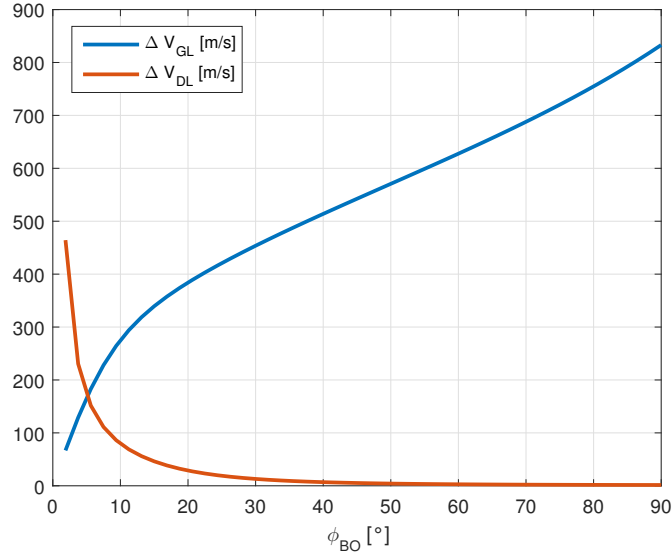


Figure 4.43: Estimated First Stage Losses in terms of  $\Delta V$

As it can be clearly seen, the largest loss is typically due to gravity rather than drag (except for very low burnout angle), therefore, this implies that an exact and detailed model of the drag losses is not crucial.

In order to develop a preliminary estimation of the propellant masses and evaluate the total mass of the Venus Ascent Rocket, a simplified model that includes the calculated  $\Delta V$  and the ideal rocket equation is needed.

Each stage of the Venus Ascent Rocket includes a fixed mass represented by the avionics, telecom, adapters, etc. and a variable mass that depends on the total propellant mass required by the stage that includes components such as tanks, lines, etc. and can be expressed as a function of the propellant fraction using the *SMF* (Structural Mass Fraction) coefficient

$$M_{var} = SMF \cdot M_{prop} \quad (4.25)$$

The *SMF* coefficient typically ranges between 8÷20%. For this analysis a value of 10% of the *SMF* coefficient has been adopted.

The dry mass of each stage can, then, be evaluated as the sum of the fixed and the variable mass:

$$M_{dry} = M_{fixed} + M_{var} = M_{fixed} + SMF \cdot M_{prop} \quad (4.26)$$

Thus, the propellant mass fraction can be estimated using the Tsiolkovsky rocket equation:

$$M_f = M_0 e^{-\frac{\Delta V}{c}} \quad (4.27)$$

where  $c$  is the ideal velocity of the exhausted gas ( $c = I_{sp}g$ , with  $g = 9.81 \text{ m/s}^2$ ).

Defining the relationship between the initial and final masses,  $M_0$  and  $M_f$  respectively

$$M_f = M_0 - M_{prop} \quad (4.28)$$

with

$$M_0 = M_{dry} + M_{PL} \quad (4.29)$$

where  $M_{PL}$  represents the payload mass, which is the entire mass of the second stage for the first stage, and the mass of the samples containers for the second stage.

The Tsiolkovsky rocket equation (Eq. 4.27) can be rewritten as follows

$$M_{prop} = \left( M_{dry} + M_{PL} \right) \left( e^{-\frac{\Delta V}{I_{sp}g}} - 1 \right) \quad (4.30)$$

The total mass of each stage is then simply calculated by

$$M_{stage} = M_{dry} + M_{prop} \quad (4.31)$$

And the rocket Gross Lift Off Mass (GLOM) is then the sum on the two stages and the payload mass:

$$GLOM = M_{st1} + M_{st2} + M_{PL} \quad (4.32)$$

GLOM usually represents the primary parameter in preliminary rocket designs. The analysis performed for the proposed mission, in fact, chose among variable parameters in order to minimize this mass. In particular, the goal of the analysis is to determine the value of the first stage burnout angle that corresponds to the minimum of the GLOM of the rocket. And then, basing on that result, in order to estimate the total  $\Delta V$  required, as well as how it splits into the two maneuvers, the burn times, the losses evaluation and finally the trajectory path of the Venus Ascent Rocket.

In order to fulfill that goal, a MATLAB spreadsheet model based on an iterative approach and capable of solving first order ordinary differential equations has been developed.

Therefore, Figure 4.44 shows the calculated behaviours of each stage mass and the GLOM with the variation of the burnout angle of the first stage that has been obtained.

It can be immediately noticed the presence of a minimum of the GLOM parameter which corresponds in this case to a burnout angle of about  $40^\circ$ . However, it can be noticed that there is a shallow minimum around this angle: changing the burnout angle by  $\pm 5^\circ$  only increases GLOM by 5 kg.

Along with the GLOM estimation, the  $\Delta V$  evaluation has been performed. Figure 4.45 shows how the two  $\Delta V_1$  and  $\Delta V_2$ , and the total  $\Delta V_{tot}$  vary with respect to the variation of the burnout angle.

As it can be noticed looking at Figures 4.44-4.45, minimizing the total  $\Delta V_{tot}$  does not minimize the GLOM. In fact, as those Figures show, it may require up to 20% less  $\Delta V$  to launch near horizontal. However, most of the total  $\Delta V_{tot}$  must be provided by the first stage. Putting too much  $\Delta V$  on the first stage is highly detrimental, adding 50% or more to

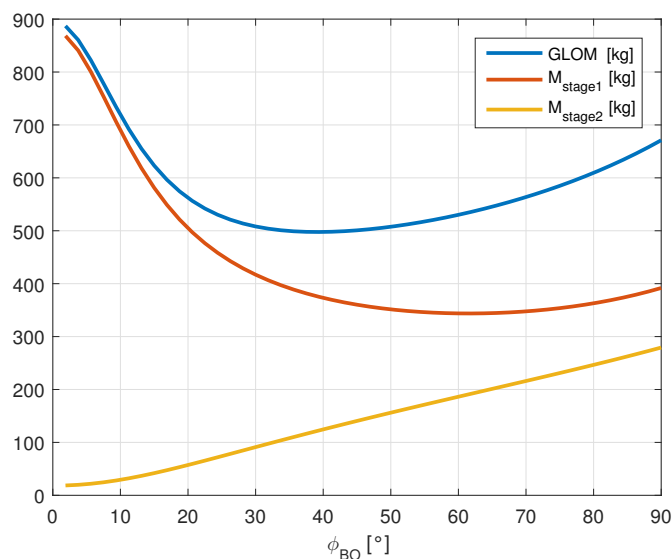


Figure 4.44: Venus Ascent Rocket GLOM vs Burnout Angle

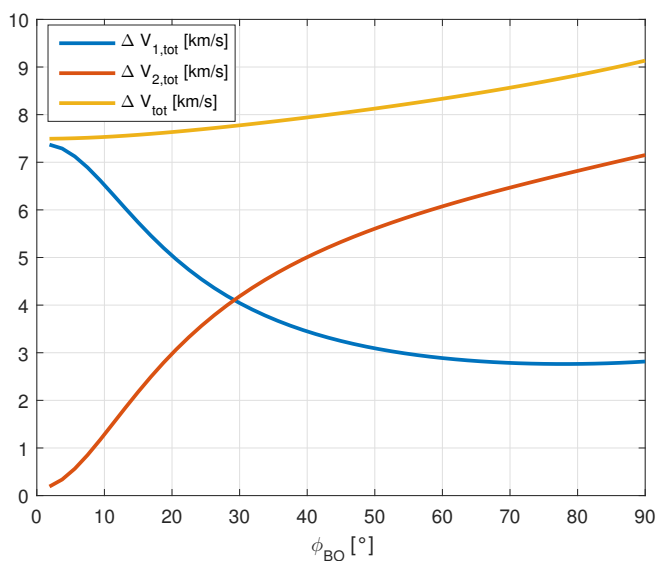


Figure 4.45: Venus Ascent Rocket GLOM vs Burnout Angle

the total mass. The balancing act between minimizing the total  $\Delta V$  and optimized staging leads to a minimum total GLOM.

Last but not least, the estimation of the burning times of each stage of the Venus Ascent Rocket has been performed and the results are shown in Figure 4.46.

Predictably, since the time of burn of a stage depends on the propellant mass (Eq. 4.21), which directly influences the mass of the stage itself, the behaviour of the burning time

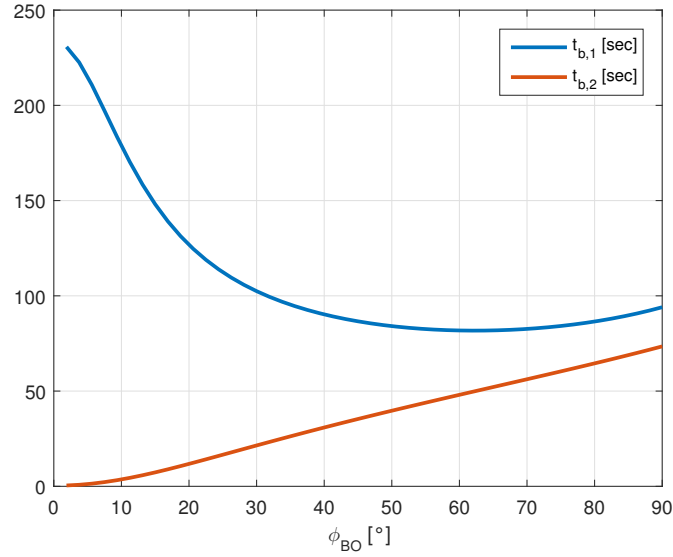


Figure 4.46: Venus Ascent Rocket Burn Times versus Burnout Angle

varying the burnout angle is similar to the one of the mass of each stage seen in Figure 4.44.

Therefore, as it has been seen from Figures 4.44-4.46, a simple analytic model has been developed in order to estimate the Venus Ascent Rocket mass and performances. The model includes preliminary estimations of the losses due to drag and gravity and represents the basis for a preliminary determination of the flight path followed by the ascent rocket from the 51 km of altitude above the Venusian surface and the achievement of the orbiting vehicle's altitude where the rendezvous is performed and the journey back to Earth starts. To summarize the results obtained with this analysis, Table 4.43 presents the values of the most important parameters obtained running the so developed MATLAB code.

Parameter	Result
$\Delta V_{1,id}$ [km/s]	3.04
$\Delta V_{GL}$ [km/s]	0.01
$\Delta V_{DL}$ [km/s]	0.526
$\Delta V_2$ [km/s]	4.90
$\Delta V_{tot}$ [km/s]	8.48
$M_{st1}$ [kg]	375.1
$M_{st2}$ [kg]	122.5
$M_{PL}$ [kg]	25.0
GLOM [kg]	497.6
$t_{b1}$ [s]	93
$t_{b2}$ [s]	29

Table 4.43: Ascent Rocket Trajectory Parameters

After having calculated the most important parameters that define the mass and the performance of the Venus Ascent Rocket, the design of the followed trajectory itself has been performed.

The first input of the study is given by the velocity at the end of the first stage impulse; with this parameter, the energy of the trajectory can be calculated using Equation 4.33:

$$\Sigma = \frac{V_i^2}{2} - \frac{\mu_{Venus}}{r_0} \quad (4.33)$$

where  $V_i$  is the initial velocity of the rocket reached thanks to the first stage burn,  $\mu_{Venus}$  is the gravitational parameter of Venus and  $r_0$  is the distance between the point where the Venus Ascent Rocket performs its first burn and the center of Venus.

From the energy it is possible to calculate the axis of the trajectory:

$$a = -\frac{\mu_{Venus}}{2\Sigma} \quad (4.34)$$

thus, the angular momentum  $h$  and the semilatus rectum  $p$  are respectively given by

$$h = r_0 \cdot V_i \cdot \cos\phi_{BO} \quad p = \frac{h^2}{\mu_{Venus}}$$

Then, the eccentricity of the trajectory can be calculated using

$$e = \sqrt{1 - \frac{p}{a}} \quad (4.35)$$

And, lastly, determining the eccentric anomaly at the first stage burnout point is then possible to evaluate the complete path the rocket follows.

The results have been obtained developing another MATLAB spreadsheet model and Figure 4.47 shows a sketch of the designed trajectory.

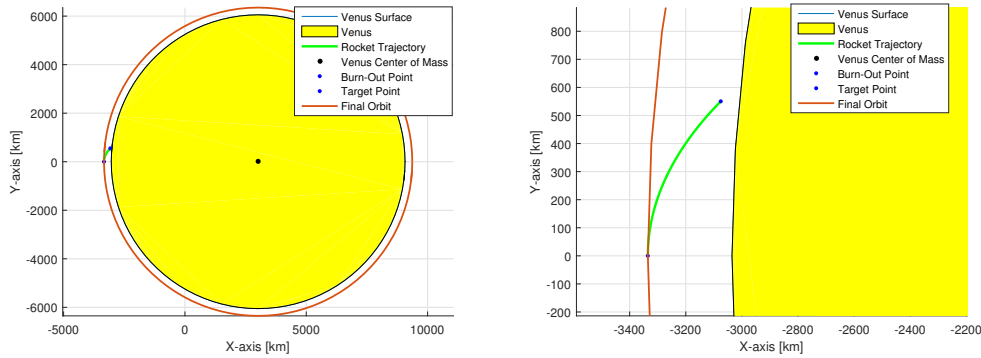


Figure 4.47: Venus Ascent Rocket Flight Path

N.B.: Figure 4.47 is not centered on the center of Venus, but on the center of the elliptical path described by the Venus Ascent Rocket.

Thanks to those calculations and the developed MATLAB spreadsheet model, the total time of flight of the rocket from the 51 km altitude above the Venusian surface to the 300

km altitude target orbit, has been estimated and resulted to be around 7 minutes and 30 seconds.

This simple model has been used to create a 3D-sketch as well (Figure 4.48), focusing on the plane where the rocket ascent takes place.

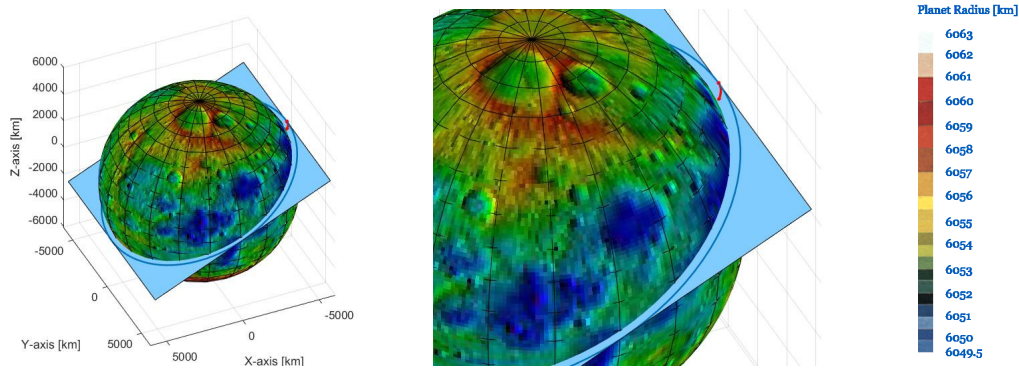


Figure 4.48: Venus Ascent Rocket Flight Path

## Rocket Design

After having designed the trajectory of the rocket and having determined the parameters that describe the amount of propellant and the mass of each stage, the design of the rocket itself has been developed. As seen from Section 4.1.1, in order to be encapsulated inside the aeroshell, the ascent rocket is required to be shorter than the maximum diameter of the heat shield, which is 3.4 m.

As for the propellant, as mentioned before, a solid propulsion has been selected, and a combination of Ammonium Perchlorate (oxidizer) and HTPB (fuel) has been chosen for the proposed mission. The properties of the propellant are presented in Table 4.44.

Oxidizer	Ammonium Perchlorate (solid)
Fuel	Aluminum + HTPB
Composition	68% AP + 18% Al + 14% HTPB
Specific Impulse [s]	287.5
Density [ $kg/m^3$ ]	287.5
Mixture Ratio	2.12
Chamber Pressure [atm]	68
Chamber Temperature [K]	2800

Table 4.44: Ascent Rocket Propellant Properties - Ref. [69]

The propellant grain geometry is selected to fit motor requirements: it should be compact and use the available volume efficiently, it should avoid or predictably control possible erosive burning and remaining unburned propellant slivers should be minimized. Therefore, an internal burning tube, progressive configuration has been designed for the propellant (Figure 4.49).

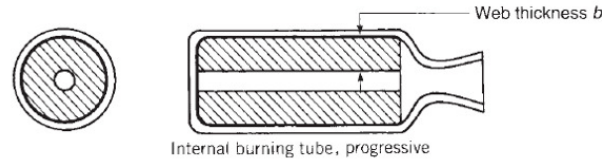


Figure 4.49: Venus Ascent Rocket Propellant Configuration - Ref. [70]

where the *web thickness* represents the ratio of the web thickness  $b$  to the outer radius of the grain:

$$b_f = \frac{b}{radius} = \frac{2b}{diameter}$$

Thus, in order to determine the size of the solid motor, an evaluation of the web fraction and the  $L/D$  ratio has been performed. In particular, solid rockets with internal burning tubes are typically characterized by web fraction between  $0.5 \div 0.9$  and  $L/D$  ratios between  $1 \div 4$  [70].

Thus, knowing the mass and the density of the propellant needed by each stage, the evaluation of the web fraction and the  $L/D$  ratio has been performed (Figure 4.50).

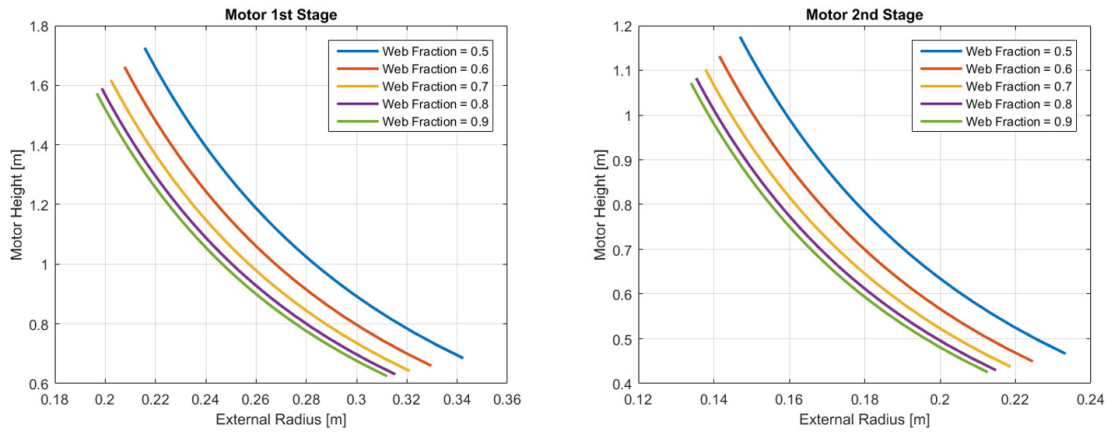


Figure 4.50: Motor Web Fraction vs  $L/D$  Ratio

Therefore, in order to satisfy the maximum rocket height requirement, the geometry properties and characteristics of the solid propellant have been determined and the results are listed in Table 4.45.

After having designed the solid motor, with the specifications of its configuration, geometry and dimensions, the design of the motor case that encapsules it has been developed.

Solid propellant rocket motor cases are used to encapsule the propellant grain and also to provide enough resistance to the system, serving as pressure vessels that protects the system from the high pressure loads. The typical loads the motor case must withstand concern the temperature changes leading to thermal stresses and strains, the stress corrosion and space environment stressors (such as vacuum or radiation). Three classes of materials that can provide enough resistance to those stresses have been typically used: high strength metals (such as steels, alloys of aluminum or titanium), wound-filament reinforced plastics

	1st Stage	2nd Stage
Propellant Mass [kg]	333.19	105.31
Propellant Volume [ $dm^3$ ]	189.2	59.8
Configuration	Internal Burning Tube, Progressive	
Web Fraction	0.8	0.8
L/D Ratio	1.2	1.3
External Radius [cm]	29.9	19.9
Web Thickness [cm]	23.9	15.9
Motor Height [cm]	70	50

Table 4.45: Ascent Rocket Motor Properties

and hybrid combination of these (such as metal cases externally wounded by reinforced plastics filaments for extra strength) [70]. Therefore, a list of possible motor case materials has been developed (Table 4.46).

Material	Density [ $kg/m^3$ ]	Ultimate Tensile Strength [Mpa]	Strength to Density Ratio (*1000)
Maraging Steel	8000	1966	246
A-286 Iron-based Alloy	7920	620	78
D6 AC Steel	7780	1483	191
Haynes 255	8220	765	93
Titanium Alloy Grade 5 (Ti-6Al-4V)	4430	950	214

Table 4.46: Possible Motor Case Materials

The properties of these materials have already been described in Section 4.2.2.

Among all these potential materials, the selection has been performed in order to minimize the mass of the motor case. However, in order to do that, a design of the motor case is needed. Therefore, the thickness of the motor case wall as well as the thickness of its torispherical head has been estimated.

According to ASME pressure vessel codes VIII section 2nd division, the thickness of the motor shell and of the torispherical head can be estimated using Eqs. 4.36-4.37 respectively.

$$T_s = \frac{P \cdot R}{2 \cdot S \cdot E + 0.4 \cdot P} \quad (4.36)$$

$$T_t = \frac{P \cdot L \cdot M}{2(SE - 0.1P)} \quad (4.37)$$

where  $P$  is the internal pressure of shell,  $R$  is the internal radius of shell (equal to the external radius of the solid motor),  $S$  is the allowable stress value and  $E$  represents the

joint efficiency;  $L$  is the Head Crown Radius that can be calculated using Eq. 4.38 and  $M$  is a parameter that is determined using Eq. 4.39.

$$L = H/2 \quad (4.38)$$

where  $H$  represents the tube length.

$$M = 0.25 \left( 3 + \sqrt{L/3} \right) \quad (4.39)$$

where  $r$  is the knuckle radius, which is 25% of  $L$ .

It is important to notice that the allowable stress factor of each material is the minimum value between the Yield Tensile Strength and the Ultimate Tensile Strength divided by the safety factor.

Table 4.48 lists the values of the parameters that does not depend on the choice of the motor case material, but that can be determined using the results obtained from the solid motor design seen previously (Table 4.45).

	1st Stage	2nd Stage
External Motor Radius [cm]	29	19
Safety Factor	1.5	1.5
Joint Efficiency	0.9	0.9
Head Crown Radius [cm]	35	25
Knuckle Radius [cm]	5.3	3.8

Table 4.47: Motor Case Thickness and Mass

As seen from Table 4.48, a safety factor of 1.5 and a joint efficiency of 0.9 has been used, according to the typical values used for structural analysis of solid rocket motor case in aerospace applications [71].

Then, the motor case thicknesses and mass have been calculated in order to choose the material that minimizes the weight of the component. As it can be clearly seen from Table 4.47, Maraging Steel resulted to be the best option for the 1st stage motor case design, whereas Titanium Alloy Grade 5 (Ti-6Al-4V) represents the best option for the 2nd stage motor case design.

Therefore, a case that can undergo combustion and can house and keep pressurized the solid motor has been designed. However, an internal layer of insulating material is typically applied between the propellant and the internal surface of the case in order to prevent the rocket motor shell from reaching temperatures that may damage its structural integrity. Typically, the insulation is bonded to the inner surface of the case and is made of materials capable of withstanding high temperature gases produced during the combustion of the grain. The most important properties this insulating material must be characterized by include [72]:

- Low ablation rate (from 0.09 to 0.2 mm/s)

1st Stage			
Material	Motor Case Thickness [mm]	Head End Thickness [mm]	Motor Case Mass [kg]
Maraging Steel	1	1.3	13.5
A-286 Iron-based Alloy	4.1	6.1	57.3
D6 AC Steel	1.2	1.7	15.6
Haynes 255	3.0	4.4	43.0
Titanium Alloy Grade 5 (Ti-6Al-4V)	1.8	2.7	13.9
2nd Stage			
Maraging Steel	1	1	6.02
A-286 Iron-based Alloy	2.8	4.4	18.1
D6 AC Steel	1	1.2	6.07
Haynes 255	2.0	3.2	13.6
Titanium Alloy Grade 5 (Ti-6Al-4V)	1.2	1.9	4.40

Table 4.48: Motor Case Design

- Low density (from 1050 to 1500  $kg/m^3$ )
- Sufficient tensile strength
- Low thermal conductivity (from 0.2 to 0.5  $W/(m \cdot K)$ )
- High specific heat (from 1000 to 2100  $J/(kg \cdot K)$ )

In particular, according to the study in Ref. [72], the proposed mission uses laminates of EPDM (Ethylene Propylene Diene Monomer) reinforced with CCF (Chopped Carbon Fiber) and aramid fiber in pulp such as KP (Kevlar Pulp) because of its great properties and high performance in rocket motor case applications. Table 4.49 lists the properties of such insulating material.

In order to estimate the mass of the insulating layer, a simple expression that relates the internal insulation thickness  $d$  at any location in the rocket motor with the exposure time  $t_e$  and the ablation rate  $r_e$  with the use of a safety factor that typically ranges between 1.2

Property	Value
Density [ $kg/m^3$ ]	1239
Tensile Strength [MPa]	7.8
Elongation [%]	1.2 ÷ 12
Specific Heat Capacity [ $J/(kg \cdot K)$ ]	1691
Thermal Diffusivity [ $mm^2/s$ ]	0.085
Thermal Conductivity [ $W/(m \cdot K)$ ]	0.178
Ablation Rate [mm/s]	0.02

Table 4.49: Properties of laminates made using six alternate layers of CCF and KP based EPDM prepreps - Ref. [72]

and 2.0 has been used [70]:

$$d = t_e \cdot r_e \cdot SF \quad (4.40)$$

As a result, the thickness of the insulating layer as been calculated for each one of the ascent rocket stages and, then, the mass of the insulating material has been estimated, as reported in Table 4.50.

	1st Stage	2nd Stage
Insulating Thickness [mm]	3.7	1
Insulating Mass [kg]	6.1	0.92

Table 4.50: Motor Case Insulating Layer Thickness and Mass

The last part of each stage of the Venus Ascent Rocket design concerned the determination of the geometry and the materials of the nozzles used by the proposed rocket. Therefore a preliminary analysis of the geometry of the nozzles has been permormed. In particular, conical nozzles have been designed since it represents the oldest and perhaps the simplest configuration, it is relatively easy to fabricate and is still used today in many small rockets. As it can be seen from Figure 4.51, the diverging section of a conical nozzle basically consists of two parts: an arc of sphere that begins at throat and characterized by radius  $R_1$ , and a linear section that begins at transition point  $N$  and is characterized by an inclination angle of  $\alpha$ .

Therefore, after having defined the input parameters (such as the expansion ratio and the radius of the exit section of the nozzle), the length of the nozzle can be rewritten as

$$L = L_N + L_1 \quad (4.41)$$

where

$$L_N = \frac{R_e - R_t + R_1(\cos\alpha - 1)}{\tan\alpha} \quad L_1 = R_1 \sin\alpha$$

Thus,

$$L = \frac{R_t(\sqrt{\epsilon} - 1) + R_1(\cos\alpha - 1)}{\tan\alpha} + R_1 \sin\alpha \quad (4.42)$$

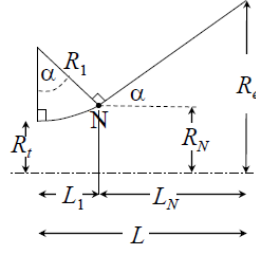


Figure 4.51: Conical Nozzle Geometry Sketch

where the expansion ratio  $\epsilon$  is defined as

$$\epsilon = \frac{A_e}{A_t}$$

and, rewriting Equation 4.42, we obtain the final expression for the length of the nozzle, given the design parameters:

$$L = \frac{R_t}{\tan\alpha} \left[ \sqrt{\epsilon} - 1 + \frac{R_1}{R_t} \left( \frac{1}{\cos\alpha} - 1 \right) \right] \quad (4.43)$$

The hot gases expand in the nozzle diverging section so in order to provide maximum thrust. As a consequence of the decrease of the pressure of the gases, energy is used to accelerate these gases. In order to design the nozzle, the expansion ratio must be determined. That is why, the exit Mach number is estimated using Equation 4.44.

$$M_e = \sqrt{\frac{2}{k-1} \left[ \left( \frac{P_c}{P_a} \right)^{\frac{k-1}{k}} - 1 \right]} \quad (4.44)$$

where  $k$  is the specific heat ratio,  $P_c$  is the chamber pressure and  $P_a$  is the atmospheric pressure at the local altitude (according to the Venus Global Reference Atmospheric Model [44]). Specific heat ratio varies depending on the composition and temperature of the exhaust gases, and is typically equal to 1.2 [70].

From the exit Mach number is, then, possible to determine the expansion ration of the divergent part of the nozzle (Eq. 4.45).

$$\epsilon = \frac{1}{M_e} \left[ \frac{1 + \frac{k-1}{2} M_e^2}{\frac{k+1}{2}} \right]^{\frac{k+1}{2(k-1)}} \quad (4.45)$$

Therefore, considering the maximum allowable diameter for the nozzle exit cone which cannot be larger than the rocket outermost diameter so that it can fit inside the lander structure and the aeroshell capsule, and knowing the expansion ratio (calculated using Eq. 4.45) a preliminary nozzle geometry can be determined following the passages presented previously (Eqs. 4.41-4.43). Generally, a theoretical correction factor, denoted as  $\lambda$ , is applied to adjust the nozzle exit momentum of any preliminary calculations that involves ideal rocket propulsion system with conical nozzles. This factor is the ratio between the

momentum of the gases exhausting with a finite nozzle angle  $2\alpha$  (see Figure 4.51) and the momentum of an ideal nozzle with all gases flowing in the axial direction [70].

$$\lambda = \frac{1}{2}(1 + \cos\alpha) \quad (4.46)$$

Predictably, for ideal rocket  $\lambda$  is equal to 1. For a rocket nozzle with a divergence cone angle of  $30^\circ$  (half angle  $\alpha = 15^\circ$ ), the axial exhaust velocity will be 98.3% of the velocity that gives the Mach exit number calculated with Eq. 4.44. In particular, nozzles characterized by small divergence angle may produce a mostly axial momentum and thus provide high specific impulses, however they present drawbacks related to the mass since they result long nozzles. On the other hand, larger divergence angles give shorter, lightweight designs, but their performances may become unacceptably low (as it can be seen from Figure 4.52).

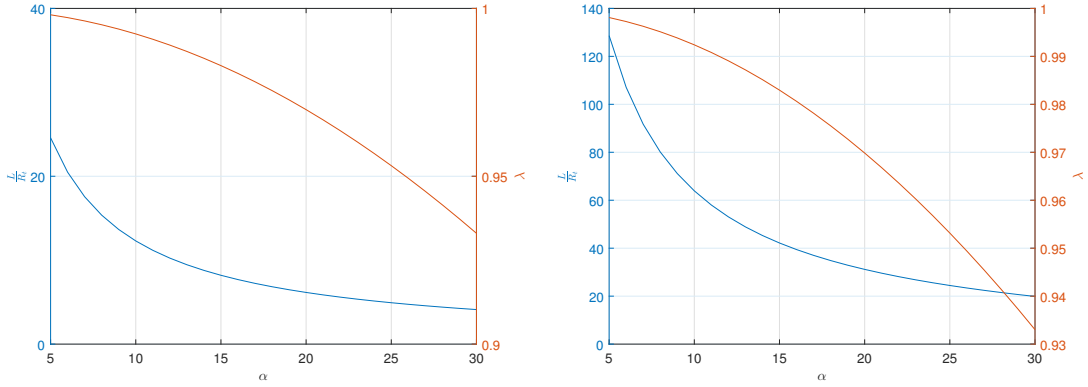


Figure 4.52: Nozzle Correction Factor and Nozzle Length to Exit Radius vs Nozzle Half Cone Angle - 1st Stage (left) and 2nd Stage (right)

Therefore, in order to avoid unacceptable low performances, a minimum correction factor of 0.97 has been considered and a resulting half cone angle of  $20.6^\circ$  has been adopted for the nozzles design.

As a result, the nozzle geometry of both the two stages of the rocket has been created and the properties of each of them are listed in Table 4.51.

	1st Stage	2nd Stage
Nozzle Throat Diameter [cm]	19	3.2
Nozzle Exit Diameter [cm]	60	40
Specific Heat Ratio	1.2	1.2
Half Cone Angle [°]	20.6	20.6
Divergent Length [cm]	54	47

Table 4.51: Venus Ascent Rocket Nozzles Properties

Lastly, following a similar process to the one used previously to determine the characteristics of the rocket motor case, the thickness, mass and material of the nozzles have been

evaluated. In particular, the thickness of both the convergent and the divergent part of the nozzle can be estimated by

$$t = \frac{P \cdot d}{2 \cos \alpha \left( \frac{UTS}{SF} - 0.6 \cdot P \right)} \quad (4.47)$$

where  $UTS$  is the Ultimate Tensile Strength of the material the nozzle is made of and  $SF$  is the Safety Factor (equal to 1.5) and  $\alpha$  is the half cone angle of the divergent (or convergent) part of the nozzle.

On the other hand, the thickness of the throat is given by

$$t = \frac{P_t \cdot d}{2 \left( \frac{UTS}{SF} - 0.6 \cdot P_t \right)} \quad (4.48)$$

where  $P_t$ , the pressure at the throat, can be estimated as  $0.54P_c$  (the pressure in the chamber).

Therefore, the nozzles thicknesses and mass have been calculated in order to choose the material that minimizes the weight of the component. As it can be clearly seen from Table 4.52, Titanium Alloy Grade 5 (Ti-6Al-4V) represents the best option for both the 1st and the 2nd stage nozzle design.

1st Stage				
Material	Nozzle Convergent Thickness [mm]	Nozzle Throat Thickness [mm]	Nozzle Divergent Thickness [mm]	Nozzle Mass [kg]
Maraging Steel	2.1	1.0	1.2	9.74
A-286 Iron-based Alloy	9.9	1.8	5.6	37.0
D6 AC Steel	2.7	1.0	1.5	11.6
Haynes 255	7.1	1.5	4.0	28.2
Titanium Alloy Grade 5 (Ti-6Al-4V)	4.3	1.2	2.4	9.6
2nd Stage				
Maraging Steel	1.4	1.0	1.0	3.65
A-286 Iron-based Alloy	6.6	1.0	3.7	11.0
D6 AC Steel	1.8	1.0	1.0	3.84
Haynes 255	4.7	1.0	2.7	8.58
Titanium Alloy Grade 5 (Ti-6Al-4V)	2.8	1.0	1.6	3.03

Table 4.52: Nozzles Design

Therefore, the calculated masses of each component of the two stages of the Venus Ascent Rocket have been estimated. The results are, then, summarized in Table 4.53.

	1st Stage	2nd Stage
Propellant [kg]	333.2	105.31
Motor Case [kg]	13.7	6.02
Insulation [kg]	6.14	0.917
Nozzle [kg]	9.60	3.03
Igniter [kg]	$1.9 \cdot 10^{-4}$	$1.9 \cdot 10^{-4}$
Electronics [kg]	12.5	7.22
<b>TOT</b>	<b>375.1</b>	<b>122.5</b>

Table 4.53: Stages Baseline Mass

Lastly, the nosecone of the of the rocket has been designed. Similarly to what has already been done for the stages and the nozzles, firstly the shape and the dimensions of the component have been determined, then the material has been selected and finally the mass is calculated.

In order to develop an optimized design of the nosecone of the rocket, a detailed aerodynamic analysis should be done in order to have the minimum mass with the maximum performances of the component (such as the minimum drag). As for this preliminary analysis, the nosecone Wolfgang Haack's series shape has been considered since it is not constructed from geometric figures, but is mathematically derived for the purpose of minimizing drag.

The equations that describe the shape of this type of nosecone include

$$\theta = \arccos\left(\frac{2x}{L}\right) \quad (4.49)$$

$$y = \frac{R}{\sqrt{\pi}} \sqrt{\theta - \frac{\sin(2\theta)}{2} + C \sin^3(\theta)} \quad (4.50)$$

where  $L$  is the total length of the nosecone,  $R$  is the radius of the nosecone's base,  $x$  varies from 0 (at the tip of the nose cone) to  $L$  and  $C$  define the shape of the series. In particular, when  $C = 0$ , the minimum drag for the given length and diameter is realized; and when  $C = 1/3$ , the minimum drag for the given length and volume is realized.

Therefore, given the diameter of the Venus Ascent Rocket, the dimensions and the shape of the nose cone have been calculated.

Lastly, a list of potential materials the nose cone can be made of has been developed (Table 4.54).

Pyrolytic Carbon is an artificially produced material similar to graphite: it is generally generated heating a hydrocarbon nearly to its temperature of decomposition, and permitting the graphite to crystalize (pyrolysis). Thanks to its high performances even at high temperatures, it is typically used for missile nose cones and ablative (boiloff-cooled) rocket motors.

On the other hand, Reinforced Carbon-Carbon (CRFC) is a composite material that consists of carbon fiber reinforcement in graphite matrix. Firstly developed for reentry vehicles of intercontinental missiles, it is mostly known for its use in parts of the Space Shuttle orbiter. It possesses great properties for structural applications at high temperatures (such

Material	Density [ $kg/m^3$ ]	Young's Modulus [MPa]	Max Operating Temperature [°C]
Pyrolytic Carbon	2250	4.8	3650
Reinforced Carbon-Carbon (CFRC)	1750	35.9	2000

Table 4.54: Nose Cone Potential Materials

as high thermal shock resistance or low thermal expansion coefficient). The minimum required thickness of the nose cone has been estimated and the mass depending on the material of the list in Table 4.54 has been evaluated in order to choose the material that gives the lightest configuration. The results are reported in Table 4.55.

Material	Thickness [mm]	Mass [kg]
Pyrolytic Carbon	7	14.4
Reinforced Carbon-Carbon (CFRC)	5	11.2

Table 4.55: Nose Cone Design

Therefore, as it can be clearly seen from Table 4.52, Reinforced Carbon-Carbon (CFRC) resulted to provide the lightest configuration and thus it has been chosen as the nose cone material.

Once all the components of the Venus Ascent Rocket have been designed, a complete CAD model has been created. Figure 4.53 gives an overview of the so designed Venus Ascent Rocket. As it can be clearly seen from the Figure, the total calculated height of the rocket resulted to be 3.27 m, thus shorter than the 3.4 m of the heat shield diameter. Therefore, the rocket resulted to be short enough to be encapsulated inside the descending aeroshell.

## 4.4 Lander Overview

During the design processes followed in the previous chapters, iterations were performed on the Lander, Balloon and Rocket components in order to provide a preliminary design of the entire lander vehicle which is supposed to successfully complete all the tasks of the mission. The aim of this chapter is to give a final complete overview of the lander vehicle. Therefore, not only the preliminary estimation of the masses of each piece of the landing probe will be presented, but also a concept of the lander will be shown, reporting some sketches from the created CAD models.

Thus, the preliminary lander mass estimation is presented in Table 4.56.

Along with the preliminary lander mass estimation, the overview of the landing probe itself is presented. Figure 4.54 shows how it is supposed to fit inside the Falcon 9 payload fairing.

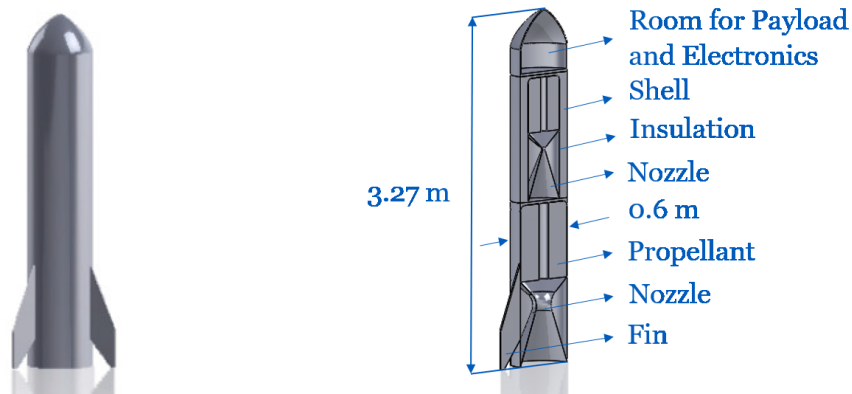


Figure 4.53: Venus Ascent Rocket CAD Model

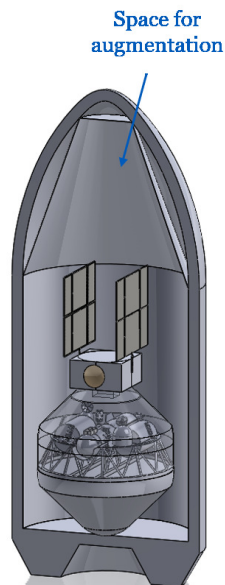


Figure 4.54: Falcon 9 Payload Fairing, Venus Lander and Orbiter

It is important to note that in Figure 4.54 it looks like there is a lot of wasted space inside the Falcon 9 upper stage, however, all that space will be used by augmentations and structures that will be useful to keep the spacecraft steady especially during the launch and the interplanetary travel.

Lastly, a Figure that shows the entire landing vehicle concept with the main subsystems and how they fit inside the lander is reported below.

Lander Component	Estimated Mass [kg]	Mass Growth Allowance [%]	Total Mass [kg]
Heat Shield	210	15	242
Backshell	192	15	221
Parachute	16	25	20
Grid Fins	24	30	31
Lander Platform	335	15	385
Helium Tanks (Balloon)	86	20	103
Landing Ring	406	15	467
Payload Vessels	59	25	74
Payload Instruments	52	20	62
Thermal Protection System	16	30	21
Drills & Mechanisms	32	30	42
Samples Handling System	12	35	16
Communication System	8	25	10
Power System	70	25	88
Balloon Lifting Gas	53	15	61
Balloon	22	30	29
Balloon Inflation Pipe	7	25	9
Ascent Rocket	523	15	601
<b>TOT</b>	<b>2123</b>		<b>2482</b>

Table 4.56: Preliminary Lander Mass Estimation

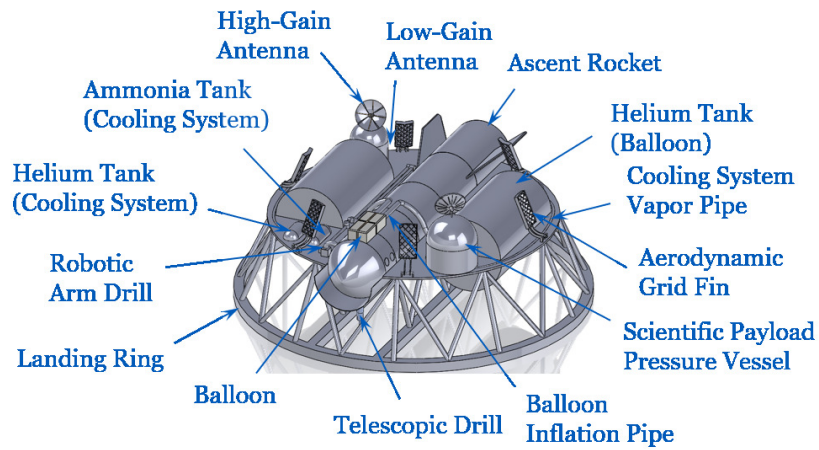


Figure 4.55: Venus Lander Overview



# Conclusions

As a conclusion, this chapter presents a brief summary of all the main investigated concepts and the most relevant results obtained during the whole work of research described in the previous chapters.

The primary objective of this thesis was to develop preliminary concepts and calculations for a Venus Sample Return space mission, satisfying a list of requirements given by NASA-JPL. Clearly, the proposed mission architecture is not intended to be the final choice of the Venus sample return mission: it is an example mission concept that both achieves the mission requirements and covers a large variety of the scientific goals related to the Venus science research, and provides enough engineering definition for first-order estimations of the needed resources. Moreover, the level of detail for the proposed mission architecture is uneven, with some elements having received advanced design and analysis work (e.g Venus ascent vehicle) and other elements not advanced beyond the rough concept stage (e.g the orbiter).

Iterations were performed on all the main systems and subsystems in order to determine the mass of each component and develop a preliminary mass estimation of the entire landing vehicle. And, with this mass in mind, the interplanetary travel, the atmospheric entry in the Venusian environment and the lift off from Venus surface have been designed in order to provide preliminary details and specifications about all the phases of the mission. However, as seen from the previous chapters, of particular interest was the implementation of the resources and the components needed by the lander to successfully perform a safe landing on the Venusian surface and a complete ascent after having collected soil and atmosphere samples (as required). In particular, new concepts of a lander and an ascent vehicle have been developed and described along with the preliminary calculations and equations used during the discussion. New strategies for the soil and atmospheric samples collection were discussed in order to both fulfill the mission requirements and provide the lander of components able to withstand the harsh Venusian environment conditions. A new combination of balloon and rocket has been discussed and developed for the Venus sample return task. Lastly, CAD models of all the developed parts and components of the entire spacecraft have been created in order to provide a global overview of every systems and subsystems together with the technological and mathematical descriptions of the parts.

As a result, even if further research and several technological breakthroughs in several key areas are obviously needed to make this mission possible, a new concept of a mission architecture that fully satisfies all the mission requirements has been developed and proposed. Therefore, this work can either provide suggestions or inspirations for related future work or represent the starting point for further and more detailed analysis that can improve the

precision and the reliability of the proposed mission concept.

# Bibliography

- [1] Venus Science & Technology Definition Team (2009), *Venus Flagship Mission Study (Final Report)*
- [2] Taylor, Fredric W. (2014), *The Scientific Exploration of Venus*
- [3] Suomi, V. E. and S. S. Limaye (1978), *Venus—Further evidence of vortex circulation*
- [4] Limaye, S. S. (1985), *Venus atmospheric circulation: Observations and implications of the thermal structure*
- [5] Way, M.J., Del Genio, A.D., Kiang, N.Y., Sohl, L.E., Grinspoon, D.H., Aleinov, I., Kelley, M., Clune, T. (2016), *Was Venus the First Habitable World of Our Solar System?*
- [6] Saunders, R.S., Stofan, E.R., Plaut, J.J., Senske, D.A. (1993), *Magellan at Venus: Summary of Science Findings*
- [7] JPL, NASA (Retrieved 29 May 2020), *Magellan Mission Summary*  
<https://www2.jpl.nasa.gov/magellan/image2.html>
- [8] Ivanov, M.A., Head, J.W. (2015), *The history of tectonism on Venus: A stratigraphic analysis*
- [9] Phillips, R.J., Raubertas, R.F., Arvidson, R.E., Sarkar, I.C., Herrick, R.R., Izenberg, N., Grimm, R.E. (1992), *Impact craters and Venus resurfacing history*
- [10] Herrick, R.R., Phillips, R.J. (1993), *Effects of the Venusian atmosphere on incoming meteoroids and the impact crater population*
- [11] Frankel, C. (1996), *Volcanoes of the Solar System*
- [12] Karttunen, H., Kroger, P., Oja, H., Poutanen, M., Donner, K.J. (2007), *Fundamental Astronomy*
- [13] Kranopol'skii, V.A. (1980), *Lightning on Venus according to Information Obtained*

*by the Satellites Venera 9 and 10*

- [14] National Space Science Data Center, NASA (Retrieved 29 May 2020), *Venera 12 Descent Craft*  
<https://www2.jpl.nasa.gov/magellan/image2.html>
- [15] Russell, C.T., Zhang, T.L., Delva, M., Magnes, W., Strangeway, R.J., Wei, H.Y. (2007), *Lightning on Venus inferred from whistler-mode waves in the ionosphere*
- [16] Marcq, E., Bertaux, J.L., Montmessin, F., Belyaev, D. (2012), *Variations of sulphur dioxide at the cloud top of Venus's dynamic atmosphere*
- [17] Filiberto, J., Trang, D., Treiman, A.H., Gilmore, M.S. (2020), *Present-day volcanism on Venus as evidenced from weathering rates of olivine*
- [18] Dziewonski, A.M., Anderson, D.L. (1981), *Preliminary Reference Earth Model*
- [19] Faure, G., Mensing, T.M. (2007), *Introduction to planetary science: the geological perspective*
- [20] Yang, Huang J., Daiyun W. (2016), *Separation of dynamic and isostatic components of the Venusian gravity and topography and determination of the crustal thickness of Venus*
- [21] Grimm, R.E., Hess P.C. (1997), *The Crust of Venus*
- [22] Aitta, A. (2012), *Venus' Internal Structure Temperature and Core Composition*
- [23] Nimmo, F. (2002), *Why does Venus lack a magnetic field?*
- [24] Nimmo, F., McKenzie, D. (1998), *Volcanism and Tectonics on Venus*
- [25] Lewis, J.S. (2004), *Physics and Chemistry of the Solar System*
- [26] Grinspoon, D.H., Bullock, M.A. (2007), *Searching for Evidence of Past Oceans on Venus*
- [27] Crisp, D., Titov, D. (1997), *Venus II - The Thermal Balance of Venus Atmosphere*
- [28] Driscoll, P., Bercovici, D. (2013), *Divergent Evolution of Earth and Venus: Influence of Degassing*
- [29] Markiewicz, W.J., Petrova, E., Shalygina, O., Almeida, M., Titov, D.V., Limaye., S.S., Ignatiev, N., Roatsch, T., Matz, K.D. (2014), *Glory on Venus Cloud Tops and the Unknown UV Absorber*

- [30] Khatuntsev, I.V., Patsaeva, M.V., Titov, D.V., Ignatiev, N.I., Turin, A.V., Limaye, S.S., Markiewicz, W.J., Almeida, M., Roatsch, T.H., Moissl, R. (2013), *Cloud Level Winds from the Venus Express Monitoring Camera Imaging*
- [31] Kamath, S., Rivera, J., Garcia, M., Benaroya, H. (2015), *Inner Solar System Prospective Energy and Material Resources - Mercury, Venus and Titan*
- [32] Zhang T.L., Baumjohann W., Delva M., Auster H.U., Balogh A., Russell C.T., Barabash S., Balikhin M., Berghofer G., Biernat H.K., Lammer H., Lichtenegger H., Magnes W., Nakamura R., Penz T., Schwingenschuh K., Vörös Z., Zambelli W., Fornaçon K.H., Glassmeier K.H., Richter I., Carr C., Kudela K., Shi J.K., Zhao H., Motschmann U., Lebreton J.P. (2006), *Magnetic Field Investigation of the Venus Plasma Environment: Expected New Results from Venus Express*
- [33] Luhmann, J.G., Russell, C.T. (1997), *Venus: Magnetic Field and Magnetosphere*
- [34] Venera-D Joint Science Definition Team (2019), *Venera-D: Expanding Our Horizon of Terrestrial Planet Climate and Geology Through the Comprehensive Exploration of Venus*
- [35] Venus Exploration Analysis Group (2019), *Venus Goals, Objectives and Investigations*
- [36] Wikipedia, The Free Encyclopedia (Retrieved 29 May 2020), *List of missions to Venus*  
[https://en.wikipedia.org/wiki/List\\_of\\_missions\\_to\\_Venus](https://en.wikipedia.org/wiki/List_of_missions_to_Venus)
- [37] Rubie, D.C., Jacobson, S.A., Morbidelli, A., O' Brien, D.P., Young, E.D., de Vries, J., Nimmo, F., Palme, H., Frost, D.J. (2014), *Accretion and differentiation of the terrestrial planets with implications for the compositions of early-formed Solar System bodies and accretion of water*
- [38] Kane, S.R., Kopparapu, R.K., Domagal-Goldman, S.D. (2014), *On the Frequency of Potential Venus Analogs from Kepler Data*
- [39] SpaceX (2019), *Falcon User's Guide*
- [40] Howard Curtis (2005), *Orbital Mechanics for Engineering Students* (1st Ed.), Butterworth-Heinemann
- [41] Machado, P., Widemann, T., Peralta, J., Ruben Goncalves, Gilli, G., Silva, M. (2017), *Meridional and Zonal winds at Venus' atmosphere from cloud-tracking, Doppler techniques and comparison with modelling*
- [42] Wiley J. Larson & James R. Wertz *Space Mission Analysis and Design* (2nd Ed.), Microcosm Inc., 2005

- [43] National Space Science Data Center, NASA (Retrieved 9 June 2020), *Venus Fact Sheet*  
<https://nssdc.gsfc.nasa.gov/planetary/factsheet/venusfact.html>
- [44] NASA Marshall Space Flight Center (2005), *Venus-GRAM (Global Reference Atmospheric Model)*
- [45] Hwang, H.H., Nasa Ames Research Center (2018), *A Common Probe Design For Multiple Planetary Destinations*
- [46] Prabhu, D.K., Allen Jr., G.A., Cappuccio, G., Spilker, T.R., Hwang, H.H., Moses, R.W. (2013), *Atmospheric Entry Studies for Venus Missions: 45° Sphere-Cone Rigid Aeroshells and Ballistic Entries*
- [47] Yajima, N., Izutsu, N., Imamura, T., Abe, Toyoo (2009), *Scientific Ballooning - Technology and Applications of Exploration Balloons Floating in the Stratosphere and the Atmospheres of Other Planets*
- [48] MS&T19 Technical Meeting and Exhibition, Gasch, M. (2019), *Heatshield for Extreme Entry Environment Technology (HEEET) Thermal Protection System (TPS)*
- [49] 13<sup>th</sup> International Planetary Probe Workshop, Ellerby, D., Gage, P., Kazemba, C., Mahazari, M., Nishioka, O., Peterson, K., Stackpoole, M., Venkatapathy, E., Young, Z., Poteet, C., Splinter, S., Fowler, M., Kellermann, C. (2016), *Heatshield for Extreme Entry Environment Technology (HEEET) Development Status*
- [50] Knacke, T.W. (1991), *Parachute Recovery Systems Design Manual*
- [51] Fryer, D.M., Harvey, J.F. (1998), *High Pressure Vessels*
- [52] Plascore (Retrieved 17 June 2020), *Plascore CrushLite™*  
<https://www.plascore.com/honeycomb/energy-absorbtion/crushlite/>
- [53] Schroeder, K., Bayandor, J., Samareh, J. (2018), *Structural Sizing and Synthesis of Venera-Class Landers*
- [54] Plascore (Retrieved 17 June 2020), *Plascore CrushLite - Lightweight, Constant Force Energy Absorber*
- [55] Jaworske, D.A., Kline, S.E. (2008), *Review of End-of-Life Thermal Control Coating Performance*
- [56] Aegerter, M.A., Leventis, N., Koebel, M.M. (2008), *Aerogels Handbook*
- [57] Lee, K.L., Tarau, C. (2019), *24 Hours Consumable-based Cooling System for Venus Lander*

- [58] Rehnmark, F., Cloninger, E., Hyman, C., Bailey, J., Traeden, N., Zacny, C., Kriechbaum, K., Melko, J., Wilcox, B., Hall, J., Sherrill, K. (2018) *Environmental Chamber Testing of a Rock Sampling Drill for Venus Exploration*
- [59] Zacny, C., Rehnmark, F., Cloninger, E., Rabinovitch, J. (2017) *Development of Venus Drill*
- [60] Bugga, R., *High Temperature-resilient And Long-Life (HiTALL) Primary Batteries for Venus and Mercury Surface Missions*
- [61] Yavrouian, A., Plett, G., Yen, S., Cutts, J., Baek, D. (1999) *Evaluation of materials for Venus aerobot applications*
- [62] Burgess, R.J. (1978) *Zero and Superpressure Free Flight Ballooning*
- [63] Smith, M.S., et al. (1997) *Development of Venusian Aerobots*
- [64] Rubin, L.S., et al. (1999) *Liquid Crystalline Polymers Expand the Capabilities of Interplanetary Aerobots*
- [65] Colozza, A. (2004) *Solar Powered Flight on Venus*
- [66] Braeunig, R.A. (2014) *Model of Venusian Atmosphere, 0 to 100 km*
- [67] Joyner, C.R., Levack, D.J.H., Rhodes, R.E., Robinson, J.W. (2010) *Propulsion System Choices and Their Implications*
- [68] Woolley, R. (2014) *A Simple Analytic Model for Estimating Mars Ascent Vehicle Mass and Performance*
- [69] Mason, P.B., Roland, C.M. (2019) *Solid Propellants*
- [70] Sutton, G.P., Biblarz, O. (2017) *Rocket Propulsion Elements*
- [71] Kumar, D.B., Nayana, S.B., Shree, S.D. (2016) *Design and Structural Analysis of Solid Rocket Motor Casing Hardware used in Aerospace Applications*
- [72] Ahmed, A.F., Hoa, S.V. (2011) *Thermal insulation by heat resistant polymers for solid rocket motor insulation*